UNIVERSITÀ DEGLI STUDI DI PADOVA

DIPARTIMENTO DI SCIENZE CHIMICHE

CORSO DI LAUREA MAGISTRALE IN CHIMICA

TESI DI LAUREA MAGISTRALE

Synthesis and Proprieties of Oligo(2-ethyl-2-oxazoline)-Based Polymers with Discrete Architecture

Relatore: Prof. Edmondo M. Benetti

Controrelatore: Prof.ssa Marcella Bonchio

Laureando: Matteo Cavaliere

ANNO ACCADEMICO 2024/2025

INDEX

ABSTRACT **3**

CHAPTER ONE: INTRODUCTION **4**

1.1 Polyoxazolines for surface modification 4

1.2 Cationic ring opening polymerization (CROP) 6

1.3 RAFT polymerization 12

1.4 Polymer brushes 15

1.5 Discrete vs polydisperse: the effect of dispersity on the properties of polymer brushes 20

1.6 Aim of this thesis 27

CHAPTER 2: MATERIALS AND METHODS **29**

2.1 Materials 29

2.2 Instruments 29

2.3 Oligo(ethyl-2-oxazoline)s through CROP 31

2.4 Chromatographic separation of discrete oligo(2-ethyl-2-oxazoline)s 32

2.5 Methylation of CDPA 33

2.6 Poly[oligo(2-ethyloxazoline)]s through RAFT polymerization 34

2.7 End-capping of POEOXMAs through aminolysis of trithiocarbonyl groups 34

CHAPTER 3: RESULTS AND DISCUSSION **36**

3.1 Synthesis of $OEOX_pMA$ 36

3.2 Chromatographic separation of discrete $OEOX_nMAs$ 44

3.4 Methylation of CDPA 48

3.5 RAFT polymerization of OEOXMAs 51

3.6 End-capping of POEOXMAs through aminolysis of trithiocarbonyl groups 56

3.7 LCST of $POEOX_nMA$-SH 59

CHAPTER 4: CONCLUSIONS AND FUTURE PERSPECTIVES **67**

BIBLIOGRAPHY **69**

SUPPORTING INFORMATIONS **72**

^{1}H-NMR spectra of purified OEOX$_p$MAs 72

MS analysis of OEOX$_p$MAs 75

^{1}H-NMR and MS spectra of isolated OEOX$_n$MAs 78

^{1}H-NMR spectra and GPC elugrams of purified POEOX$_n$MAs 84

UV-Vis absorbance spectra of POEOX$_n$MA and POEOX$_n$MA-SH (superimposed) 94

Fitting of T_c for POEOX$_n$MA-SH 97

Quantities used for the synthesis of OEOX$_p$MAs 104

Quantities used for the synthesis of POEOX$_n$MAs 105

ABSTRACT

Dispersity within polymer brushes plays a major role in determining interfacial proprieties such as hydrophilicity, lubrication and interaction within proteins in biological media, thus critically influencing the performance of brush-functionalized surfaces and materials. In particular, side-chain dispersity in polymer brushes bearing functional oligomeric side chains can deeply influence their interfacial proprieties, due to the occurrence of solvophobic intermolecular polymer-polymer interactions. In recent years, the development of controlled radical polymerization (CRP) techniques, together with the possibility of synthesizing tailored macromonomers subsequently separated into discrete fractions through preparative chromatography, has led to the design of polymeric architectures with precisely defined structure. This thesis focuses on synthesizing a library of polymer brushes bearing polydisperse and discrete oligo(2-ethyl-2-oxazoline) (OEOXA) side chains with precisely defined number of 2-ethyl-2-oxazoline units. The discrete macromonomers employed for the synthesis of polymer brushes were obtained by purifying methacrylate-terminated OEOXAs by flash chromatography. The LCST behaviour of each polymer in solution was studied, to determine the influence of side-chain dispersity on hydration.

CHAPTER ONE: INTRODUCTION

1.1 Polyoxazolines for surface modification

Achieving control over chemical composition and morphology of surfaces is crucial for obtaining tailored materials, employed in many areas of material science and technology such as colloidal stabilization[1], adhesion, lubrication[2] and, more recently, bioengineering, (bio)sensors and biomedicine[3]. One of the most used polymer for surface modification in biological applications is polyethylene glycol (PEG), due to its high biocompatibility[4], being currently applied to passivate cargos for drugs in nanomedicine or to functionalize implants and medical devices[5]. Despite its excellent bioinert proprieties, recent studies[6–8] issued the potential presence of anti-PEG antibodies in a certain percentage of the human population, that could induce allergic responses upon treatment with PEGylated formulations, including COVID-19 vaccines, further stimulating research on alternative polymers that suppress non-specific interactions.

In recent years, research efforts are devoted to find non-immunogenic alternatives to PEG, and one promising class of polymers are poly(2-alkyl-2-oxazoline)s (PAOXA)s[9]. These are obtained by Cationic Ring Opening Polymerization (CROP) of 2-alkyl-2-oxazoline, which are five membered cyclic imino-ethers with an alkyl R-group on position 2 (Figure 1). CROP is a type of chain-growth polymerization[10], characterized by a high control over chain length and functionalities.

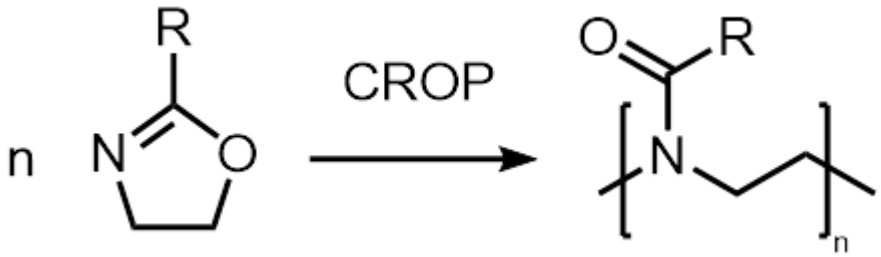

Figure 1 Polymerization of 2-alkyl-2-oxazoline through cationic ring opening.

Many studies are focusing on PAOXAs obtained through CROP because of the high reliability and reproducibility of this type of polymerization, together with the possibility of obtaining polymers with predictable molecular weight distribution and controlled α,ω-functionalities[11]. In addition, since PAOXAs present antifouling proprieties similar to PEGs, they could potentially be the most promising non-ionic alternatives for surface modification

and the functionalization of biomaterials[12], since they tend to inhibit non-specific adsorption of proteins in biological media. Because of that, they have already been used to create functional polymers[13], bioconjugates[14], tissue-reactive graft polymers[15] and bioactive surfaces[3], for application in the biomedical field[16] and in material science (Figure 2).

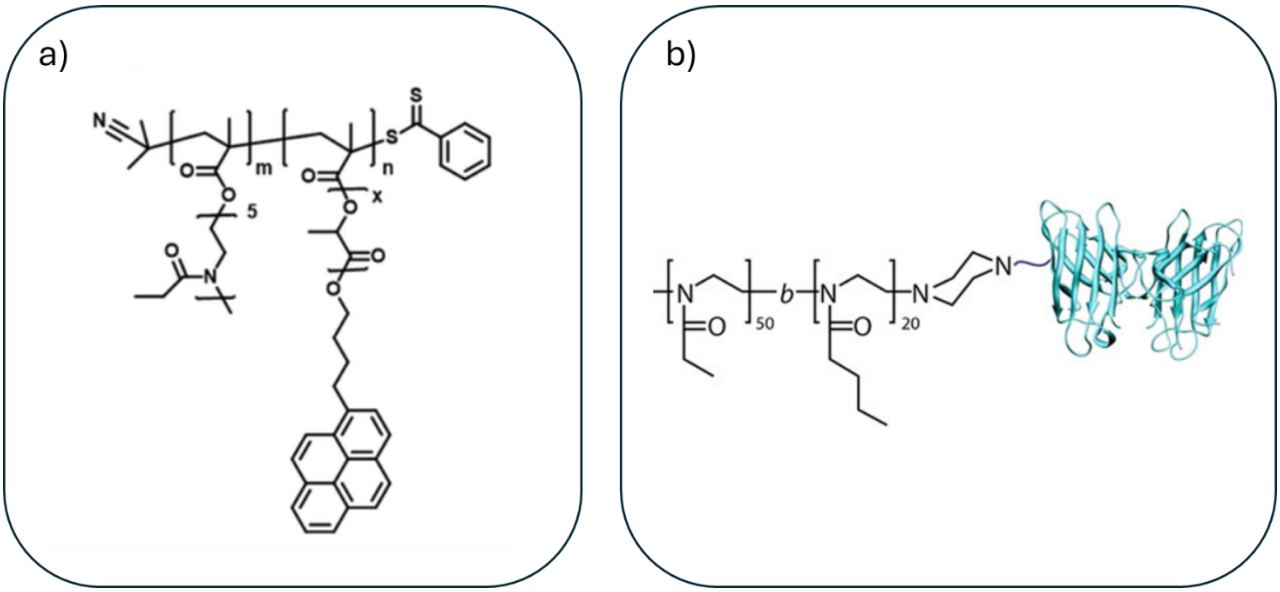

Figure 2 Examples of PAOXA-based functional polymers: (a) fluorescent amphiphilic comb polymers with PLA and PAOXA side chains; (b) conjugate of Superoxide Dismutase 1 with PAOXA block copolymers (pictures adapted from Yildirim et al.[13], Tong et al.[14]).

One propriety of PAOXAs that is similar to PEGs is hydrophilicity, which allow for the formation of an hydration coating when used as graft polymers, acting as a barrier against non-specific interactions, such as protein adsorption in biological systems, that become thermodynamically disfavoured[17]. Moreover, they can be further functionalized through reaction with initial or terminal groups, to deliver novel proprieties to grafted surfaces.

Specifically, poly(2-ethyl-2-oxazoline) (PEOXA) has been approved as an indirect food additive by FDA, opening the way for the design of new polyoxazoline-based materials[18].

1.2 Cationic ring opening polymerization (CROP)

Ring Opening Polymerization (ROP) is a type of chain-growth polymerization based on strained cyclic compounds used as monomers. The driving force of the polymerization is indeed the opening of the ring, which is made possible by having nucleophilic/electrophilic centres on the ring, such as heteroatoms that gets attacked to form propagating species, giving rise to a linear growing chain, with high control on the degree of polymerization (DP). Among different types of ROPs, Cationic Ring Opening Polymerization (CROP) is based on electrophilic initiators that generate positively charged growing chain-ends, and it constitutes the main way for obtaining PAOXAs.

The mechanism of CROP starts with a nucleophilic attack of the cyclic monomer on an electrophilic initiator, forming an iminium ion. Various types of electrophilic initiators can be used, but nowadays the most used are alkylating reagents such as methyl iodide, benzyl bromide, methyl triflate or methyl tosylate, the latter being mostly preferred for its higher stability and lower toxicity (Figure 3).

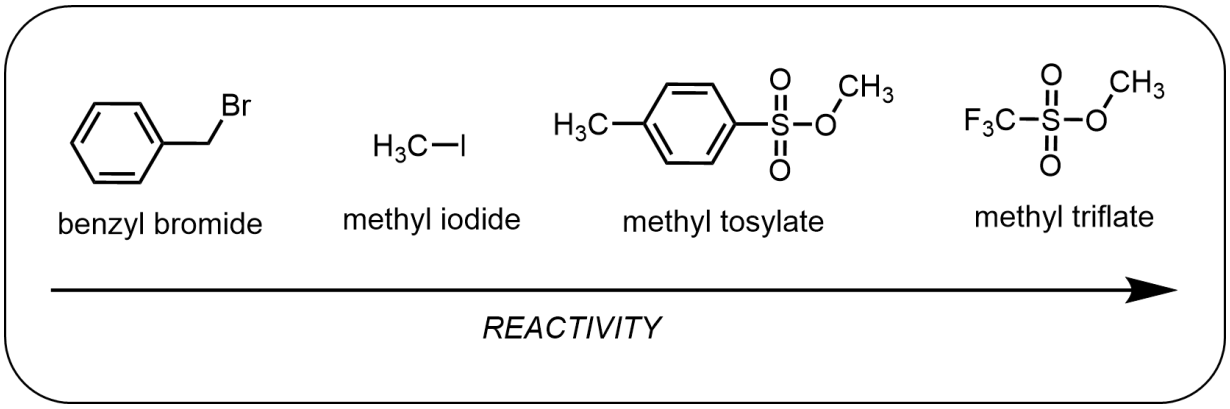

Figure 3 Various types of alkylating agents, in increasing order of reactivity.

Each chain is initiated by a nucleophilic attack of the oxazoline monomer onto the R_1 group of the initiator, causing the release of a counterion X^- and the formation of an activated cationic monomer (iminium ion). After that, another molecule of oxazoline attacks on the 5 position of the activated monomer, forming a cationic propagating chain; the latter is in equilibrium with a covalent amide form, resulting from the attack of the counterion of the initiator on the 5 position of the iminium ring (Figure 4).

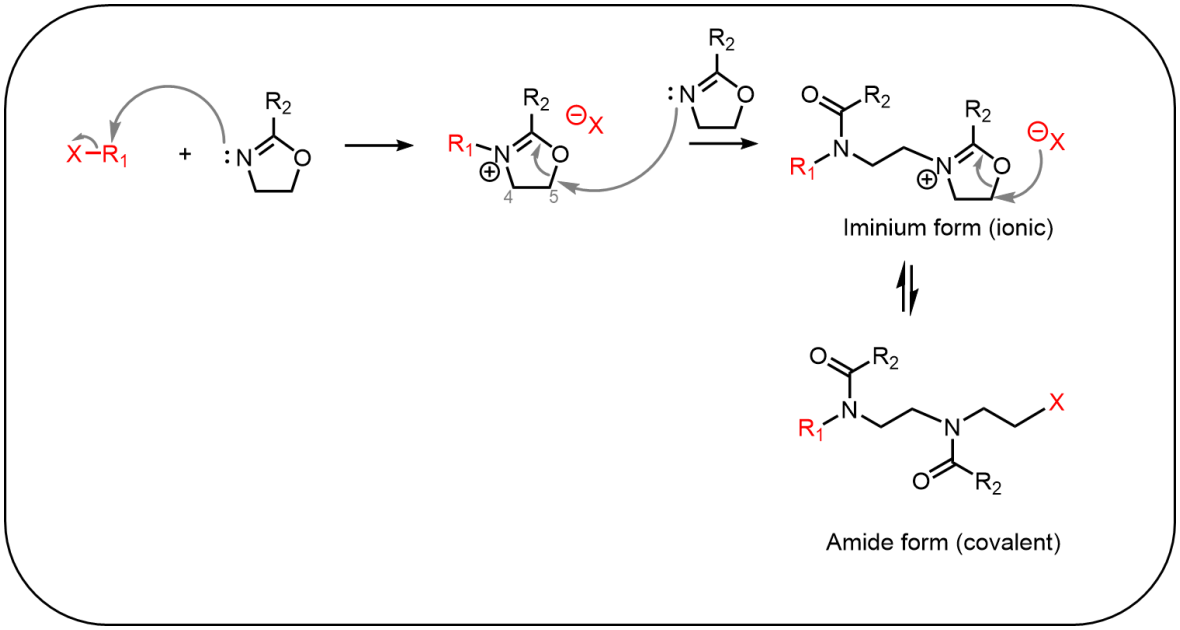

Figure 4 General mechanism for initiation in CROP.

The polymerization goes on following either a cationic pathway or covalent pathway (Figure 5), depending on various electronic factors such as nucleophilicity of the monomer, stability of the counter ion, stabilization of the positive charge, type of solvent. Various combinations of monomers and initiators can lead to different reaction pathways[9], whilst increased solvent polarity favours the ionic pathway. The general rule of thumb is that, if the X^- counterion of the initiator is a stronger nucleophile than the monomer (*i.e.*, X^- has a low stability in solution), the preferred pathway will be covalent, because the anion will quickly attack on the 5 position, making the ionic form an unstable intermediate. On the other hand, if the monomer is a stronger nucleophile than X^- (*i.e.*, X^- is stable in solution), the preferred pathway will be ionic, since the ionic form will be stabilized (Figure 6).

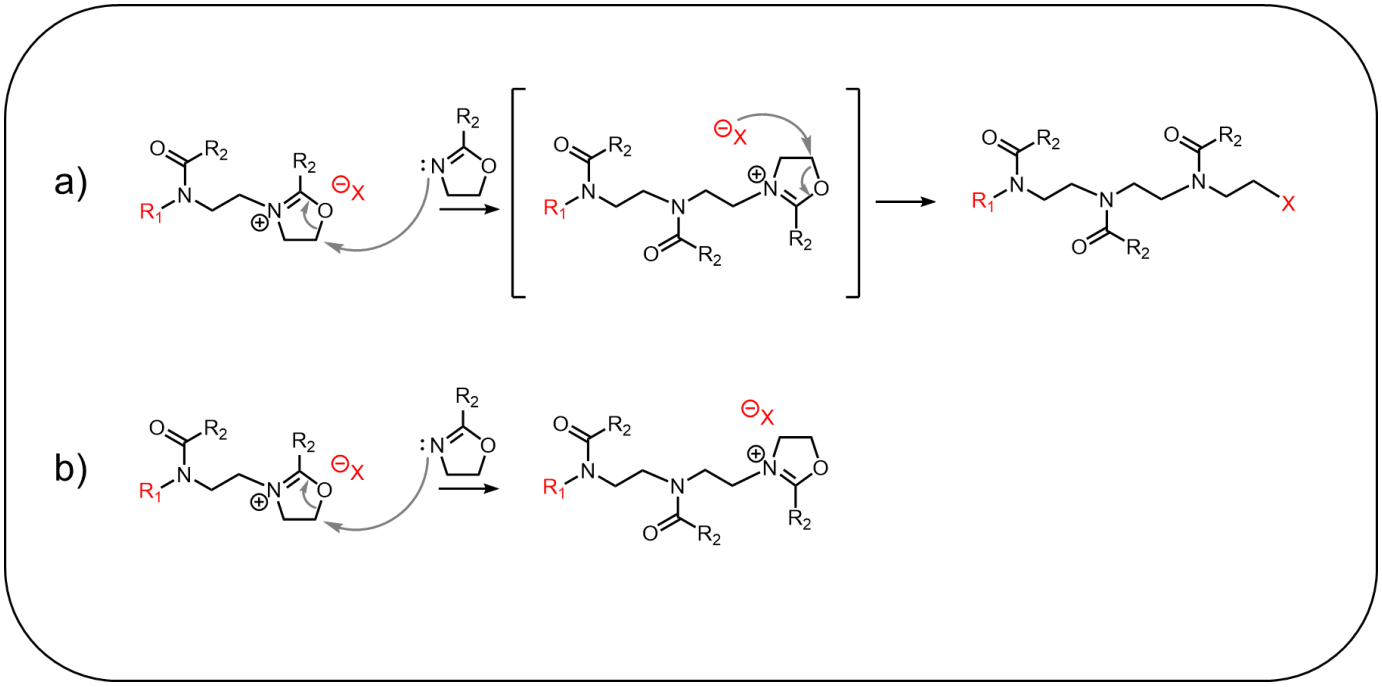

Figure 5 Mechanisms of propagation in CROP: (a) covalent, (b) ionic.

Monomers	Counteranions, X^- (Nucleophilicity ←) Cl	I	TsO	TfO
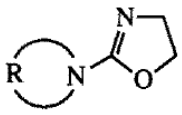	ionic and covalent (DIP)	ionic and covalent (DIP)	ionic	ionic
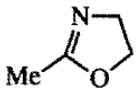	covalent	ionic	ionic	ionic
	covalent	covalent	ionic	ionic
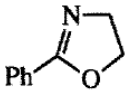	-	covalent	ionic	ionic
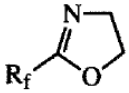	-	covalent	covalent	ionic

Nucleophilicity ↑

R_f = C_2F_5, C_3F_7

Figure 6 Different combinations of initiators and monomers give rise to varying reaction pathways (picture adapted from Aoi et al.[9]).

The kinetics of the propagation is generally described as a two-step mechanism (Figure 7): the first step is rate determining and involves the addition of the monomer M to the activated monomer from initiation P_1* (with rate constant $k_{p,1}$); the following step is the propagation of

the growing chain end P_n* by addition of another monomer M (with rate constant $k_{p,n}$, with n ≥ 2)[19].

After the complete initiation and the first propagation step, the propagation rate constant ($k_{p,n}$, with n ≥ 2) increases, probably due to a neighbouring, intra-molecular dipole-ion polarization effect, which stabilizes the transition state and possibly shifts the equilibrium to the more reactive cationic species, depending on parameters such as concentration, solvent and temperature[11], making the cationic pathway almost exclusively responsible for propagation.

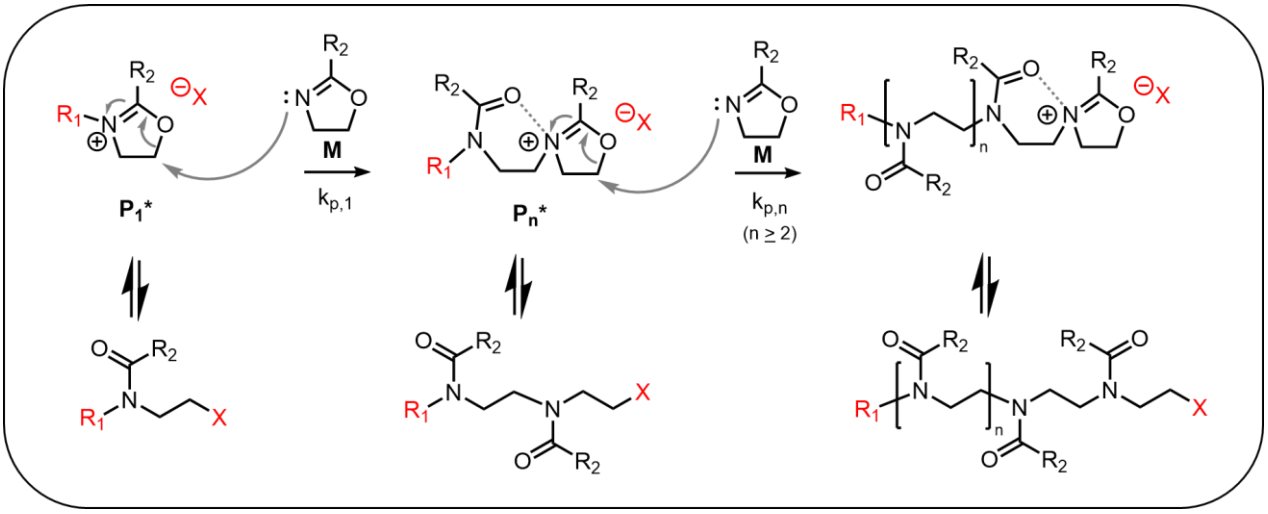

Figure 7 Kinetics of initiation and propagation of CROP.

An ideal living polymerization is characterized by a fast initiation and absence of undesired termination (such as chain-transfer reactions). Therefore, the rate of propagation of an ideal living CROP of PAOXA follows pseudo-first order kinetics since, if ideal conditions are met, the concentration of active growing chains [P*] is constant and equal to the initial concentration of initiator $[I]_0$:

$$-\frac{d[M]}{dt} = k_p[P^*][M] = k_p[I]_0[M] = k'_p[M]$$

Therefore, the integrated equation is:

$$\ln\frac{[M]_0}{[M]_t} = k_p[I]_0 t = k'_p t$$

The termination is carried out by adding a terminating agent, which is generally a nucleophile that attacks the growing chain end. Two different termination mechanisms can occur, depending on the nucleophile strength[20]:

- weak terminating agents (e.g. H_2O) will perform a kinetically controlled attack on the C2 of the iminium chain-end, forming a quaternary intermediate that evolves into an ester-terminated secondary amine (typically an unwanted product) (Figure 8a);
- strong terminating agents (e.g. carboxylates) will perform a thermodynamically controlled attack on the C5 of the iminium chain-end, end-capping the growing chain with a chosen R_3 substituent and formally obtaining an α,ω-bifunctionalized polymer (Figure 8b).

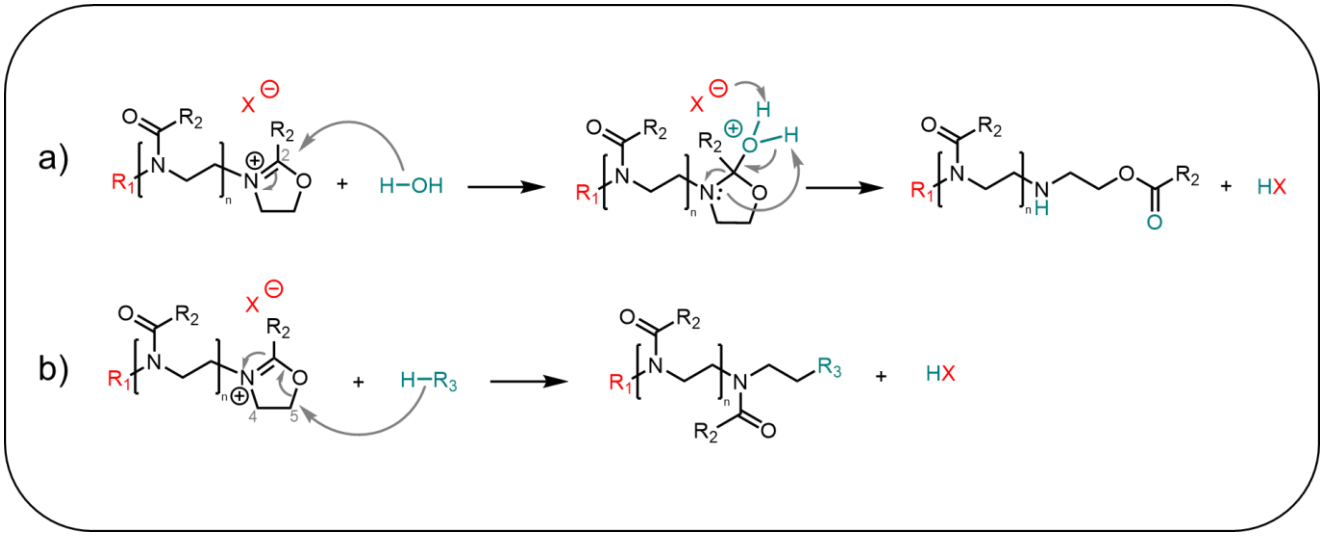

Figure 8 Different types of terminating agents give rise to different products: (a) water as weak terminating agent, (b) strong terminating agent.

For this reason, it is crucial that the system is kept completely dry throughout the entire polymerization. This is achieved by using freshly dried and distilled reagents, and by conducting the reaction under an inert atmosphere (nitrogen gas or argon gas). That is because water might compete with the monomer in the nucleophilic attack on the growing chain end, causing the formation of irreversible inactive chains and unwanted side-products.

The most used classes of terminating agents are:

- methanolic potassium hydroxide (MeOH/KOH), resulting in an −OH terminated chain[21] (Figure 9a);
- nitrogen based reactants such as primary/secondary/tertiary amines, resulting in a secondary/tertiary/quaternary amine end-group[22] (Figure 9b);

- carboxylate derivatives for introducing styrenics, acrylates or methacrylates ω-function that can be further polymerized for making PAOXAs-based polymer brushes[22,23] (Figure 9c).

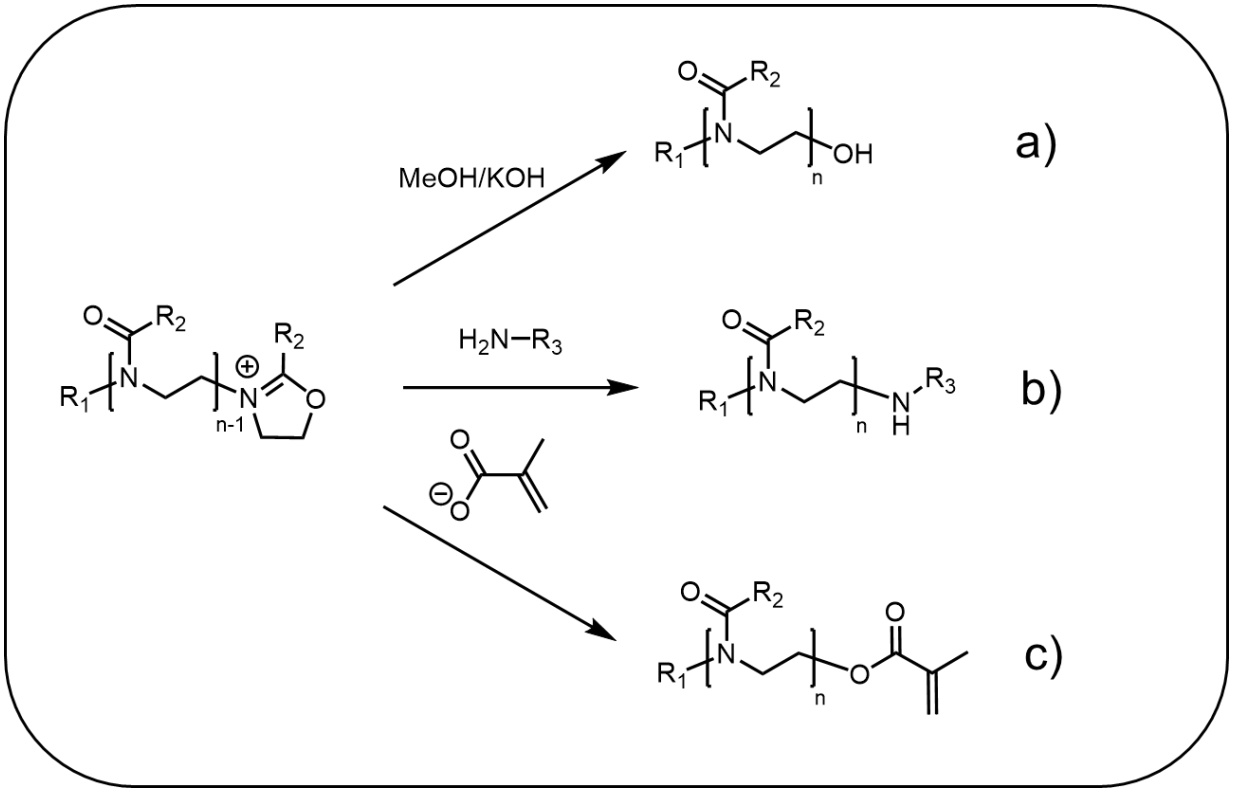

Figure 9 Most used types of terminating agents for CROP of PAOXAs.

Chain transfer reactions can occur if the polymerization is not ideal (*e.g.,* termination is slow), leading to unwanted termination and dispersity broadening.

One of the most frequent side reactions for propagating oxazolinium species is β-elimination, which can formally be seen as an imine-enamine rearrangement. This results in the formation of a proton-initiated oxazolinium cation, which will behave as a novel active monomer, and a dead enamine-terminated polymer chain[24], that can subsequently react as nucleophile with another propagating iminium, leading to chain coupling and the formation of branching points (Figure 10).

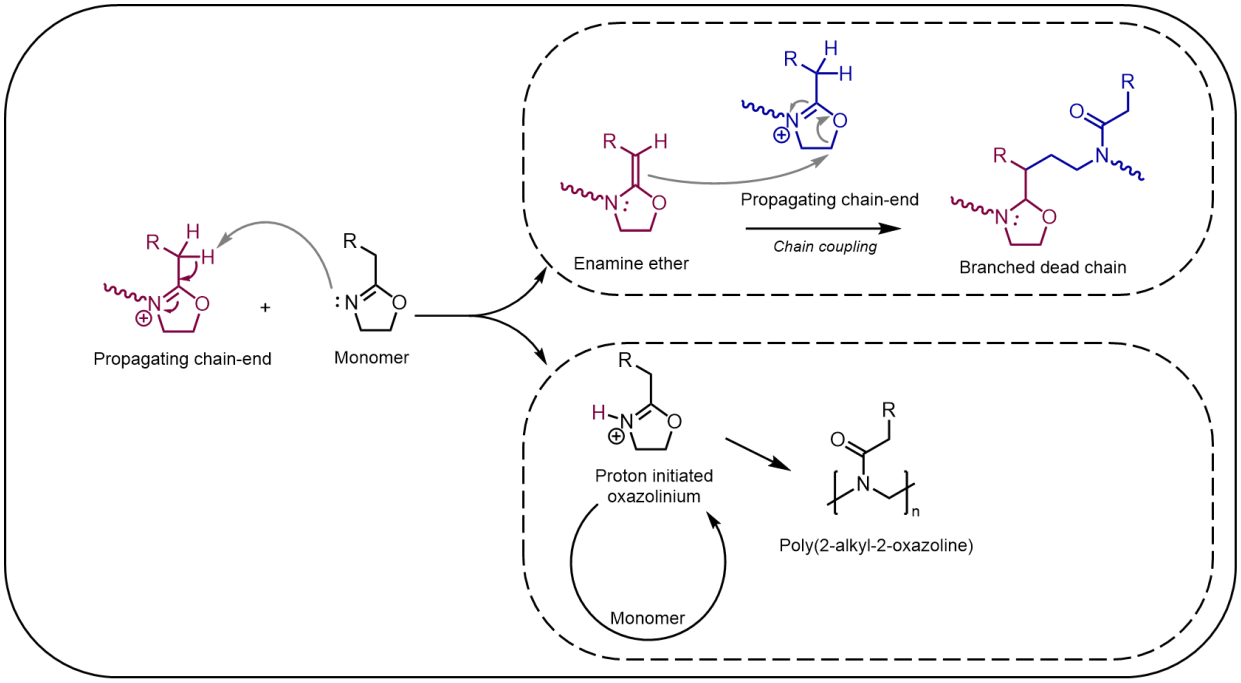

Figure 10 Chain transfer mechanism for propagating 2-alkyl-2-oxazolinium species.

Generally, the reactivity of enamine species is lower compared to the remaining monomer, as they mostly react at extended heating, thus at higher conversion. At the same time, the proton-initiated oxazolinium cation can form new growing chains, resulting in lower molecular weight polymers as side-products, broadening the overall dispersity.

Nevertheless, if carried out in the proper experimental conditions, the CROP of 2-alkyl-2-oxazolines is usually characterized by low dispersity and high end group fidelity[25].

1.3 RAFT polymerization

Reversible Addition-Fragmentation Polymerization (RAFT) is a type of controlled radical polymerization that involves an addition-fragmentation equilibrium between the active growing chains and a chain transfer agent (CTA), a molecule added to the system that creates stable dormant radical species while keeping the number of radicals the same throughout the entire process[26]. The main upside of RAFT is its capability of mimicking a living polymerization, which is fundamental for the synthesis of polymeric architectures with predictable molecular weight, low dispersity and high end-group fidelity, while also having the benefits of radical polymerization, such as high feasibility and the possibility of block copolymer growth[27].

In a thermal RAFT, the initiator (typically a diazo or peroxide compound) is activated by heating the system, causing the homolysis of a specific bond and generating free radicals, with different half-lives depending on temperature and radical stability[28]. Generally, to ensure a sufficient rate of radical generation, the reaction is conducted at a temperature corresponding to a 10 hours half-life for the chosen initiator. The CTA is typically a thiocarbonylthio-based compound, which forms radical species by addition of the growing chain-end to the thiocarbonyl group.

The mechanism of RAFT involves different steps that can be divided in:

- propagation steps (Figure 11b, d), typical of a radical polymerization, during which the polymer chains grow by reacting with monomers;
- addition/fragmentation steps (Figure 11c, e), during which the CTA reacts with growing chains, causing the reversible transfer of the radical chain-ends between dormant and active forms.

This eventually results in the insertion of the polymer chain between the R-S bond of the CTA, giving rise to a polymer end-capped with a chosen functionality R- and the thiocarbonylthio group.

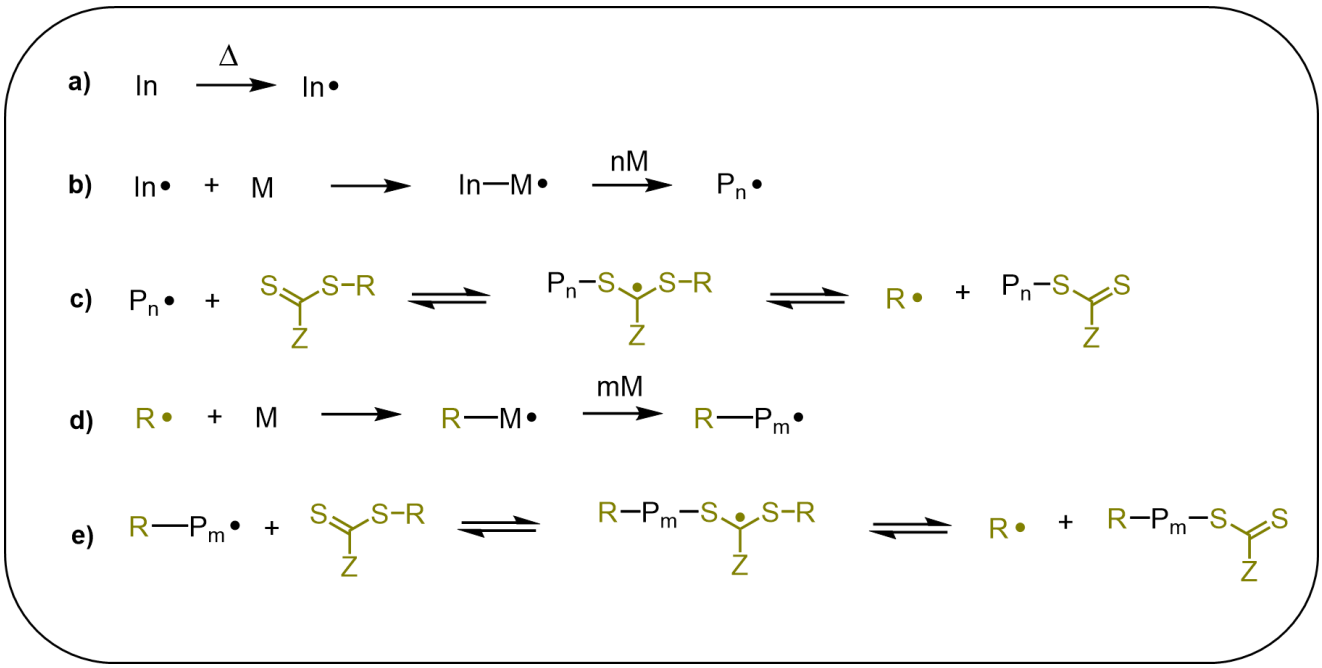

Figure 11 General mechanism for a RAFT polymerization.

In this way, the CTA limits the number of active chains in the system by keeping a certain number of chains dormient. In particular, if the rate of the addition/fragmentation steps is much higher than the rate of the propagation steps, the overall growth is controlled, giving rise to polymer chains with highly predictable molecular weights and low dispersity.

In a RAFT, the target degree of polymerization (DP_{target}) can be predicted by using the formula[26]:

$$\mathrm{DP_{target}} = \frac{[\mathrm{M}]_0}{[\mathrm{CTA}]_0}$$

where $[M]_0$ is the initial concentration of monomer and $[CTA]_0$ is the initial concentration of CTA. This comes from the fact that each CTA molecule can initiate and terminate one chain, so the ratio between the number of monomers and the number of CTAs gives out the average length of the final chains obtained.

During the years, many types of CTAs have been synthesized, with different -R and -Z groups, based on their reactivity towards different types of monomers (Figure 12). The general rule is that:

- For more activated monomers (MAMs), which form stable radical during polymerization (e.g. methacrylate, acrylate, styrene), a more reactive CTA is needed, to ensure a fast attack on the C=S bond. For this reason, the most preferred CTAs for MAMs includes trithiocarbonates (–Z = –SR') and dithiobenzoates (–Z = –Ph), because they react with monomers by forming a stabilized radical intermediate.
- For less activated monomers (LAMs), which form unstable radical during polymerization (e.g. vinyl acetate, vinyl chloride), a less reactive CTA is needed, to ensure a greater control over reactivity towards the CTA. Hence, the most preferred CTAs for LAMs are xantates (–Z = –OR') and dithiocarbamate (–Z = –NHR').

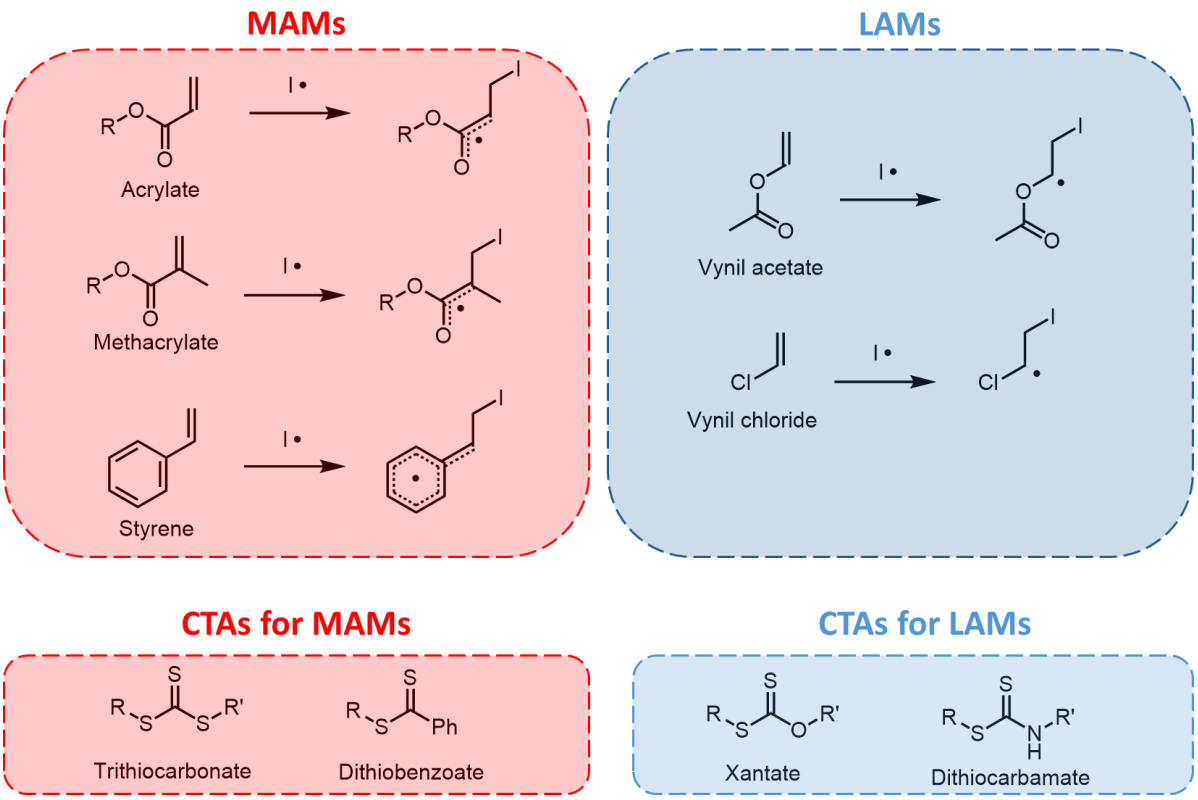

Figure 12 Most used MAMs and LAMs, and their corresponding CTAs.

1.4 Polymer brushes

Surface structuring through polymer grafting represents nowadays one of the most efficient ways for controlling and modifying physicochemical properties and interfacial interactions in different (bio)materials. Above all types of surface grafted architectures, polymer brushes are of great interest, since they can completely alter the interfacial properties of a surface and its interactions in a certain environment, while bearing functional groups with low cytotoxicity and high biocompatibility, making them the ideal choice for designing biomaterials and implantable medical devices.

Polymer brushes are thin polymer layers tethered to a surface, which assembly in a specific “brush-like” shape, used for modulating surface interaction. They find applications in various fields, with particular focus on biomedicine, biomaterial and sensoring[29]. They are typically composed of long hydrophilic or amphiphilic chains grafted to a surface (2D brush) or branching from a polymeric backbone (1D brush, also referred as bottle brushes or comb-like polymers)[30] (Figure 13).

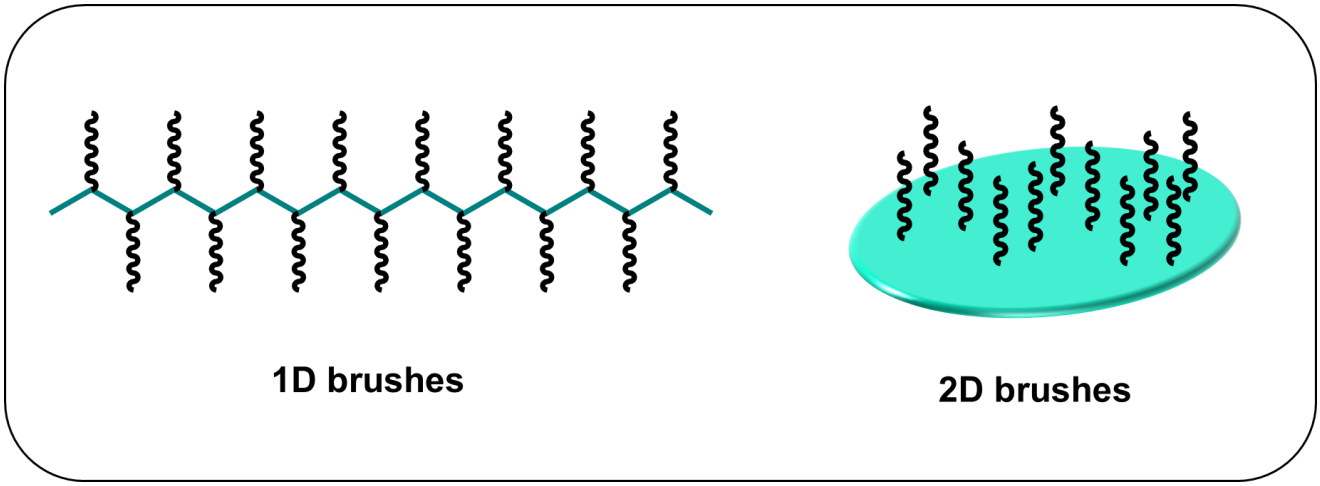

Figure 13 Schematic representation of one dimensional (left) and bidimensional (right) polymer brushes.

The structure of polymer brushes and their interfacial proprieties can be tuned by controlling various factors[31]:

- polymer composition and topology
- molar mass distribution
- surface coverage (grafting density)
- dispersity *Đ*

By varying these parameters, new proprieties can be given to grafted surfaces, such as hydrophilicity, lubrication or anti-fouling (Figure 15). In particular, fouling is the deposition of retained particles, colloids, or macromolecules on a surface[32]; this phenomenon can also happen when foreign bodies are inserted into biological systems, like prosthetics or implantable medical devices[33,34], which can undergo non-specific protein adsorption, followed by an immunogenic response and eventually rejection of the foreign body (Figure 14).

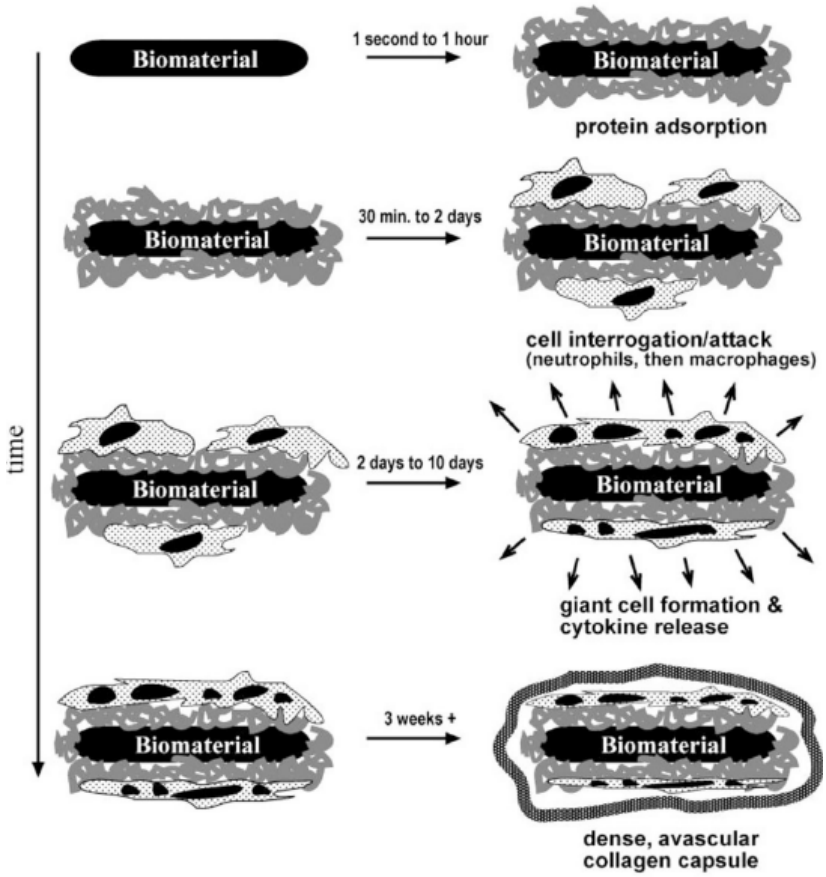

Figure 14 Implantation of a biomaterial in a biological environment (e.g., living organism) leads to protein adsorption, immunological response and isolation of the foreign material (picture adapted from Yang et al.[35]).

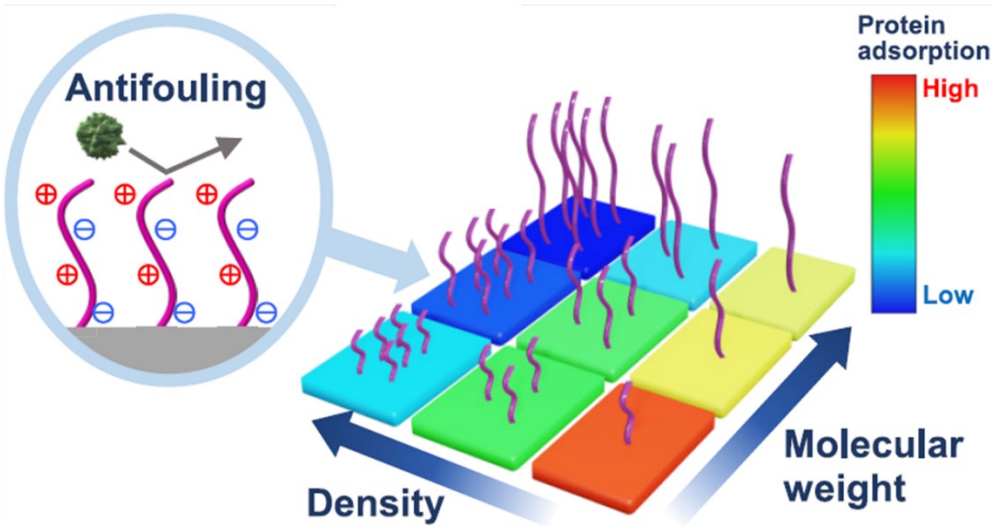

Figure 15 Varying parameters of polymer brushes can affect protein adsorption (picture adapted from Okuyama et al.[36]).

Since anti-fouling is closely related to hydrophilicity of a surface[34], the chemical composition and grafting density of the grafted polymers plays a crucial role, since proteins adsorption is a function of the grafted polymer surface coverage[37]. The grafting density itself depends on how the polymer brushes have been grafted to the surface, either by "grafting-to" or "grafting-from"[38] (Figure 16):

- The "grafting-to" approach is performed by submerging a surface in a solution of polymer molecules that covalently bind through some functional groups to the surface, to form tethered chains. It can be easily achieved but doesn't allow to reach high grafting densities, because it becomes progressively difficult to adsorb more chains on the surface due to steric repulsion.
- The "grafting-from" approach is a more promising method for the synthesis of polymer brushes with high grafting density, because the polymerization starts from initiator/monomers that are covalently bonded to the substrate surface, while being submerged in a solution of monomers. In this way, molecules of monomer penetrate through the already grafted polymer layer easily, progressively growing the polymer chains from the surface.

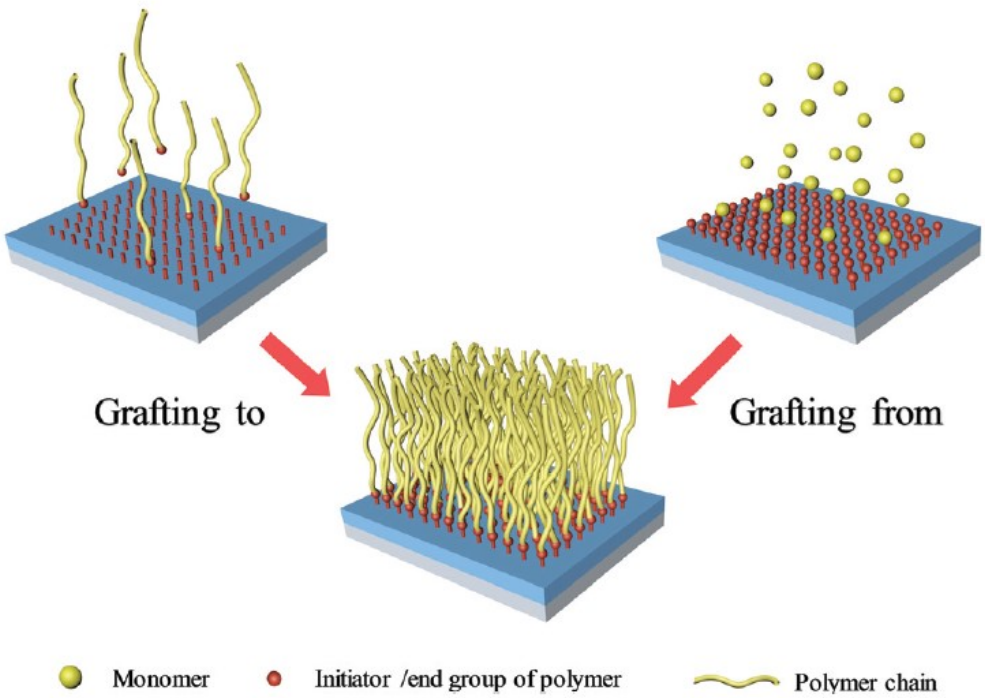

Figure 16 Schematic illustration of grafting to/from methods (picture adapted from Wang et al.[39]).

The design of polymer brushes-based surface coatings that successfully suppress non-specific protein adsorption requires an understanding of interfacial properties and how they

can be modulated to give unique features to materials for specific applications. The anti-fouling proprieties of long-chain polymer brushes emerge from two combined phenomena: surface hydration and steric repulsion, that eventually make non-specific adsorption of proteins in aqueous media thermodynamically disfavoured[40]. When hydrophilic graft polymers are put in an aqueous environment, H_2O molecules form a hydrogen-bond network around the polymer film that makes protein adsorption enthalpically disfavoured ($\Delta H_{ads} > 0$), because it would cause the desolvation of the polymer chains by solvent exclusion, breaking the intermolecular hydrogen-bonds. Moreover, the steric repulsion resulting from the compression of long polymer chains makes adsorption entropically disfavoured ($\Delta S_{ads} < 0$), because it would cause the chains to collapse in a packed conformation (Figure 17).

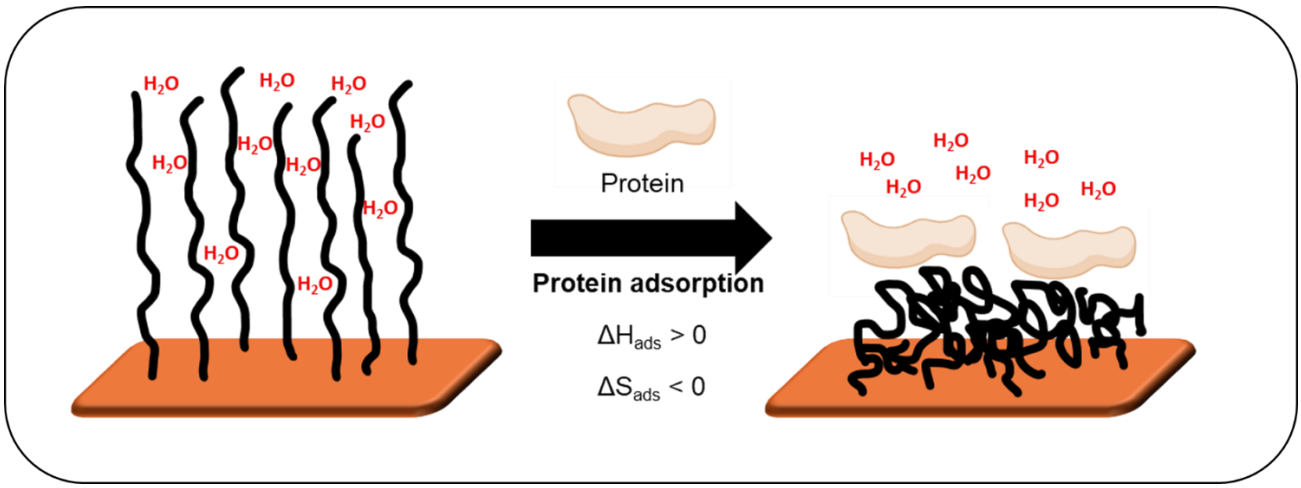

Figure 17 Schematic representation of protein fouling on a grafted surface.

Since hydrophilic proprieties are closely related to anti-fouling, any decrease in the surface hydration might lead to a decrease of resistance to non-specific adsorption, reduced lubrication and biopassivity. This underlines a clear direct correlation between polymer composition and physiochemical properties of the grafted surface[41].

Recent progress in polymer science have led to the design of precise polymer brushes architectures, allowing to modulate surface proprieties in an unique way, for example for the creation of stimuli responsive materials or (bio)sensors[29].

1.5 Discrete vs polydisperse: the effect of dispersity on the properties of polymer brushes

Natural macromolecules with defined biological functions (e.g. proteins, polynucleotides), are often characterized by discrete molar masses and precise composition, both of which are essential for ensuring structural control, distinctive properties, and specific functions. For this reason, polymer scientists have been striving to develop robust synthetic protocols to access polymeric structures with homogeneous composition and predictable molar mass, to discover new correlations between polymer structure and physicochemical proprieties.

New controlled polymerization techniques, like ring opening polymerization (ROP) or reversible deactivation radical polymerization (RDRP) have opened the way for the synthesis of narrow dispersed polymers, making dispersity (*Đ*) an additional tuning parameter in polymer synthesis[42], both for application on polymers in solution and grafted on surfaces. The possibility of modulating *Đ* within a relatively large range while maintaining control over the chain's growth process and chain end fidelity of modern polymerization techniques paved the way towards the design of innovative precisely tailored polymeric architectures, eventually constituting a potential, additional tool for varying the interfacial physiochemical properties of the grafted surface. Indeed, achieving perfectly monodisperse polymers is not only a remarkable synthetic achievement but also provides fundamental building blocks for new classes of polymeric materials, potentially free of defects, or exhibiting properties that are precisely tunable in a quantized manner[43]. For example, a variation of *Đ* within a brush can be exploited to modulate the way brush-functionalized nanomaterials, such as grafted nanoparticles or macroscopic surfaces, interact with the surrounding environment, in terms of hydrophilicity, steric stabilization, lubrication and biopassivity[31].

An even more precise way to achieve macromolecular discreteness is through preparative flash column chromatographic separation, a widely used technique in organic chemistry that is recently being applied for oligomers separation. Through flash column chromatography, complex mixtures of polydisperse oligomers or polymers with varying compositions are separated based on differential chemical affinity (adsorption) to a stationary phase (typically silica), in order to easily generate libraries of well-defined polymers with compositional differences. This technique often requires a fine tuning of the eluent, which can be a mixture of many organic solvents or a gradient of them, to achieve separation of compounds that differ for just one repetitive unit[44], even with a retention factor $R_f \leq 0.1$.

Chromatographic separation has been employed by various research groups to fractionate (meth)acrylate, styrene and acrylamide oligomers and polymers, as well as commercial oligo(ethylene glycol) and oligo(2-alkyl-2-oxazoline)[45–48]. This allowed scientists to obtain oligomeric macromonomers of defined chain length, with unique control over side-chain dispersity, that could be further polymerized with CRP techniques to give rise to libraries of synthetic polymers brushes (Figure 18).

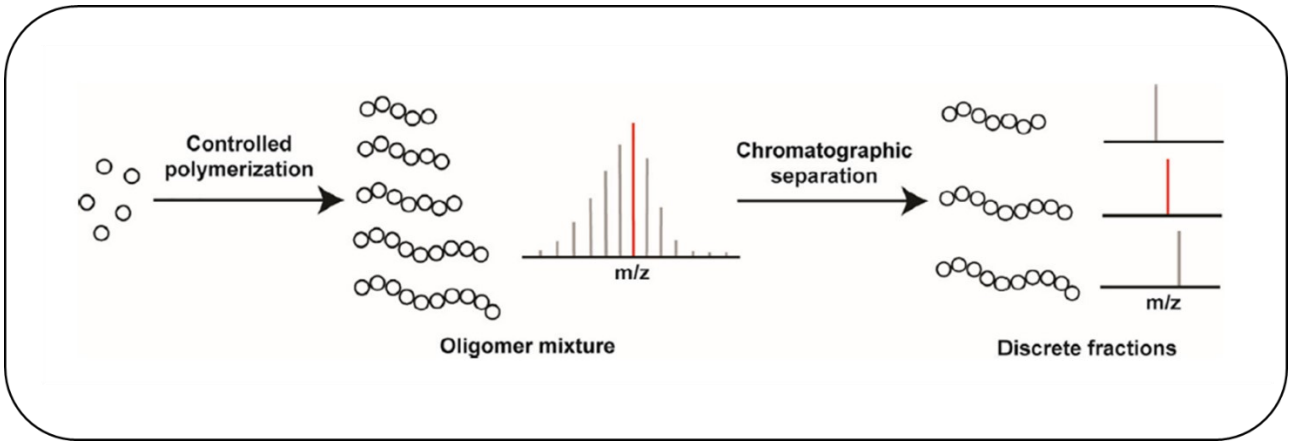

Figure 18 Controlled polymerization combined with chromatographic separation can open the way to macromolecular discreteness (picture adapted from Genabeek et al.[49]).

One of the most interesting types of polymer architectures are bottle-brush polymers, which are a type of comb-like polymers, composed of a long backbone chain and functional, oligomeric (or polymeric) side chains. Their design is reminiscent of the structure of some biopolymers, such as proteoglycans[50], which owe their lubricating proprieties to an intrinsically complex architecture, composed of many branched unit with polydisperse glycosaminoglycan side chains[51] (Figure 19).

Thanks to the above-mentioned developments, it is possible to mimic the structure of some natural macromolecules, obtaining synthetically built biopolymers, or even to generate totally new polymeric architectures, moving towards the discovery of emergent proprieties deriving from defined macromolecular structures.

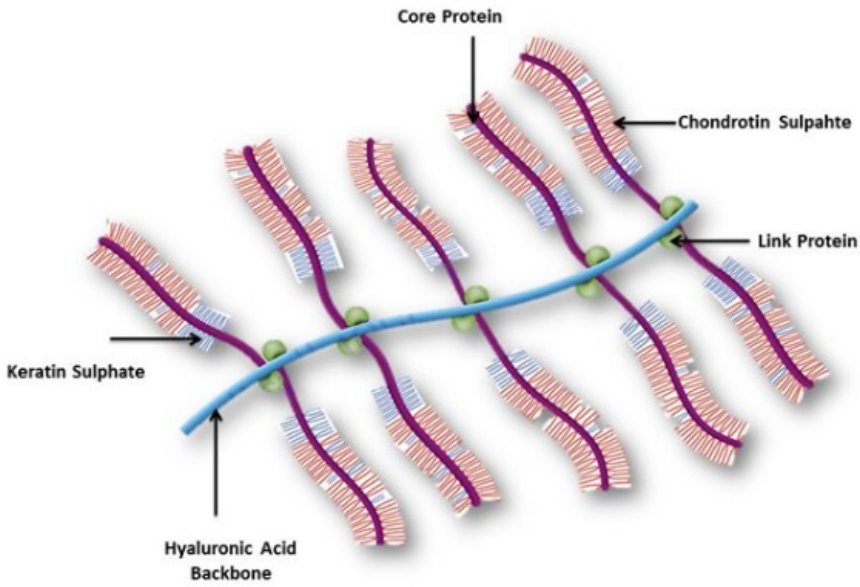

Figure 19 Representation of a proteoglycan (picture adapted from Joshi et al.[52]).

Using discrete oligomers as building blocks for branched polymer brushes could help studying macromolecules with discrete structures compared to polydisperse analogues, and how dispersity could affect crucial proprieties such as hydration, protein fouling and biocompatibility. In a study by Pavón *et al.*[53], polydisperse $POEG_pMAs$ were compared to discrete $POEG_8MAs$, obtained from isolating OEG_8MA macromonomer through column chromatography from a commercial OEG_pMA mixture. The resulting studies on interaction with anti-PEG-antibodies (APAs) showed that structural monodispersity within OEG side chains of polymer brushes grafted to Au nanoparticles enhanced the stealth proprieties of the grafted surface, since the structural homogeneity of $POEG_8MA$ ensured that the brushes formed a more uniform layer, hiding the methoxy-specific binding sites of OEG chains from the biological environment, while $POEG_pMA$ brushes with polydisperse side chains showed higher interaction with APAs, due to an augmented exposure of longer OEG chains, increasing epitope binding of APAs (Figure 20).

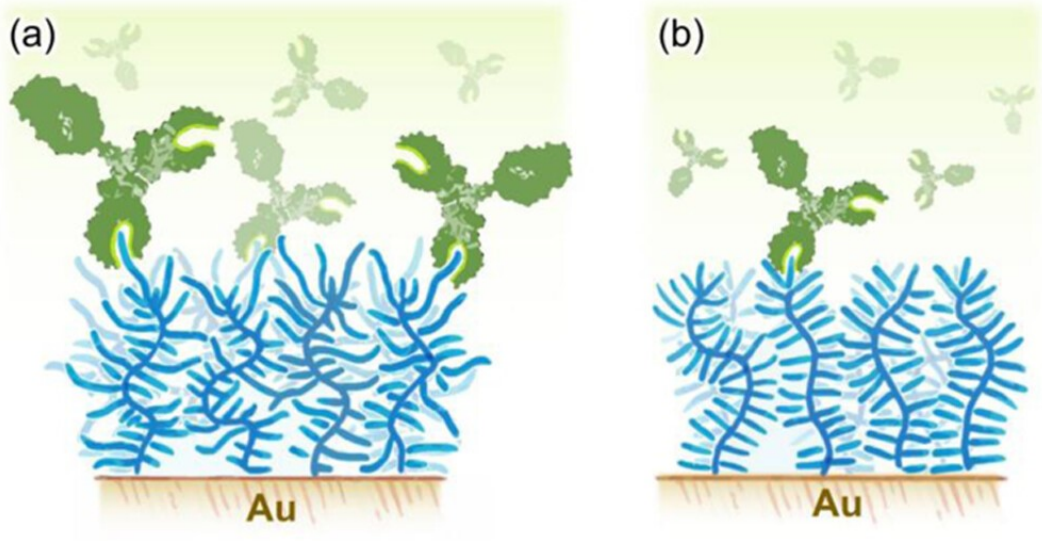

Figure 20 Representation of Au-grafted polydisperse $POEG_pMA$ (a) vs monodisperse $POEOG_8MA$ (b) in interaction with APAs (picture adapted from Pavon et al.[53]).

One way to indirectly evaluate the tendency of a polymer to hydrate in water is by investigating its temperature-responsive behaviour, for example by determining the lower critical solution temperature (LCST). The LCST is a parameter deriving from the Flory and Patterson theory of thermodynamics of polymer solutions: when an initially homogeneous polymer solution in water undergoes phase separation upon increasing the temperature, the cloud point vs volumetric fraction (Φ) curve is convex upward, and its minimum point is called lower critical solution temperature[54] (Figure 21). This model was introduced for predicting behaviour of polymers with anisotropic interactions (*e.g.*, dipole-dipole interactions, H-bonding, electrostatic forces) that would deviate from the upper critical solution temperature (UCST) predicted by the Flory-Huggins theory.

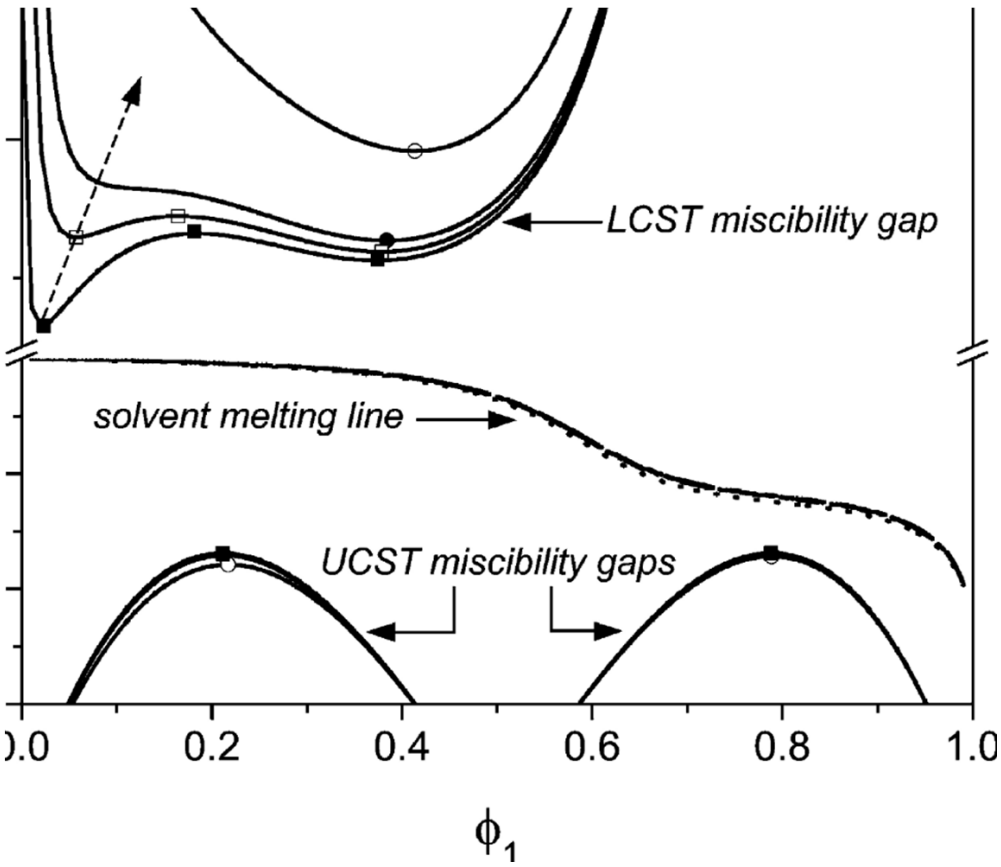

Figure 21 Theoretical reduced temperature-composition phase diagram for model polymer solutions with different values of the polymer chain length (picture adapted from Van Mele et al.[55]).

The LCST can be experimentally estimated by measuring the cloud point temperature (T_c) which is the temperature at which the transmittance of an aqueous solution of a polymer becomes 50% of the transmittance at room temperature[56]. It is important to notice that, by definition, the LCST corresponds to the minimum of the T_c vs Φ plot[57]. To understand how LCST is linked to the hydrophilicity of a polymer, the thermodynamic of a polymer solution system needs to be considered, starting from the free energy of mixing at equilibrium for a polymer solution:

$$\Delta G_{mix} = \Delta H_{mix} - T_c \Delta S_{mix}$$

For a polymer with LCST behaviour, going above T_c will make the mixing not spontaneous anymore ($\Delta G_{mix} > 0$). This comes from considering the thermodynamic parameters of the system, since for LCST polymer solutions:

- $\Delta H_{mix} < 0$, since solvent-polymer interactions that allow for the polymer solubilization are exothermic;

- $\Delta S_{mix} < 0$, since the solvent needs to organize in an ordered structure to solvate the polymer chains.

This means that, for $T<T_c$, the mixing is spontaneous ($\Delta G_{mix} < 0$), and the solution appears clear, while for $T>T_c$, clouding is observed because mixing becomes not spontaneous anymore ($\Delta G_{mix} > 0$), so aggregation of polymer chains happens. Hence, the thermal energy introduced in the system breaks the hydrogen bonds between water molecules and hydrophilic side chains of the polymers, causing aggregation and making the solution macroscopically cloudy, due to the occurrence of new lateral-chain and main-chain interactions (Figure 22). For this reason, the LCST can be considered an experimental parameter linked to the hydrophilicity of a polymer: for example, the ΔH_{mix} of highly hydrophilic polymers will be more negative, due to stronger interactions with water, resulting in a high LCST.

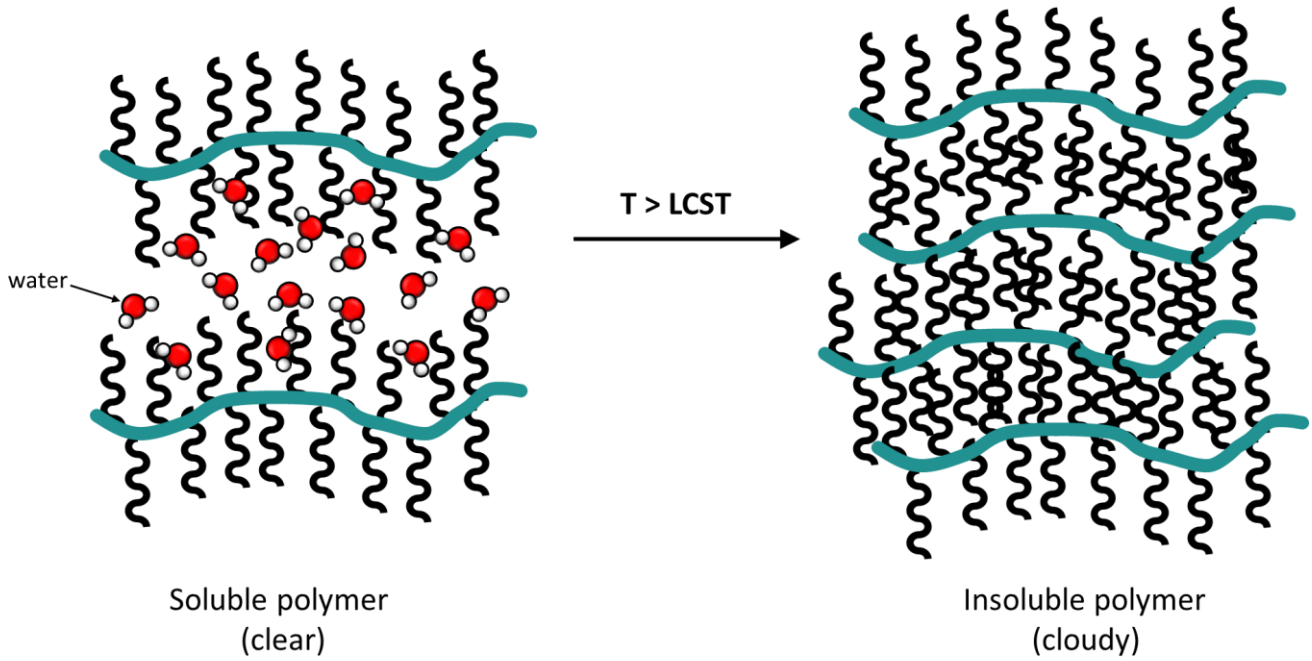

Figure 22 Schematic representation of aggregation due to increasing temperature for polymers with LCST behaviour.

For polymer brushes, the LCST depends on the balance between hydrophilic and hydrophobic interactions, and can strongly depend on the length and composition of the hydrophobic backbone (*e.g.,* methacrylate, acrylate, vinyl, *etc.*) and on the length, composition and dispersity of the side chains (*e.g.*, oligo ethylene glycols, oligo oxazolines). For $POEG_nMA$, as the length of the OEG chains increases, the polymer becomes more hydrophilic, resulting in an increase in LCST. More specifically, the ether oxygen atoms of the hydrophilic OEGMA side-chain form hydrogen bonds with water, while the hydrophobic

methacrylate backbone reduces water solubility by forming intermolecular polymer-polymer interactions[46]. This highlights the close relationship between side-chain length and thermoresponsiveness, and the importance of discrete well-defined polymer libraries for examining structure/property relationships.

While there are many studies on dispersity of side chains for OEGMA-based polymers, there are fewer examples of how dispersity can influence more complex polymer architectures, such as oligo(2-alkyl-2-oxazoline)s-based polymer brushes. In a recent work by Romio *et al.*[48], polymer brushes with a backbone of poly(methacrylate) bearing monodisperse oligo(2-ethyl-2-oxazoline)s side-chains ($POEOX_nMA$) were synthetised and compared with polydisperse ones, studying how hydrophilicity changes with side-chain dispersity for this class of polymers. This study demonstrates how polydisperse side chains on a long polymeric backbone increase hydration of the surface-grafted polymers in comparison to polymer brushes with monodisperse oligomeric side chains. This is due to the more favourite polymer-polymer hydrophobic interactions between the monodisperse side chains compared to water-polymer hydrophilic interactions with the aqueous media, giving an effect similar to hydrophobic exclusion (Figure 23). Moreover, atomic force microscopy (AFM) studies showed that longer monodisperse OEOX side-chains favoured hydration and reduced the occurrence of hydrophobic interaction between PMA backbones (similarly to POEGMA), while the presence of polydisperse side chains determined an increment in hydration and simultaneously hindered hydrophobic interactions within brushes.

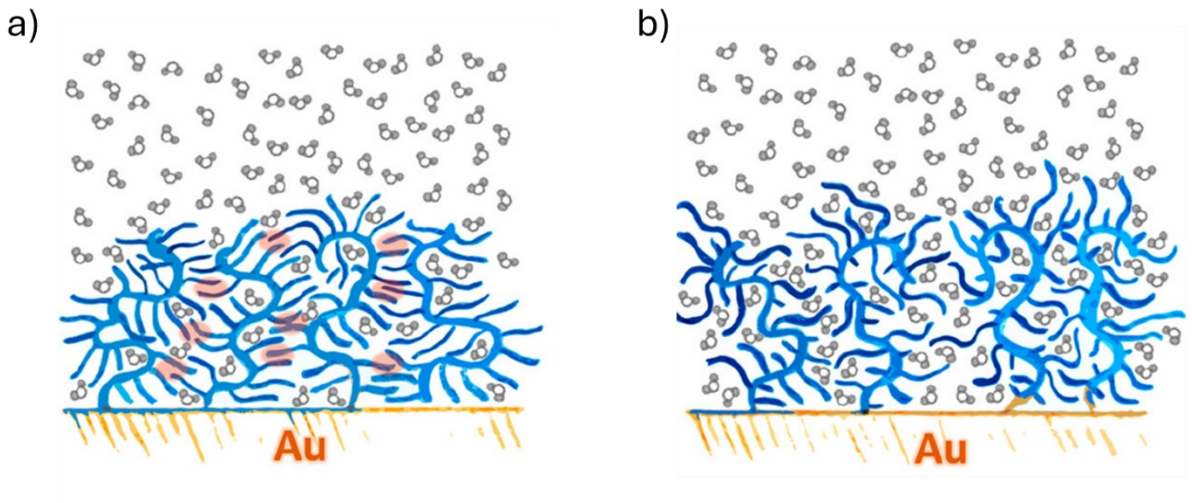

Figure 23 Representation of Au-grafted polydisperse $POEOX_pMA$ (a) vs monodisperse $POEOX_nMA$ (b) in interaction with water molecules (picture adapted from Romio et al.[48]).

In conclusion, the presence of side chains with a well-defined length within brushes with homogeneous structure can profoundly influence the behaviour of polymers in solution and on surfaces, since dispersity has significant impact on interfacial physicochemical properties. This relationship between polymer architecture and hydrophilic proprieties can be exploited to produce surfaces with modulated hydrophilicity, achieving precise control over proprieties directly dependent from hydration, such as lubrication, anti-fouling and biocompatibility.

1.6 Aim of this thesis

In this project, oligo(2-ethyl-2-oxazoline)methacrylate (OEOXMA) were synthesized through CROP of 2-ethyl-2-oxazoline monomers (EOXA), to obtain a mixture of polydisperse $OEOX_pMA$, which could be subsequently purified into discrete oligomers of defined chain length ($OEOX_nMA$, with n defined, $Đ = 1$) by flash column chromatography (Figure 24).

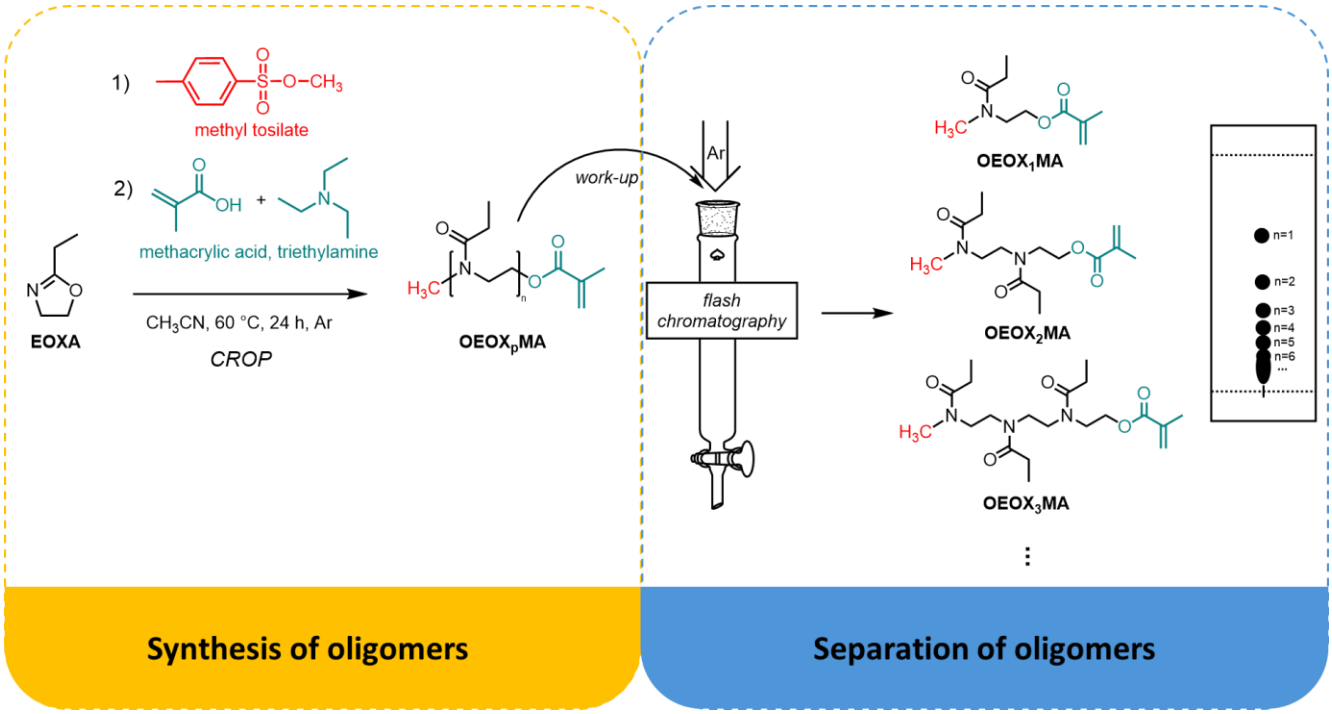

Figure 24 Scheme of the first two steps of this thesis project: oligomer synthesis through CROP (left) and oligomer separation through flash column chromatography (right).

The separated oligomers could then be used as macromonomers for the growth of a polymethacrylate backbone through RAFT polymerization, using methyl 4-cyano-4-(((dodecylthio)carbonothioyl)thio)pentanoate (MCDP) as a chain transfer agent, obtaining a library of poly[oligo(2-ethyl-2-oxazoline)methacrylate] ($POEOX_nMA$) brushes with defined n.

The RAFT polymerization was performed also on polydisperse oligomers as control, obtaining $POEOX_pMA$ brushes (Figure 25).

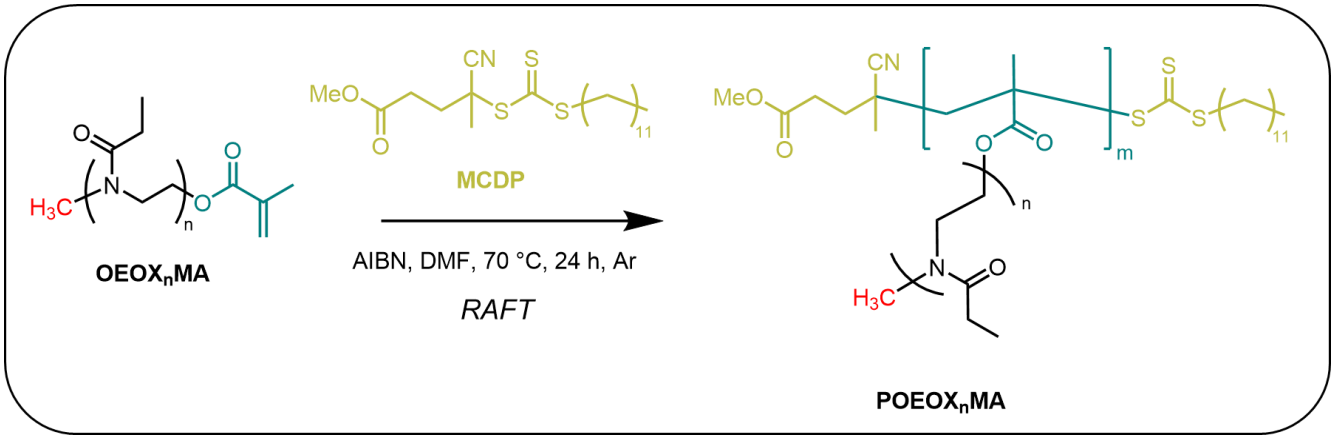

Figure 25 Reaction scheme for the RAFT polymerization on monodisperse and polydisperse oligomers.

By obtaining a series of polymers with constant main-chain length and increasing side-chain length (Figure 26), it was possible to study how dispersity within lateral chain for this type of bottle-brush (or comb-like) polymers influences thermoresponsiveness and water solubility, indirectly determined through LCST measurements, to study how different polymer architectures influences proprieties related to hydrophilicity,

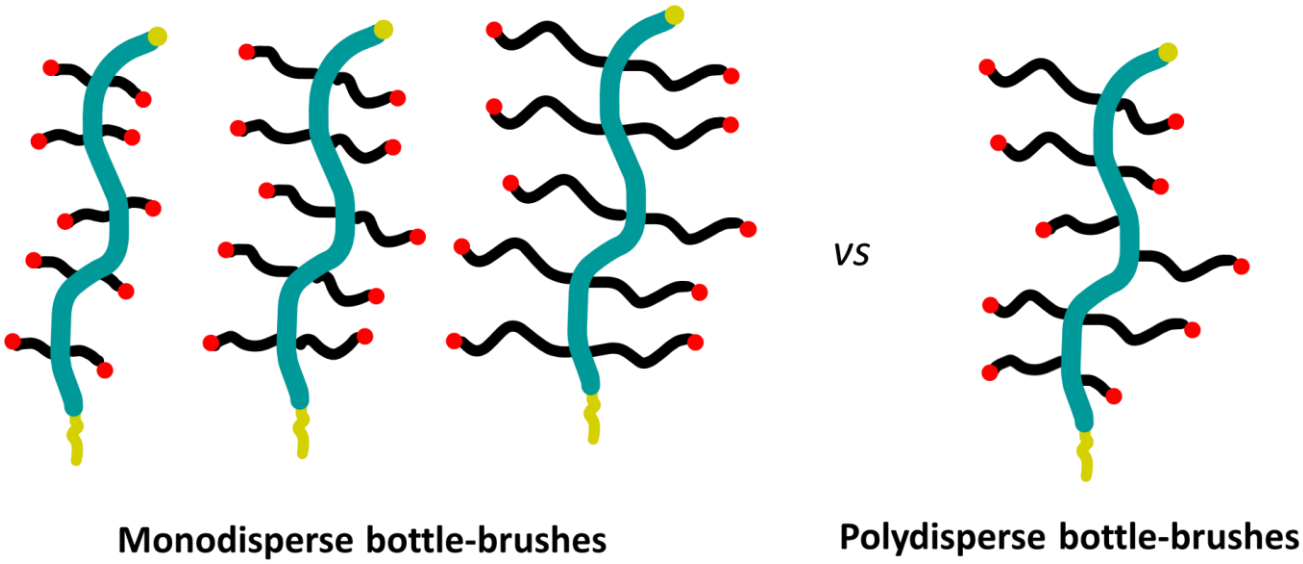

Figure 26 Representation of the final polymers obtained: bottle-brushes with monodisperse OEOX side chains (left) vs bottle-brushes with polydisperse OEOX side chains (right).

CHAPTER 2: MATERIALS AND METHODS

2.1 Materials

2-ethyl-2-oxazoline (Sigma-Aldrich), methyl tosylate (Sigma-Aldrich), acetonitrile (dry, Sigma-Aldrich), calcium hydride (Sigma-Aldrich), methacrylic acid (Sigma-Aldrich), triethylamine (TCI), chloroform-D (99.8% atom, Sigma-Aldrich), dimethylformamide (Carlo Erba), lithium bromide (Sigma-Aldrich), acetonitrile (Carlo Erba), TLC plate 60 F254 (Merck), silica gel 230-400 mesh (Sigma-Aldrich), sand 50-70 mesh (Sigma-Aldrich) potassium hydroxide (Sigma-Aldrich), chloroform (Sigma-Aldrich), sodium bicarbonate (Sigma-Aldrich), sodium chloride (Sigma-Aldrich), sodium sulphate (Sigma-Aldrich), tetrahydrofuran (stabilized with BHT, Sigma-Aldrich), dichloromethane (Sigma-Aldrich), ethanol (VWR), methanol (Sigma-Aldrich), potassium permanganate (Sigma-Aldrich), 4-cyano-4-(((dodecylthio)carbonothioyl) thio)pentanoic acid (BLD pharm), tetrahydrofuran (dry, Sigma-Aldrich), diazabicyclo[5.4.0]undec-7-ene (Sigma-Aldrich), methyl iodide (Sigma-Aldrich), petroleum ether (Sigma-Aldrich), hydrochloric acid (≥37%, Sigma-Aldrich), 2,2′-Azobis(2-methylpropionitrile) (Sigma Aldrich), diethyl ether (Sigma-Aldrich), n-butylamine (Sigma-Aldrich), n-hexane (VWR), aluminum oxide (activated, basic, Sigma-Aldrich), acetone (VWR).

2.2 Instruments

Nuclear Magnetic Resonance Spectroscopy (NMR): ^{1}H-NMR and ^{13}C-NMR spectra were recorded using a Bruker AVANCE NANOBAY spectrometer operating at 400 MHz and equipped with a Varian 400/54 magnet (9.39 T) and Probe BBFO. For conversion determination, ^{1}H-NMR spectra were recorder on a Bruker AVANCE 200 operating at 200 MHz, equipped with an Oxford Instruments superconducting magnet (4.7 T) and Probe BBFO. All the spectra were taken using $CDCl_3$ as solvent.

Gel Permeation Chromatography (GPC): GPC chromatograms were recorded on a Shimadzu NEXERA chromatograph, equipped with two Agilent 300x8 mm PSS columns with SDV packing, 5 µm particle size, with pore size of 500 and 1000 Å respectively, with molecular weight range 100-30 kDa and 100-60 kDa respectively, and a refractive index detector. The mobile phase used was N,N-dimethylformamide (DMF) with lithium bromide (LiBr) 1 g/L, with a measurement flow of 1 mL/min and oven temperature of 60 °C. A calibration was performed on the instrument using poly(methyl methacrylate) (PMMA) standards of known molecular weight in the range of 550 to 64000 Da, supplied by Polymer

Laboratories Ltd. Each sample (~2 mg/mL) was filtered through a PTFE membrane with a porosity of 0.20 µm before the injection.

Mass spectrometry with Electrospray Ionization (MS-ESI): Mass spectrometry measures were performed using fast flow injection analysis (FIA) with an Agilent Technologies 1100 series HPLC system equipped with a mass spectrometer detector (MSD Trap SL, model G2245D) and an ESI source operating at a flow rate of 50 µL/min. Ionization was performed in positive ion mode under the following conditions: nebulizer pressure of 20 psi, dry gas flow rate of 5 L/min, dry gas temperature of 325 °C, capillary voltage of 3.5 kV, capillary exit voltage of 177.3 V, and skimmer voltage of 40 V.

UV-Vis spectroscopy: UV-Vis spectra were taken on an Agilent CARY 60 UV-Vis spectrophotometer equipped with an 18-seater thermostated cuvette holder operating at 25 °C. For turbidity measures, an Agilent CARY 60 UV-Vis spectrophotometer equipped with thermoelectric cuvette holder with ethylene glycol as coolant was used, programmed to perform a temperature ramp of 1°C/min from 20°C to 80°C (and backwards). The cuvette used was a quartz cuvette with 10 mm optical path, and transmittance was read at a fixed wavelength of 700 nm. All spectra were taken in MilliQ water at polymer concentration of 5 mg/mL. Some of the turbidity measures were taken in a similar device, but without a programmable temperature ramp, though still allowing to perform a manual ramp of 1 °C/min.

Ultra High-Performance Liquid Chromatography – Mass Spectroscopy (UHPLC-MS): UHPLC-MS measurements were obtained by conducting reverse phase chromatography coupled with a mass spectrometer, with a gradient of H_2O and CH_3CN, using a 1100 Series Agilent Technologies system, equipped with:

- HiP sampler (G4226A), with the following conditions: draw speed of 100 µL/min, eject speed of 100 µL/min, injection volume of 5 µL;
- binary pump (G4220A), with the following conditions: flow of 0.55 mL/min, solvent composition gradient as follows:

Time (min)	H_2O	CH_3CN
0.00	95.0%	5.0%
5.50	70.3%	39.7%
10.00	60.2%	39.8%
11.00	0.0%	100.0%
12.00	0.0%	100.0%
13.00	95.0%	5.0%

Figure 27 Gradient of eluent for UHPLC-MS measures.

- column compressor (G1316C), with the following conditions: temperature of 25 °C;
- UHPLC column: ZORBAX reversed-phase HPLC column;
- diode array detector (G4212A), with the following conditions: bandwidth of 4 nm, reference wavelength of 360 nm, acquired wavelength of 200 nm;
- time of flying / quadrupole-time of flying (TOF/Q-TOF) mass spectrometer (G6550B) with Dual AJS ESI as ion source, with the following conditions: gas temperature of 250 °C, gas flow of 15 L/min, nebulizer pressure of 35 psig, sheath gas temperature of 320 °C and sheath gas flow of 12 L/min, with positive polarity, 0 collision energy (no MS^n measures were performed), nozzle voltage of 500 V. The electrospray ionization of sample molecules was done using 0.1% v/v formic acid as a protonating agent.

2.3 Oligo(ethyl-2-oxazoline)s through CROP

Synthesis of $OEOX_pMA$ with a DP target of 4: 12 mL of 2-ethyl-2-oxazoline (EOXA) were transferred to an oven-dried round bottom flask and anhydrified with CaH_2 for 24 h, then distilled at 155 °C under argon into a 50 mL oven-dried double neck round bottle flask with a screwable plastic cap, to keep the distilled EOXA under argon atmosphere. The distillation apparatus was treated with 3 cycles of vacuum-argon prior to use, in order to remove any trace of humidity. The final volume of EOXA distilled was 11.5 mL (0.114 mol, 4 eq).

6 mL of methyl tosilate (MeOTs) were transferred to an oven-dried round bottom flask and anhydrified with CaH_2 for 24 h, then distilled at 145 °C under vacuum into a round bottom flask with a rubber septum under argon atmosphere. The distillation apparatus was treated

with 3 cycles of vacuum-argon prior to use, in order to remove any trace of humidity The final volume of MeOTs distilled was 4.3 mL (0.0285 mol, 1 eq).

For the terminating solution, 4.6 mL of methacrylic acid (MAA, 0.0556 mol, 2 eq) were filtered through basic alumina and transferred to and oven-dried round bottom flask, closed with a rubber septum and degassed with argon for 15 min. Then 10.4 mL of dry acetonitrile (ACN) were added, to obtain a 1 g/mL solution. 12 mL of triethylamine (TEA) were transferred to an oven-dried round bottom flask and anhydrified with KOH for 2h. Then, 7.7 mL of TEA (0.0556 mol, 2 eq) were filtered through a PTFE filter into the MAA solution, and let it react for 5 minutes.

For the polymerization, 17 mL of dry ACN were added with an argon degassed syringe into the distilled EOXA, to obtain a 4 M solution. Then, all the 4.3 mL of MeOTs were transferred with an argon degassed syringe into the EOXA solution. The reaction was then kept for 2 h at 70 °C. The conversion was determined through ^{1}H-NMR spectra, by taking samples of reaction crude at 0 h and 2 h, with an argon degassed syringe. After 2 h, all the volume of the terminating solution was transferred into the polymerization solution with an argon degassed syringe and kept at 60 °C for 24 h (90 % conversion).

For the work-up, the solvent was removed under reduced pressure, and the residue was redissolved in chloroform (250 mL). The organic phase was extracted by washing with a saturated solution of $NaHCO_3$ (2 × 200 mL) and finally with brine (1 × 200 mL). The organic phase was dried over Na_2SO_4, filtered, and the solvent was evaporated under reduced pressure prior to addition of 10 mL of THF stabilized with BHT, to prevent self-polymerization of the oligomers. The final product was freeze dried to obtain a highly hygroscopic wax-like yellow solid (9 g). The chemical structure and molecular weight distribution of the final $OEOX_pMA$ were determined by ^{1}H-NMR and UHPLC-MS.

2.4 Chromatographic separation of discrete oligo(2-ethyl-2-oxazoline)s

1.5 g of $OEOX_pMA$ was dissolved in the minimum amount of DCM:MeOH 99:1. The obtained solution was then purified by flash silica gel column chromatography (100 cm of length, 4 cm of diameter, packed with 230-400 silica mesh for 15 cm of height) using a manually performed gradient of mobile phase from 99:1 DCM:MeOH to 95:5 DCM:MeOH. In particular, after detecting the spot corresponding to the first oligomer, the eluent was changed to 98:2 DCM:MeOH, then changed again by increasing the polarity for every new

spot detected. When all the desired oligomers were eluted, the stationary phase was washed with DCM:MeOH 80:20. For 1.5 g of $OEOX_pMA$, the volume of solvents used were approximatively:

- 1 L of 99:1 DCM:MeOH
- 0.5 L of 98:2 DCM:MeOH (after the first spot detection)
- 0.5 L of 97:3 DCM.MeOH (after the second spot detection)
- 0.5 L of 96:4 DCM:MeOH (after the third spot detection)
- 1 L of 95:5 DCM:MeOH (to fully separate the last spots)
- 0.5 L of 80:20 DCM:MeOH (to wash the column)

To ensure a steady flow, argon gas was insufflated into the column, using a pressure reducer set at 0.5 psi. Single-fraction detection was performed using SiO_2-coated TLC sheets stained with $KMnO_4$ solution, and DCM:MeOH 95:5 as eluent. Each fraction was isolated by solvent evaporation under reduced pressure, redissolution in water and drying under vacuum, to obtain an oil (shorter isolated oligomer appeared colourless, while longer ones had a yellowish colour). All the fractions were stored below −20 °C prior to use. The purified oligomers were characterized by ^{1}H-NMR and MS-ESI.

2.5 Methylation of CDPA

The procedure followed is patented by DUPONT ELECTRONICS - WO2005/113493, 2005, A1, Page/Page column 3; 5.

A solution of 4-cyano-4-(((dodecylthio)carbonothioyl)thio)pentanoic acid (CDPA, 0.1017 g, 1 eq) in dry THF (3 mL) was transferred to a round bottom flask, degassed with Ar (closed with a rubber septum) for 15 min and then kept in a ice bath at 5-10°C before adding diazabicyclo[5.4.0]undec-7-ene (DBU, 0.076 mL, 2 eq) dropwise through an Ar degassed syringe. The mixture was stirred for 5 min, then methyl iodide (MeI, 0.078 mL, 5 eq) was added through an Ar degassed syringe, and the resulting mixture was stirred for 18 h. The reaction was followed through TLC on silica, performed using DCM:Petroleum ether 9:1 as eluent and using a 264 nm UV lamp for spot detection. After that, the reaction mixture was diluted with n-hexane, filtered, and the solid was rinsed with n-hexane. The filtered mixture was washed with dilute sodium chloride (100 mL), HCl 1M (100 mL), dilute sodium bicarbonate solution (100 mL), and water (100 mL), and the organic phase was anhydrified with sodium sulphate and filtered. Then, the filtered organic phase was transferred in a round

bottom flask, and the solvent was removed under reduced pressure to obtain an amber oil (0.0639 g, 61 % yield). The final product was characterized through ^{1}H-NMR, ^{13}C-NMR and MS-ESI.

2.6 Poly[oligo(2-ethyloxazoline)]s through RAFT polymerization

POEOX$_p$MA and POEOX$_n$MAs (n discrete) were synthesized by RAFT polymerization with 50:1:0.2 macromonomer:MCDP:AIBN molar ratios, using DMF as solvent (0.5 M monomer concentration). In a typical procedure, OEOX$_p$MA$_{5.5}$ (macromonomer $\overline{DP}$ = 5.5, M_n = 634 g/mol, 0.4438 g, 50 eq), MCDP (5.8 mg, 1 eq), AIBN (0.5 mg, 0.2 eq), and DMF (1.4 mL) were loaded in a 10 mL oven dried schlenk flask, and the mixture was degassed with Ar for 30 min. The polymerization was carried out under argon atmosphere at 70°C. Samples for conversion determination were taken at 0 h and 24 h through an Ar degassed syringe, under strong Ar flux. After 24 h, the reaction was stopped by exposure to air, and the crude product was precipitated into a large excess of cold diethyl ether, then centrifuged at 5000 rpm for 12 minutes. The precipitate was transferred with the minimum quantity of THF in a round bottom flask, the solvent was removed under reduced pressure, and the final product (POEOX$_p$MA, 90% conversion) was freeze-dried to obtain a white powder (0.3822 g). The final product was characterized by ^{1}H-NMR and GPC.

2.7 End-capping of POEOXMAs through aminolysis of trithiocarbonyl groups

POEOX$_p$MA and POEOX$_n$MAs (n discrete) were end-capped with thiols through aminolysis with a large excess of n-butylamine. In a typical procedure, POEOX$_p$MA$_{5.5}$ (M_n = 30.0 kDa, 57.4 mg, 1 eq) and THF (3 mL) were transferred to a round bottom flask, then closed with a rubber septum and the headspace was degassed with Ar for 15 minutes. After that, n-butylamine (16.6 mg, 50 eq) was injected through a degassed syringe into the mixture and kept under stirring for 24 h. Then, the crude was precipitated into a large excess of diethyl ether, then centrifuged at 5000 rpm for 12 minutes. The precipitate was transferred with the minimum quantity of THF in a round bottom flask, the solvent was removed under reduced pressure, and the final product (POEOX$_p$MA$_{5.5}$–SH) was freeze-dried to obtain a white powder (42.8 mg, 75% yield) and stored at 0 - 4 °C. The reaction was followed by performing UV-Vis absorbance spectra (wavelength range of 200 nm – 700 nm) of the purified polymers,

before and after aminolysis, to observe the decrease of intensity of the trithiocarbonyl moieities absorbance bands.

CHAPTER 3: RESULTS AND DISCUSSION

3.1 Synthesis of OEOX$_p$MA

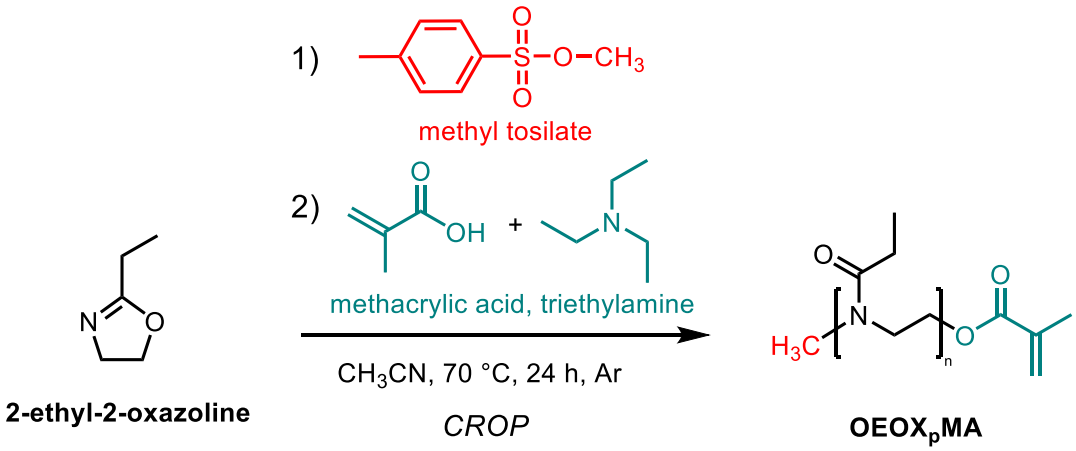

Figure 28 Reaction scheme for the synthesis of OEOX$_p$MA.

Oligomer	[EOXA] : [MeOTs] : [MAA] : [TEA]	p % (2 h)	$\overline{DP}_{NMR}$	$\overline{DP}_{MS}$	M_n (g/mol)	Đ
a) **OEOX$_p$MA$_{4.0}$**	4 : 1 : 2 : 2	> 95%	4.0	/	/	/
b) **OEOX$_p$MA$_{3.4}$**	3 : 1 : 2 : 2	90%	3.4	/	/	/
c) **OEOX$_p$MA$_{1.7}$**	2 : 1 : 2 : 2	> 95%	1.6	1.7	270	/
d) **OEOX$_p$MA$_{5.5}$**	5 : 1 : 2 : 2	> 95%	5.6	5.4	634	1.15
e) **OEOX$_p$MA$_{4.5}$**	4 : 1 : 2 : 2	88%	4.4	4.5	544	1.13

Table 1 Molar ratios of monomer, initiator and terminating compounds, conversion after 2 hours (calculated through ^{1}H-NMR), average DP (calculated through ^{1}H-NMR), average DP (calculated through MS), number average molar mass (calculated through MS), dispersity (calculated through MS) of all the OEOX$_p$MAs synthesized.

The average degree of polymerization ($\overline{DP}$) were calculated via ^{1}H-NMR and MS (Table 1). All the conversion at 2 hours were calculated through ^{1}H-NMR, by following the decrease in intensity of the signals of the protons on the monomer (4.1 ppm, t, O-CH$_2$ and 3.7 ppm, t, N-CH$_2$) (Figure 29). All signals were integrated by normalizing with respect to the signal of the

carbonylic proton of DMF (8 ppm, s), added as reference (20 µL of DMF in 100 µL of crude sample). The formula used for calculating conversion is:

$$p\,\% = \frac{I_t - I_0}{I_0} \times 100$$

where I_t is the intensity of the signal of the monomer at time t and I_0 is the intensity of the signal of the monomer at time 0.

The $\overline{DP}$ of each batch could be calculated through ^{1}H-NMR, by dividing each integral (normalized to the signal of N-CH_3 at 3.01 ppm) by the number of protons of every signal corresponding to the ethyl lateral chains (-CH_2- at 2.32 ppm, -CH_3 at 1.10 ppm) (Figure 30).

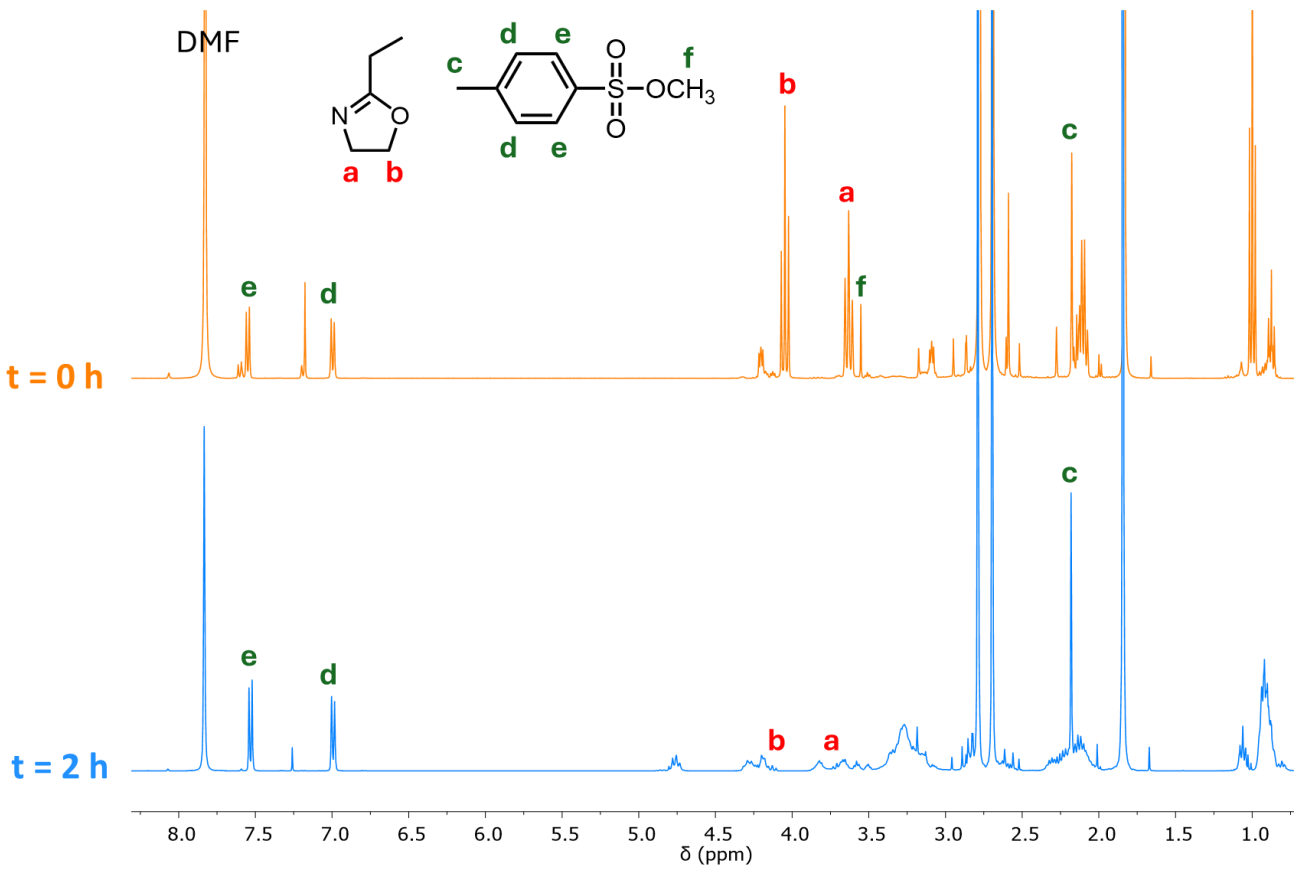

Figure 29 ^{1}H-NMR spectra of OEOX$_p$MA reaction crude, at different reaction time (disappearing of signals a and b can be observed).

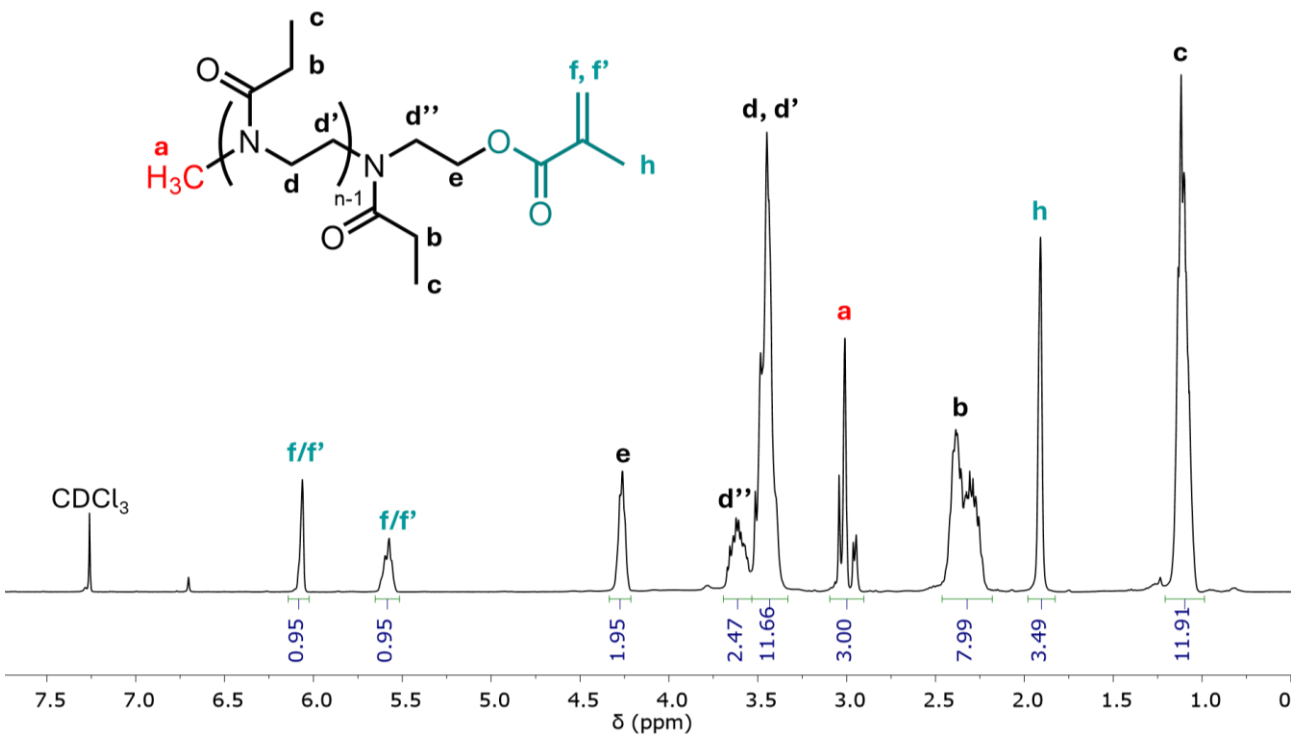

Figure 30 ^{1}H-NMR spectrum of purified OEOX$_p$MA$_{4.0}$

^{1}H-NMR (400 MHz, $CDCl_3$): δ 6.06 (s, 1H), 5.60 (s, 1H), 4.26 (m, 2H), 3.62 (m, 2H), 3.45 (m, 12 H), 3.01 (m, 3H), 2.32 (m, 8H), 1.91 (s, 3H), 1.10, (m, 12H).

$$\overline{\mathrm{DP}}\,(\mathrm{CH_2}) = \frac{7.99}{2} \approx 4.0$$

$$\overline{\mathrm{DP}}\,(\mathrm{CH_3}) = \frac{11.91}{3} \approx 4.0$$

In the ^{1}H-NMR spectrum of the purified OEOX$_p$MA (Figure 30), some signals appear broad (*e.g.,* -CH_2- at 3.62, -CH_2- at 3.45, -CH_2- at 2.32 ppm, -CH_3 at 1.10 ppm), and this is due to the fact that the product synthesized is a mixture of oligomers, with different chain lengths, distributed with a certain dispersity around a central value, calculated as $\overline{\mathrm{DP}}$. Indeed, all the signals related to protons that do not repeat throughout the chain (*e.g.,* =C-H at 6.06 ppm, =C-H at 5.60 ppm, O-CH_2 at 4.26, N-CH_3 at 3.01 ppm, =C-CH_3 at 1.91 ppm) appear as sharp singlet, or otherwise as multiplets, indicating that different chain lengths can influence the chemical shift of initial and terminal protons on the oligomers. The ^{1}H-NMR signals are in accordance with spectra reported in literature for OEOXMA obtained with the same procedure[58].

Through UHPLC-MS analysis, it was possible to calculate the M_n, M_w, $\overline{DP}$ and *Đ* for the polydisperse oligomers. The UHPLC-MS analysis was performed using a diode array detector (DAD), which detected the variation in the intensity of absorbance due to the presence of methacrylate moieties. The wavelength observed was 200 nm, which corresponds to the absorbance maximum of methacrylates. By assuming that every oligomer of different chain length absorbs with the same intensity (*i.e.,* chain length does not influences the molar extinction coefficient *ε* at 200 nm for the terminal methacrylates), it was possible to calculate the relative abundance of each oligomer in the mixture, by integrating each peak of the DAD elugram, and then converting the values to a relative intensity, using the formula:

$$\mathrm{I}\,\%_{\mathrm{i}} = \frac{\mathrm{Int_i}}{\sum_{\mathrm{i}} \mathrm{Int_i}} \times 100$$

where $\mathrm{Int_i}$ are the integrals of each signal. In this way, a relative intensities distribution was obtained, which would be equivalent to a molar fraction distribution of oligomers of each chain length.

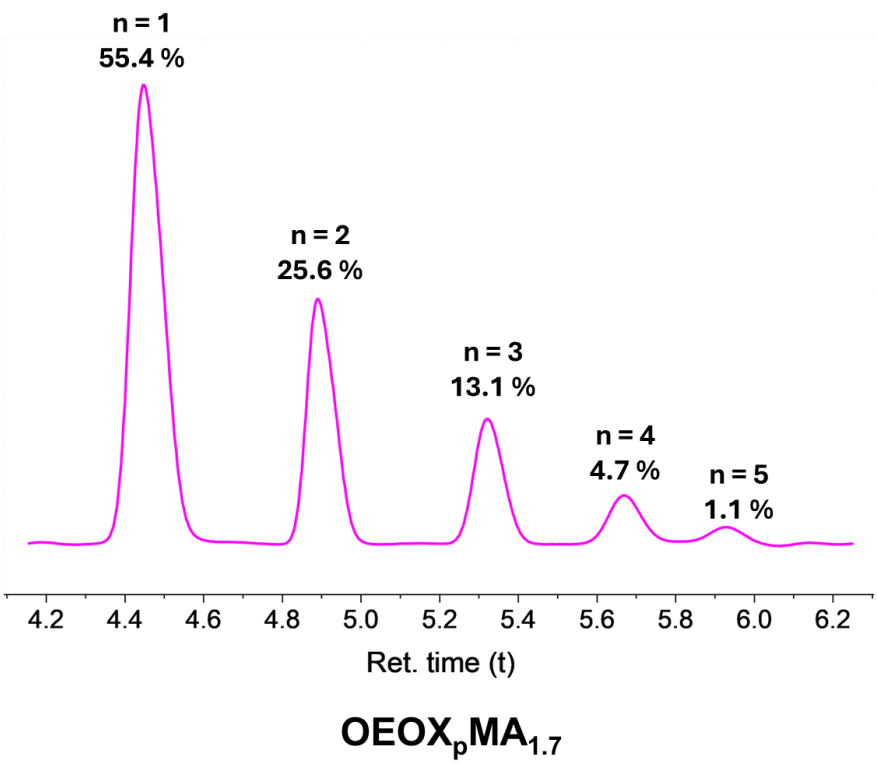

Figure 31 DAD elugram of $OEOX_pMA_{1.7}$, observed at 200 nm.

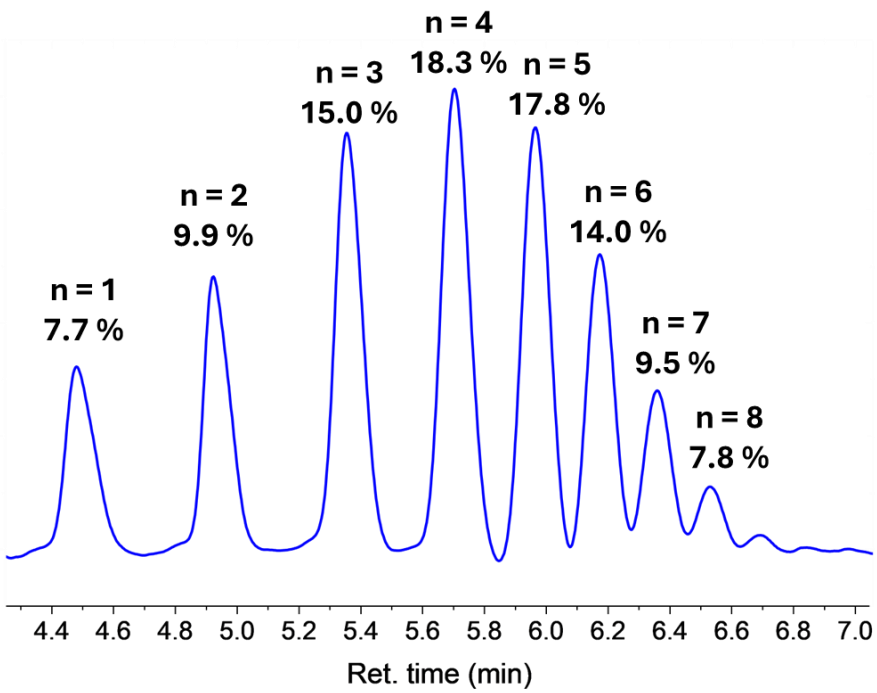

Figure 32 DAD elugram of OEOX$_p$MA$_{4.5}$, observed at 200 nm.

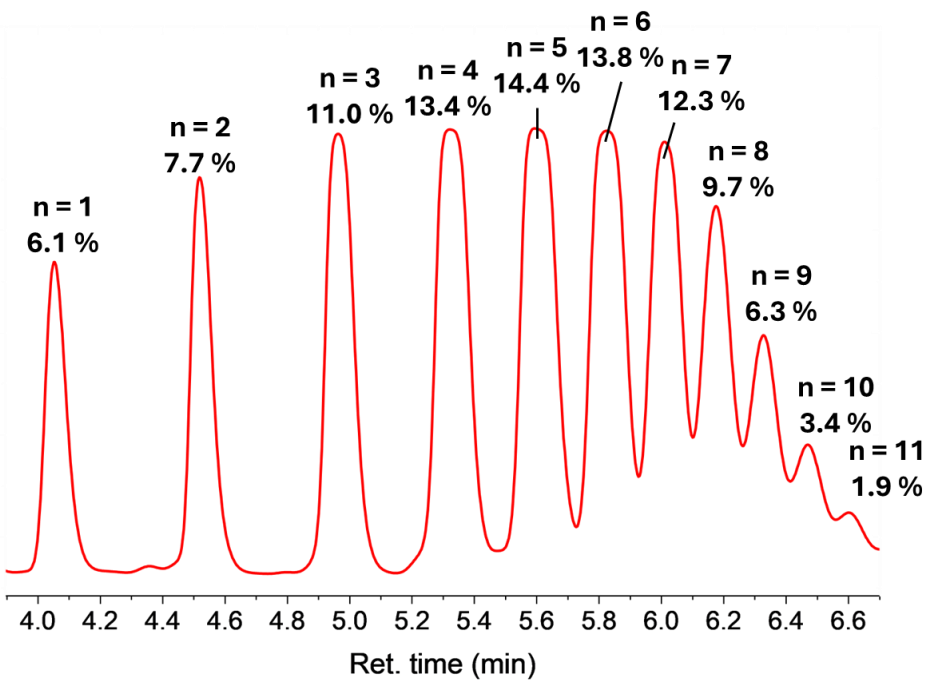

Figure 33 DAD elugram of OEOX$_p$MA$_{5.5}$, observed at 200 nm.

M_n, M_w, and $Đ$ could be calculated from their definitions, replacing the number of moles N_i of each oligomer species with the integrals Int_i obtained from the MS analysis, and using MW_i as the molecular weight of each oligomer species:

$$M_n = \frac{\sum_i MW_i N_i}{\sum_i N_i} \rightarrow M_n = \frac{\sum_i MW_i Int_i}{\sum_i Int_i}$$

$$M_w = \frac{\sum_i MW_i m_i}{\sum_i m_i} = \frac{\sum_i {MW_i}^2 N_i}{\sum_i MW_i N_i} \rightarrow M_w = \frac{\sum_i {MW_i}^2 Int_i}{\sum_i MW_i Int_i}$$

$$Đ = \frac{M_w}{M_n}$$

$\overline{DP}$ was calculated as the sum of the molar fractions of each oligomer in the mixture, weighted by the chain length n_i of each oligomer, through the formula:

$$\overline{DP} = \frac{\sum_i n_i Int_i}{\sum_i Int_i}$$

The DAD elugrams showed a bell-like relative intensity distribution (Figure 31, Figure 32, Figure 33), whose medium values were in accordance with the $\overline{DP}$ calculated through ^{1}H-NMR. For higher molecular weight oligomers (n ≥ 6), the relative intensities calculated were less reliable, due to an insufficient separation in the UHPLC run and broadening of the peaks, that resulted in unresolved DAD peaks. However, since the main contribution to $\overline{DP}$ came from the lower molecular weight oligomer species (*i.e.* the most present), the final values of $\overline{DP}$ calculated from the relative intensity distribution were close to the one calculated through ^{1}H-NMR, differing only by ±0.1.

For $OEOX_pMA_{1.7}$, dispersity was not reported, since it resulted smaller than one. This is due to the fact that, for that oligomer mixture, the most abundant species are n = 1 and n = 2 oligomers, resulting in an asymmetric bell-like distribution of frequencies (Figure 32), with a maximum at n = 1, hence calculating dispersity loses its meaning (since dispersity is related to standard deviation of molar weights distribution[42]).

The first two batches of oligomers synthesized ($OEOX_pMA_{4.0}$ and $OEOX_pMA_{3.4}$) were not analysed through UHPLC-MS, and the $\overline{DP}$ could only be calculated through ^{1}H-NMR.

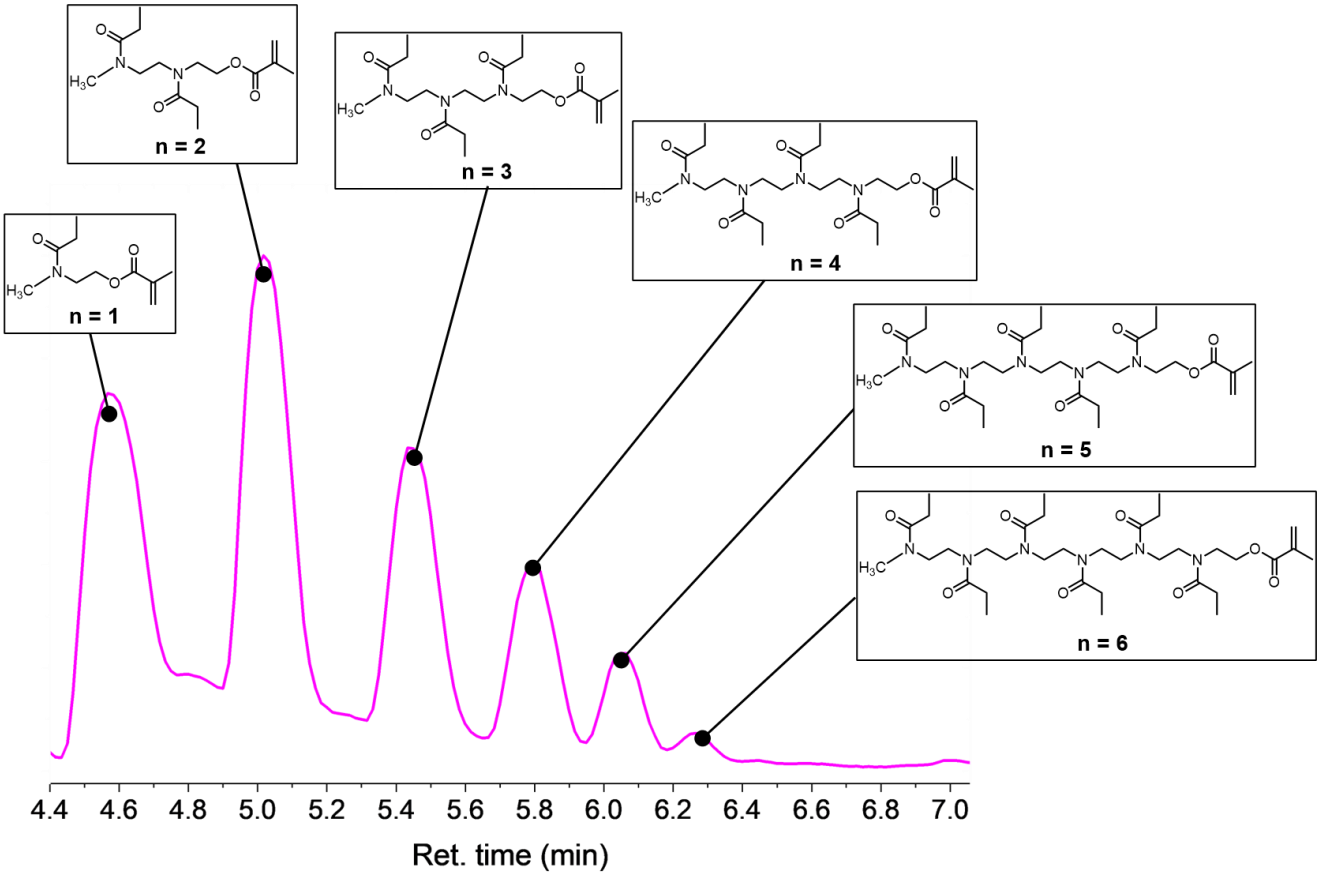

Figure 34 TIC elugram of $OEOX_pMA_{1.7}$.

UHPLC-MS analysis was also performed in total ion current (TIC) mode, to obtain an elugram with similar retention times of the DAD elugram, but different distribution of intensities, meaning that oligomers with varying length could have different ionization efficiencies (Figure 34). By extracting the ion current associated with the estimated mass of the protonated molecular ion for each oligomer (EIC mode), every peak of the elugram could be assigned to the corresponding oligomer, confirming that species from n = 1 to n = 7 were present in a detectable amount in $OEOX_pMA_{1.7}$, while the exact masses measured were close to the estimated one (Table 2).

Molecule	n	MW_{th} (g/mol)	MW_{exp} (g/mol)
$[OEOX_1MA + H]^+$	1	200.1281	200.1281
$[OEOX_2MA + H]^+$	2	299.1965	299.1969
$[OEOX_3MA + H]^+$	3	398.2649	398.2657
$[OEOX_4MA + H]^+$	4	497.3334	497.3342
$[OEOX_5MA + H]^+$	5	596.4018	596.4023
$[OEOX_6MA + H]^+$	6	695.4702	695.4717
$[OEOX_7MA + H]^+$	7	794.5386	794.5393

Table 2 Protonated molecular ion, number of repeating units, theoretical molecular weight (calculate from molecular formula) and experimental molecular weight (measured through MS) of oligomer species present in $OEOX_pMA_{1.7}$.

GPC analysis were conducted on the oligomer mixture, but since their molecular weights were mostly smaller than the lower limit of the instrument (500 Da), M_n and *Đ* could not be calculated in a reliable way using this method. However, each peak could still be identified and assigned to the smaller most present oligomers (Figure 35).

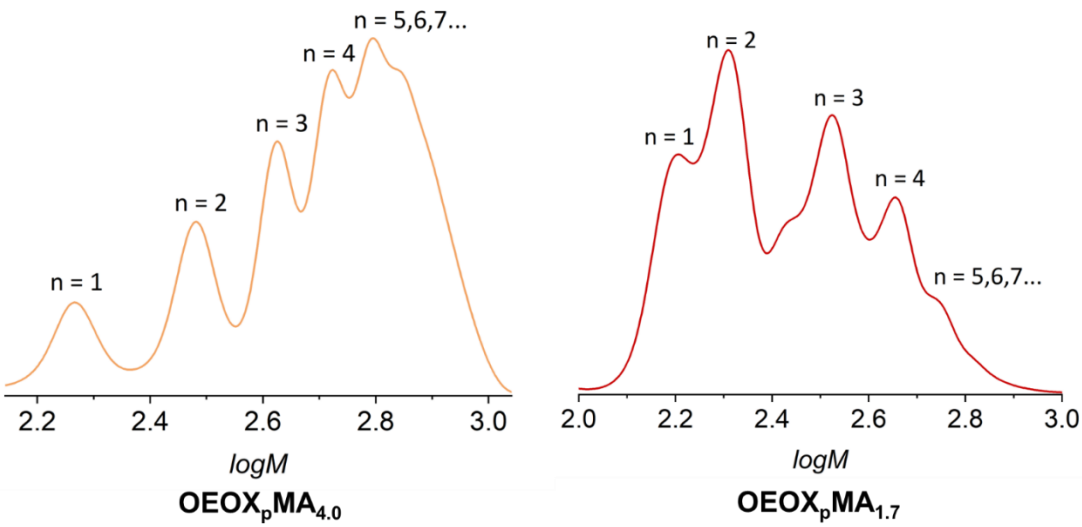

Figure 35 GPC elugrams for $OEOX_pMA_{4.0}$ and $OEOX_pMA_{1.7}$:

In every batch of oligomers synthesized, the conversion reached was always near or above 90 %, and this means that almost all the monomers were incorporated into the chains. Moreover, the $\overline{DP}$ measured was always consistent with the ratios of monomer:initiator of

the corresponding reaction, meaning that the DP_{target} was reached every time. This eventually proves that CROP on 2-ethyl-2-oxazoline is a reproducible and reliable reaction to obtain oligomers of desired average chain length.

3.2 Chromatographic separation of discrete $OEOX_nMAs$

For optimizing the oligomers separation, various ratios of DCM:MeOH were tested on TLC plates to find the best gradient to use. 95:5 DCM:MeOH emerged as the best option for separating each oligomer on silica, allowing for identification of single spots corresponding to oligomers with chain length from n = 1 to n = 5. To ensure the complete and quantitative separation of the oligomers, the column chromatography required a gradient of mobile phases, achieved by preparing mixtures of DCM and MeOH eluents with different ratios, from 99:1 to 95:5, and changing the eluent running in the column every time a new spot was detected on TLC, performing a manual gradient of eluent. For an even better separation, aiming for the isolation of oligomers with n greater than 5, it is actually necessary to perform an automated preparative flash column chromatography, with more sophisticated systems that can hold higher pressure of N_2 or Ar, an UV detector system and an automatic fraction collector, in order to precisely tune the gradient, reach better separation, and even scaling up the procedure, to separate grams of isolated oligomers. In this work, the manual gradient performed has allowed to obtain isolated oligomer species in quantities spanning from 0.1 to 0.05 g, starting from 1.6 g of mixture, indeed losing some of the oligomers with higher molecular weights, but eventually proving that this type of precise separation is possible in a quantitative way.

The relative recovered moles matched quite well the frequency distribution obtained through MS analysis: the highest quantity of oligomers recovered from the separation of $OEOX_pMA_{4.5}$ were $OEOX_4MA$ and $OEOX_5MA$, while for $OEOX_pMA_{1.7}$ the most present were $OEOX_1MA$ and $OEOX_2MA$, both in accordance with the $\overline{DP}$ for the starting batch (Table 3). Relative recovered mass and relative recovered moles were calculated with the formulas:

$$\%\,m = \frac{m\ (g)}{m_{tot}\ (g)} \times 100$$

$$\%\,n = \frac{n\ (mol)}{n_{tot}\ (mol)} \times 100$$

where m is the recovered mass of the oligomer specie, m_{tot} is the total recovered mass, n is the number of moles of the oligomer specie, n_{tot} are the total recovered moles.

Sample	m (g)	Oligomer species	MW (g/mol)	m (g)	n (mmol)	m %	n %
$OEOX_pMA_{4.5}$	**1.6**	**$OEOX_1MA$**	199	0.08	0.40	7.4 %	15.3 %
		$OEOX_2MA$	298	0.13	0.44	12.0 %	16.9 %
		$OEOX_3MA$	397	0.23	0.58	21.3 %	22.2 %
		$OEOX_4MA$	496	0.32	0.65	29.6 %	24.9 %
		$OEOX_5MA$	595	0.32	0.54	29.6 %	20.7 %
$OEOX_pMA_{1.7}$	**1.0**	**$OEOX_1MA$**	199	0.47	2.36	49.9 %	61.9 %
		$OEOX_2MA$	298	0.32	1.07	33.9 %	28.1 %
		$OEOX_3MA$	397	0.15	0.38	15.9 %	10.0 %

Table 3 Mass of the starting oligomer mixture, isolated oligomer species, recovered mass, recovered moles, relative recovered mass, relative recovered moles of the column separations conducted.

Each purified oligomer was analysed through ^{1}H-NMR and MS-ESI, to fully characterize the oligomer species isolated and to confirm monodispersity for the isolated fractions (see supporting information). The MS-ESI spectrum of $POEOX_pMA_{4.5}$ (oligomer mixture before separation) shows signals with m/z corresponding to the masses of $[M+Na]^+$ oligomer species, with a constant difference of 99 m/z between peaks, which corresponds exactly to the mass of one repeating unit. By comparing this spectrum with the MS-ESI spectra of the isolated oligomers (Figure 36), same values of m/z are found, proving that the separation was indeed successful (*i.e.*, true monodispersity was achieved).

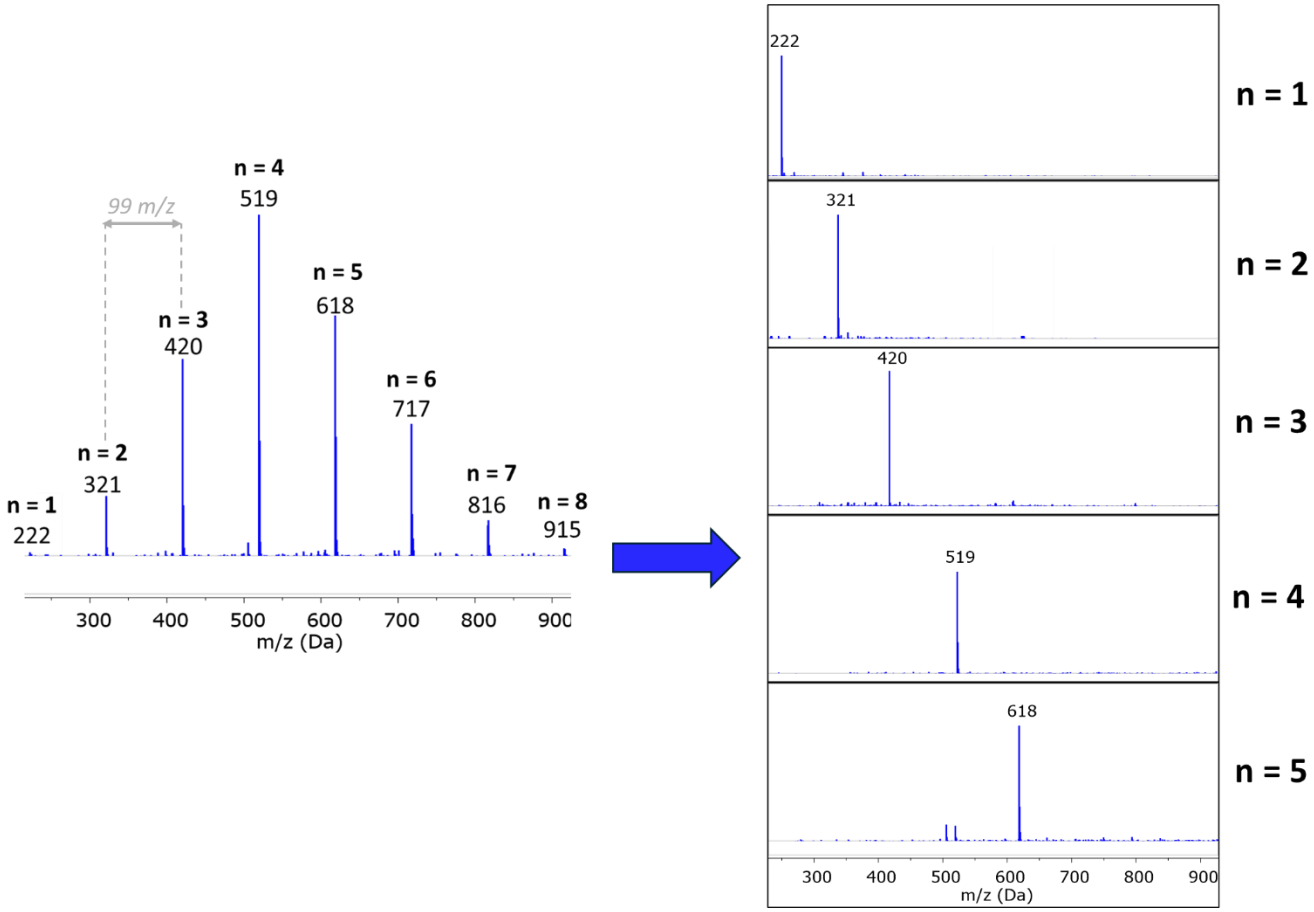

Figure 36 MS-ESI of the oligomers before and after the column separation.

As expected, from the stacked ^{1}H-NMR spectra of the oligomers (Figure 37), the intensities of the ^{1}H-NMR signals related to repeating units increase with increasing chain length (normalized to the N-CH_3 at 3.01 ppm). Moreover, a broadening of the ^{1}H-NMR signals can be observed as the oligomers become longer, due to the overlap of different signals of the same type of protons with slight variation in chemical shift, especially for those on repeating units. Moreover, the broadening of NMR peaks can also be attributed to reduced mobility in solution for longer oligomeric chains.

While $OEOX_1MA$ can be considered a small molecule, its ^{1}H-NMR spectrum presents some peculiarities, such as the splitting of the N-CH_3 methyl protons signal (at 3.01 ppm), that appears as a doublet. This is due to the partial double bond character of the N-C=O bond between the carbonylic carbon and the nitrogen of the amide, that creates an exchanging equilibrium between two low energy position for the groups directly bonded to the nitrogen, hence splitting the signal of the methyl. This effect can also be seen for the CH_2 directly bonded to the nitrogen (at 3.62 ppm), which appears as a doublet of triplets (instead of a simple triplet). The signals associated with protons that are further from the amide are

gradually less influenced from this effect (for instance, the methyl of the methacrylate at 1.91 ppm appear as a singlet).

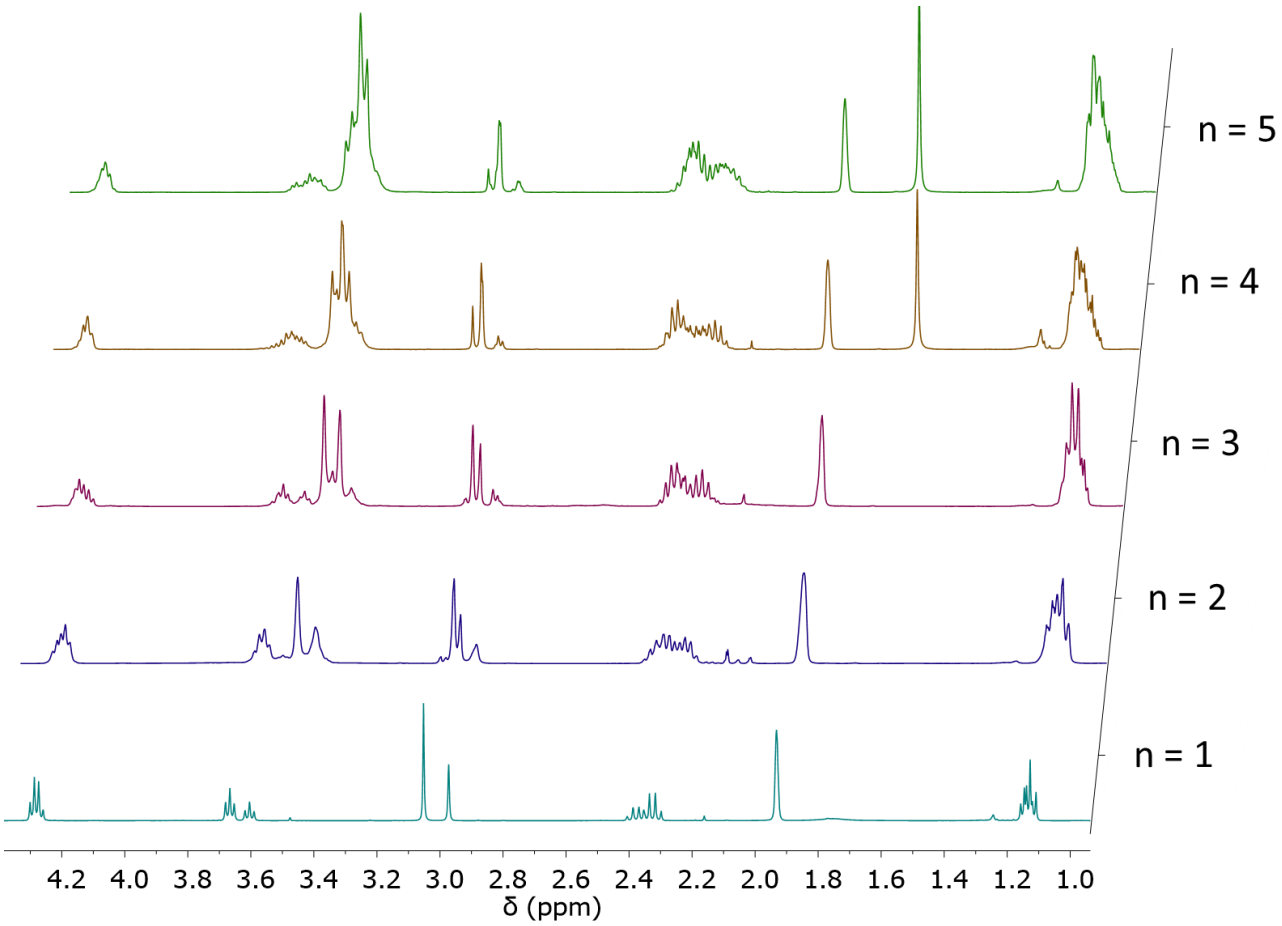

Figure 37 Stacked ^{1}H-NMR spectra of the isolated oligomers (n from 1 to 5).

3.4 Methylation of CDPA

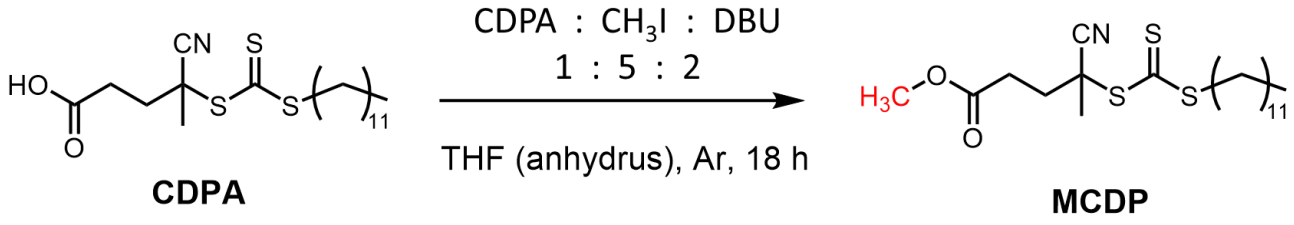

Figure 38 Reaction scheme of methylation of the CTA.

This reaction was performed to methylate the chain transfer agent 4-cyano-4-(((dodecylthio)carbonothioyl)thio)pentanoic acid (CDPA, a commercial CTA), in order to protect the terminal carboxylic group on the final polymers (Figure 38). The procedure followed was patented by DUPONT ELECTRONICS, but the quantity of methyl iodine (MeI) used was greater (5 eq), to ensure a high yield, since MeI is highly volatile. After the addition of the methylating agent, a precipitate started forming, which was the salt of the protonated organic base with the iodine ($DBU^+ I^-$). After 18h, to ensure that the reaction took place, a TLC plate was run, containing the reaction crude and pure CDPA, using DCM:Petroleum ether 9:1 as eluent. Under UV light, a new spot appeared with a higher R_f, indicating that the new compound interacted less with the silica and therefore was less polar. After purification, the ^{1}H-NMR (Figure 39), ^{13}C-NMR (Figure 40) and MS-ESI (Figure 41) confirmed that the amber oil obtained was indeed the methyl ester of CDPA, called methyl 4-cyano-4-(((dodecylthio)carbonothioyl)thio)pentanoate (MCDP).

^{1}H-NMR (400 MHz, $CDCl_3$): δ 3.71 (s, 3H), 3.32 (t, 2H), 2.63 (m, 2H), 2.45 (m, 2H), 1.87 (s, 3H), 1.69 (quint, 2H), 1.39 (m, 2H), 1.26 (m, 16H), 0.88 (t, 3H).

^{13}C-NMR (400 MHz, $CDCl_3$): δ 217.07, 172.08, 119.14, 52.25, 46.48, 37.21, 34.04, 32.06, 29.76, 27.82, 25.01, 22.84, 14.26

MS-ESI ($MeOH/H^+$), signals from $C_{20}H_{35}NO_2S_3$: $[M+Na]^+$ 440 m/z

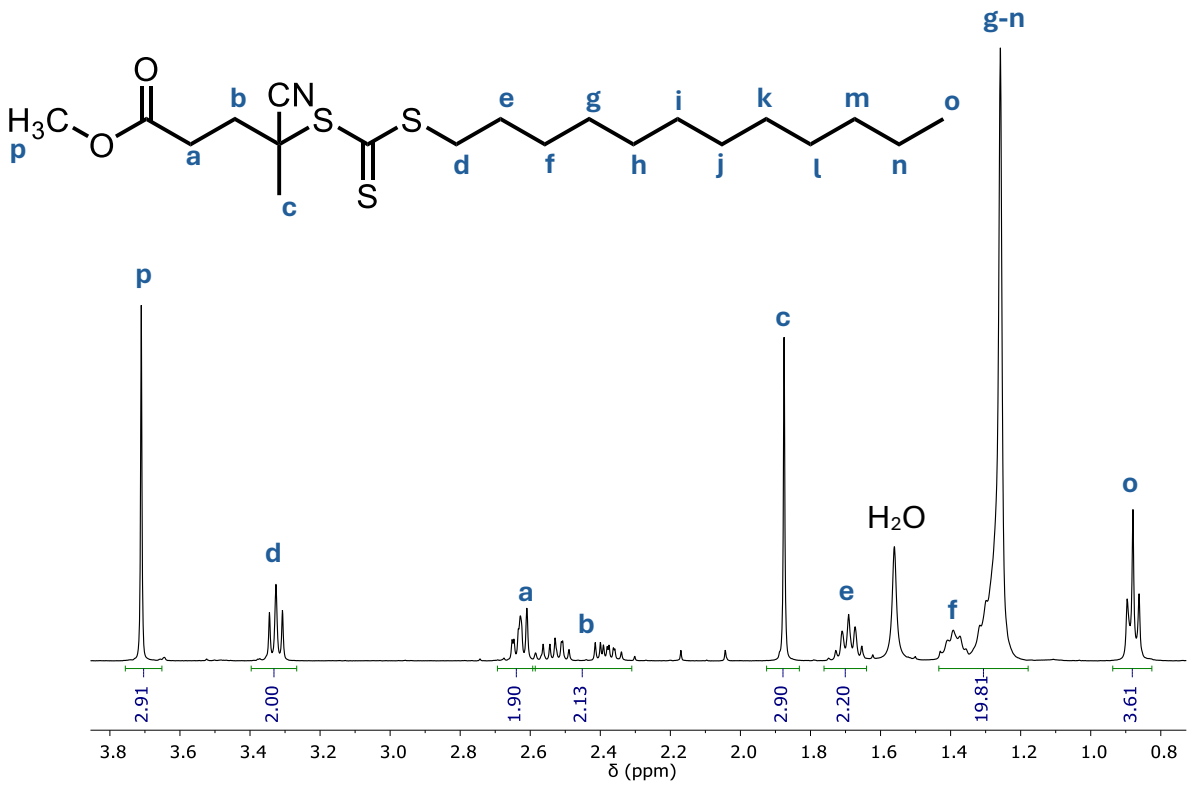

Figure 39 ^{1}H-NMR spectrum of purified MCDP.

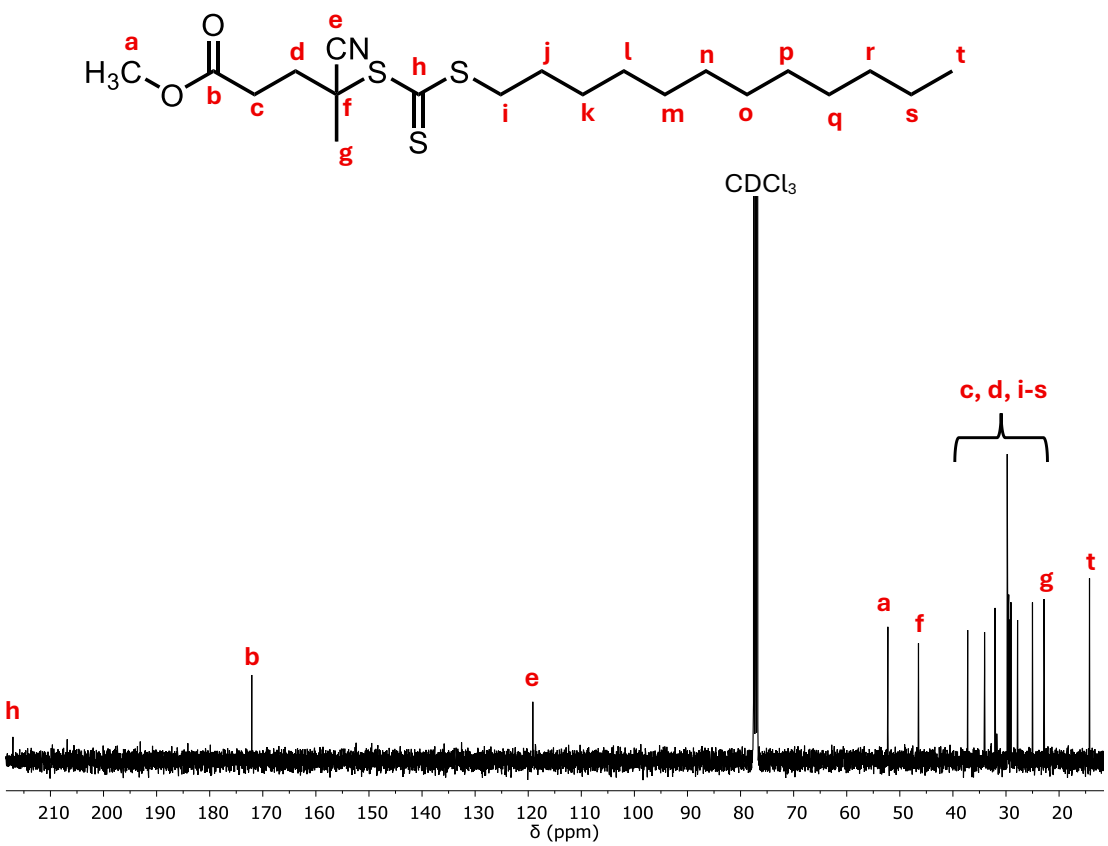

Figure 40 ^{13}C-NMR spectrum of purified MCDP.

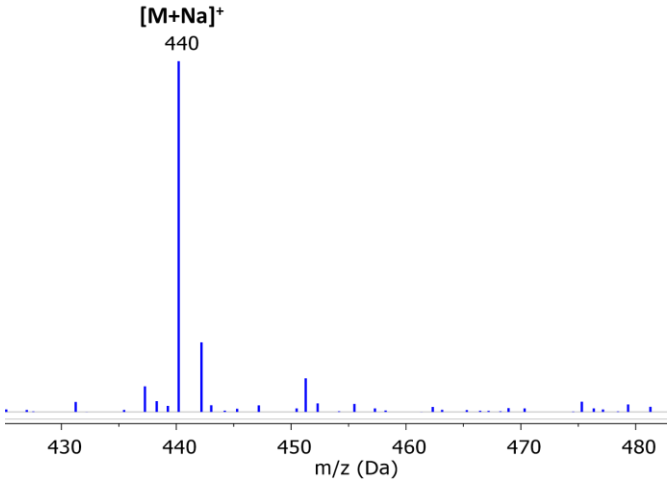

Figure 41 MS-ESI spectrum of purified MCDP.

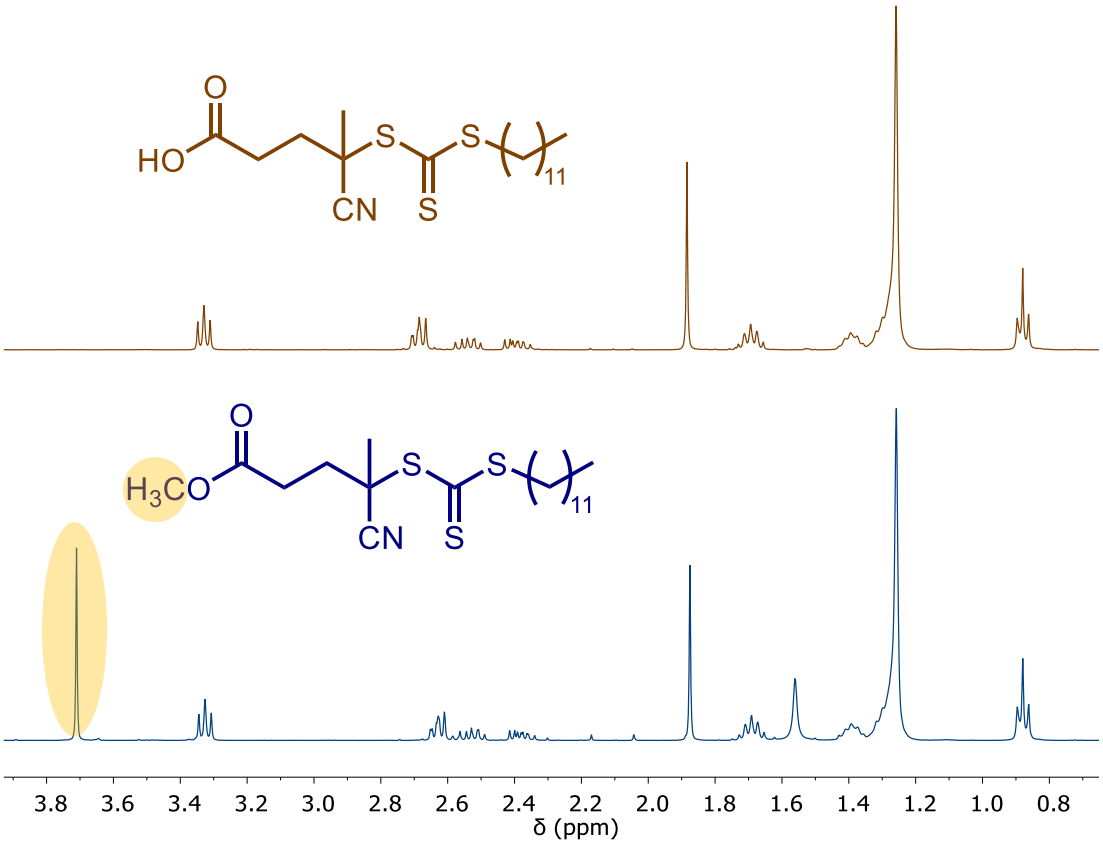

Figure 42 Comparison of ^{1}H-NMR spectra of CDPA (up) and MCDP (down).

A comparison of the ^{1}H-NMR spectra of commercial CDPA and its methylated version (MCDP) shows that all the signals kept similar chemical shifts, and a new signal corresponding to the –$COOCH_3$ protons appeared at 3.7 ppm.

3.5 RAFT polymerization of OEOXMAs

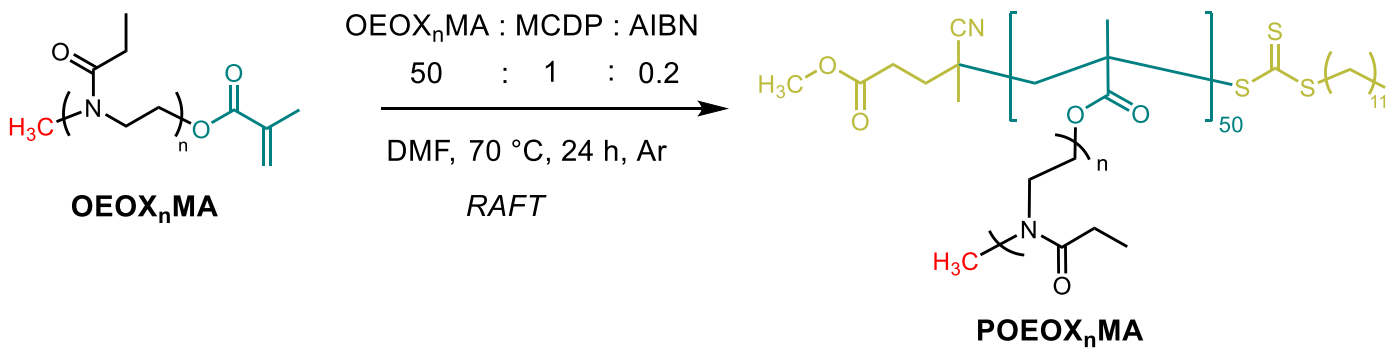

Figure 43 Reaction scheme of RAFT polymerization on OEOX$_n$MAs.

Polymer	MW$_{olig}$ (g/mol)	% p (24 h)	$M_{n,th}$ (kDa)	$M_{n,exp}$ (kDa)	$\overline{DP}$ (NMR)	$\overline{DP}$ (GPC)	Đ
POEOX$_1$MA	199	79 %	7.9	7.3	35	37	1.09
POEOX$_2$MA	298	73 %	10.9	8.4	26	28	1.09
POEOX$_3$MA	397	91 %	18.0	13.6	39	34	1.24
POEOX$_4$MA	496	76 %	18.8	14.5	/	29	1.53
POEOX$_5$MA	595	75 %	22.3	15.7	/	26	1.67
POEOX$_p$MA$_{4.5}$	~544	93 %	25.3	22.2	/	41	1.35
POEOX$_p$MA$_{5.5}$	~634	90 %	28.5	30.0	/	47	1.40

Table 4 Macromonomer molar mass, conversion at 24 hours, theoretical number average molar mass (calculated from conversion), experimental number average molar mass (measured from GPC), average DP (measured from ^{1}H-NMR), average DP (measured from GPC), dispersity (measured from GPC) of all the polymers synthesized.

All the conversions at 24 hours were calculated through ^{1}H-NMR, by following the decrease in intensity of the signals of the alkene protons of the methacrylate moieties (6.01 ppm, s, =C-H). All signals were integrated by normalizing with respect to the signal of the carbonylic proton of DMF (8 ppm, s), that was already present as solvent (Figure 44). The formula for calculating the conversion is:

$$p\,\% = \frac{I_t - I_0}{I_0} \times 100$$

where I_t is the intensity of the signal of the alkene proton at time t and I_0 is the intensity of the signal of the alkene proton at time 0.

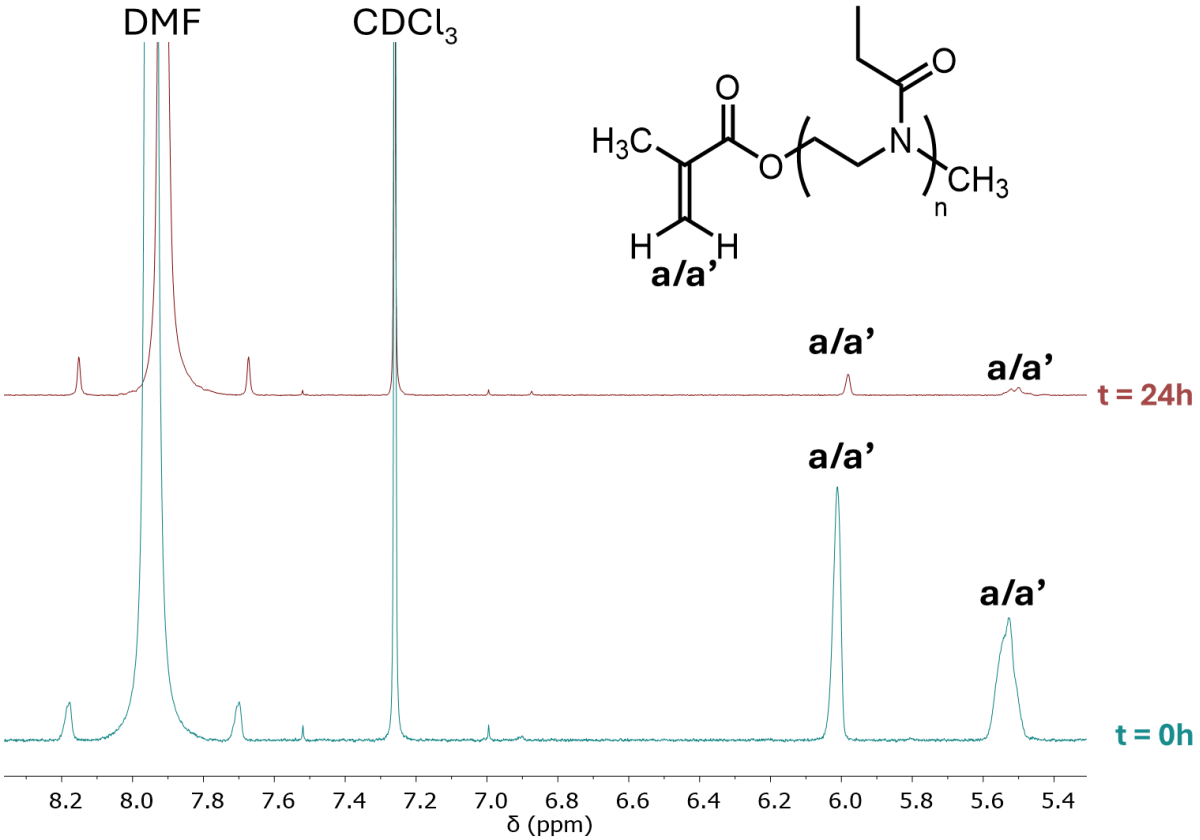

Figure 44 ^{1}H-NMR spectra of the polymerization mixtures at 0 h and 24 h.

One thing to be noted is that the monomers that reached higher conversions were the polydisperse ones ($OEOX_pMA_{4.5}$, $OEOX_pMA_{5.5}$), which could indicate that, in the oligomer mixture, some oligomer species might react with a higher polymerization rate k_p than others, having higher contribution on the overall conversion (Table 4). If compared with the conversions of monodisperse oligomers, the higher conversions are reached with macromonomers with n = 1 (79%) and n = 3 (90%). The values of *Đ* of the final polymers were compatible with a controlled polymerization, ranging from 1.20 to 1.67, with the higher being $POEOX_5MA$. $OEOX_nMA$s with n = 1 and n = 2 produced polymers with the lowest *Đ* (1.20), meaning that they went through an optimal controlled polymerization compared to other oligomers. However, all the differences observed for the different polymerizations might be due to several factors, such as residual oxygen levels, reactivity of the oligomeric species and purification procedure.

To obtain polymers of similar length, all the polymerizations were aimed at DP_{target} = 50, by using a macromonomer:CTA ratio of 50:1. This resulted in $\overline{DP}$ varying in a range of 26 – 47, since none of the polymerizations reached a conversion higher than 90 % (at 24 hours). The $\overline{DP}$ for all polymers was calculated through GPC analysis using the formula:

$$\overline{DP} = \frac{M_{n,pol}}{MW_{mon}}$$

where $M_{n,pol}$ is the number average molecular weight of the polymer measured through GPC and MW_{mon} is the molecular weight of the discrete oligomers (or the number average molecular weight for polydisperse oligomer mixtures), used as macromonomers.

Some of the molar masses measured from GPC analysis ($M_{n,exp}$) are lower than the theoretical molar masses calculated from conversion ($M_{n,th}$), and this is due to the polymer architecture which influences the hydrodynamic volume of the polymers. Indeed, comb polymers have much smaller hydrodynamic volumes in solution compared to linear polymers, because the chains are forced into a more compact conformation, closer to each other. As the calibration of the GPC was carried out with linear standard polymers (PMMA), comb polymers appear at a later elution volume, resulting in an underestimation of the molar masses[59]. This was true for all the polymers except for $POEOX_pMA_{5.5}$, whose $M_{n,exp}$ was actually greater than the $M_{n,th}$. This could be deriving from an error in determining conversion, possibly from an overestimation of the integral under the methacrylic proton signals due to partial evaporation of the reference DMF.

For some of the polymers with smaller side chains ($POEOX_1MA$, $POEOX_2MA$, $POEOX_3MA$), it could be possible also to calculate $\overline{DP}$ using ^{1}H-NMR, by normalizing each integrals to the signal of the proton of the terminal methyl-ester group, deriving from the methylated CTA used ($COOCH_3$ at 3.7 ppm) (Figure 45). For longer polymers, this signal was almost totally covered by the broad bands of the EOX side chains, while other sharp signals of the CTA could not be identified (see supporting information).

^{1}H-NMR (400 MHz, $CDCl_3$): δ 4.05 (68H), 3.70 (s, 3H), 3.65 (66H), 3.01 (105H), 2.40 (73H), 1.85 (66H), 1.15 (113H), 0.90 (105H).

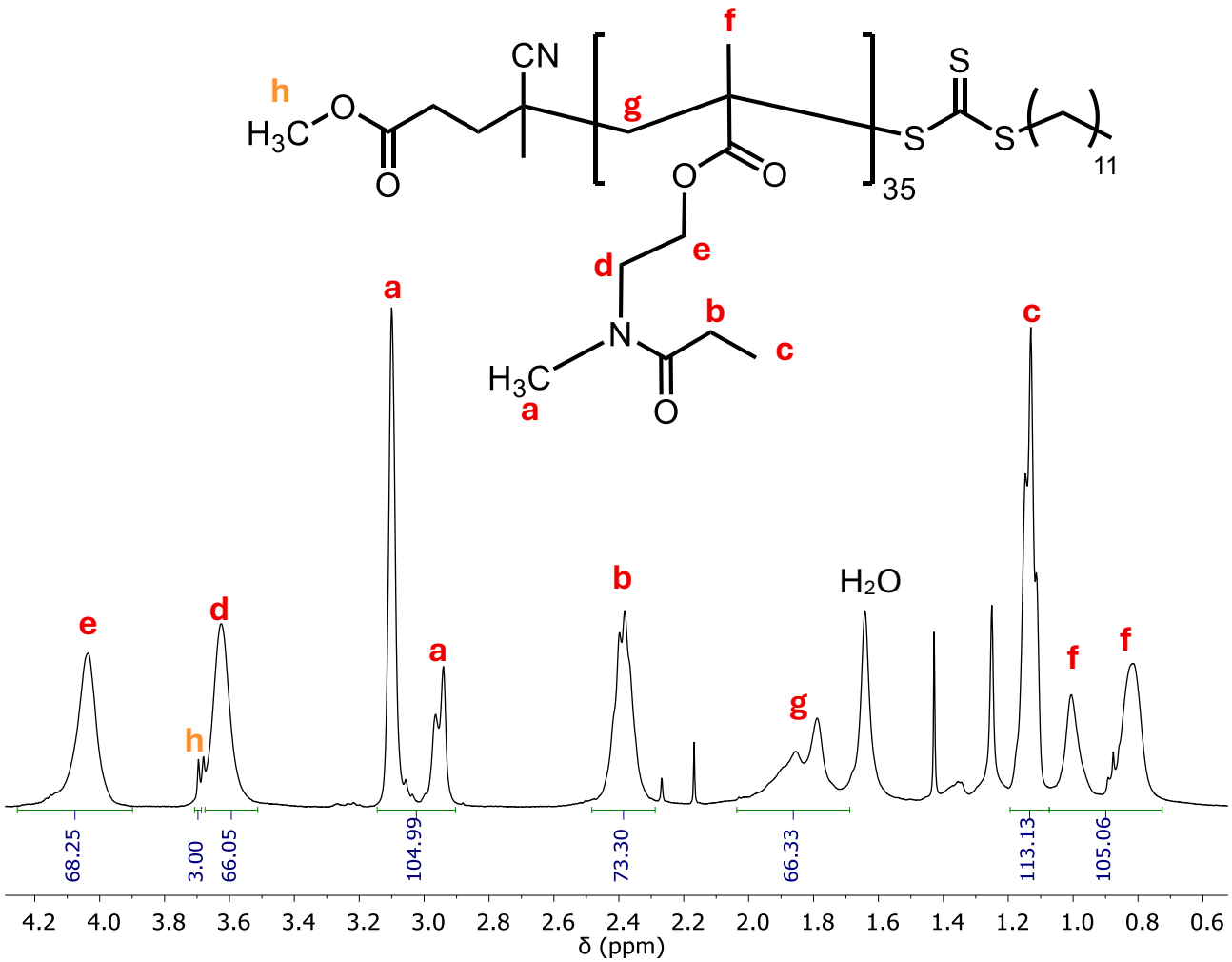

Figure 45 ^{1}H-NMR spectrum of purified POEOX$_1$MA.

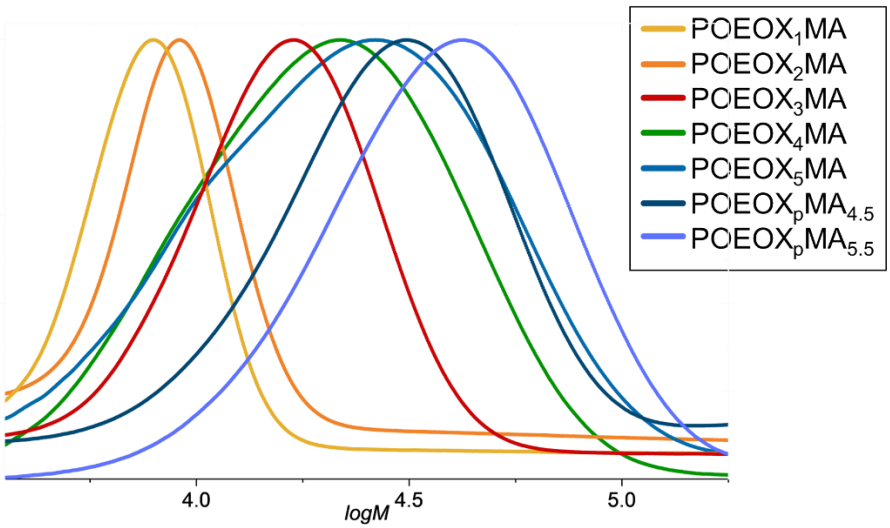

Figure 46 GPC traces of all the polymers with normalized intensities.

Stacked GPC traces of all polymers show increasing M_n with increasing side chain length (Figure 46). This was expected, as the M_n depends mainly on the molar weight of the starting macromonomer and on the degree of polymerization reached.

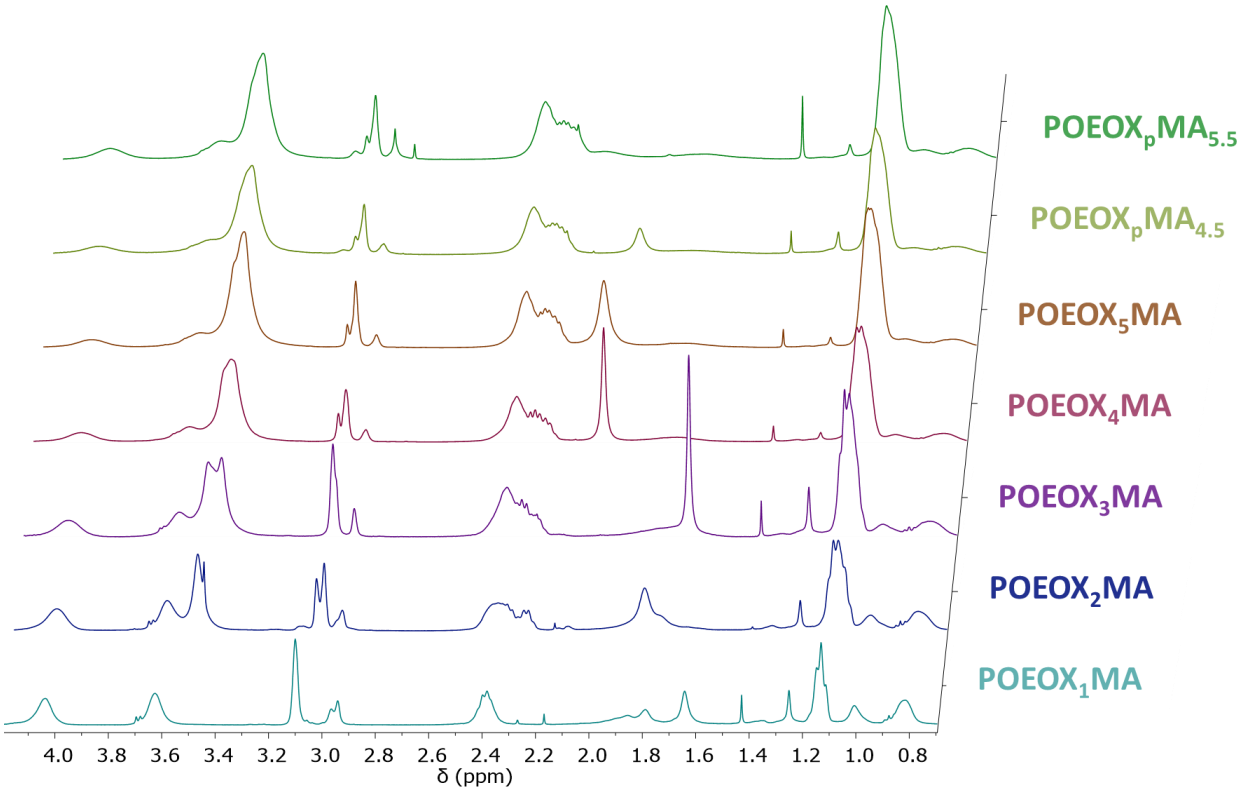

Figure 47 Stacked ^{1}H-NMR spectra of all the polymer synthesized.

Stacked ^{1}H-NMR spectra of all polymers shows that the signals of the OEX side chains become broader and more intense as side chains gets bigger, while the signals of the backbone (–CH_2– at 1.8 ppm and –CH_3 at 0.9 ppm) remains almost the same, since they depend on the degree of polymerization of each polymer (Figure 47).

3.6 End-capping of POEOXMAs through aminolysis of trithiocarbonyl groups

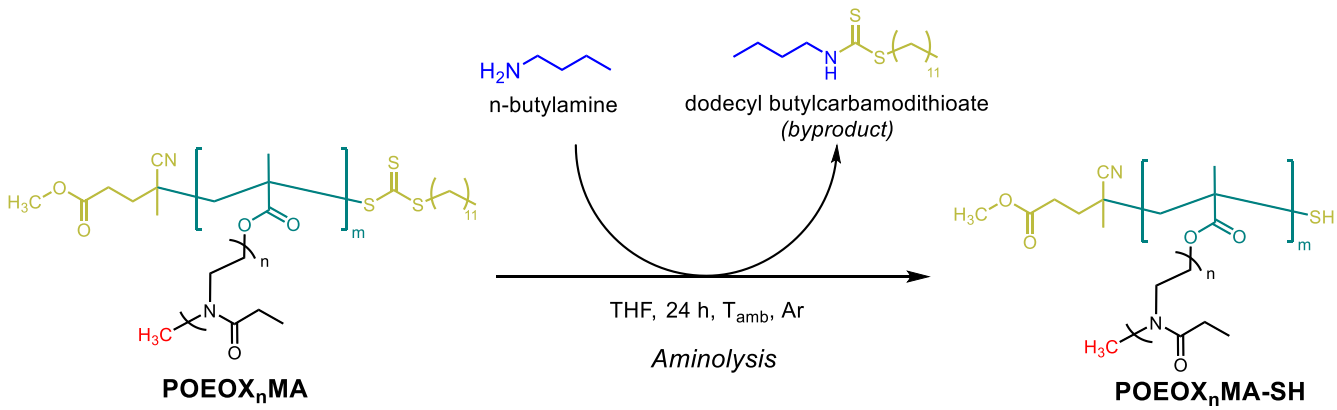

Figure 48 Reaction scheme of aminolysis of POEOX$_n$MAs.

This reaction was conducted to end-cap the polymers with a thiol group, by removing the trithiocarbonyl terminal group bearing the dodecyl chain. In this way, more reliable LCST measures could be conducted, since the contribute to polymer-polymer aggregation of the dodecyl end-chain was removed, making the LCST mostly dependent on side-chain interactions.

One main indicator that the reaction has happened was the change in colour of the polymer solution after the addition of n-butylamine. Indeed, after only 1 hour of reaction under stirring, the solution went from yellow (due to the absorbance in the visible range of light of the trithiocarbonyl group via a n→π* transition) to colourless, meaning that all the trithiocarbonyl groups got cleaved. Moreover, UV-Vis absorbance spectra of the polymers before and after aminolysis were taken (see supporting information), together with a UV-Vis absorbance spectrum of the isolated CTA (Figure 49).

The spectrum of MCDP presents two absorbance bands which are typical of trithiocarbonyl groups. They can be associated to a π→π* transition (~310 nm, very intense) and a n→π* transition (~450 nm, very low intensity), and these bands could also be found in the polymers obtained via RAFT polymerization. After cleaving the trithiocarbonyl groups through aminolysis, the absorbance band at 310 nm disappeared (while the 450 nm band could not be detected since the polymers was too low in concentration), while new bands with lower intensities appeared at 270 nm and 300 nm, that could be attributed to the formation of terminal thiols (Figure 50).

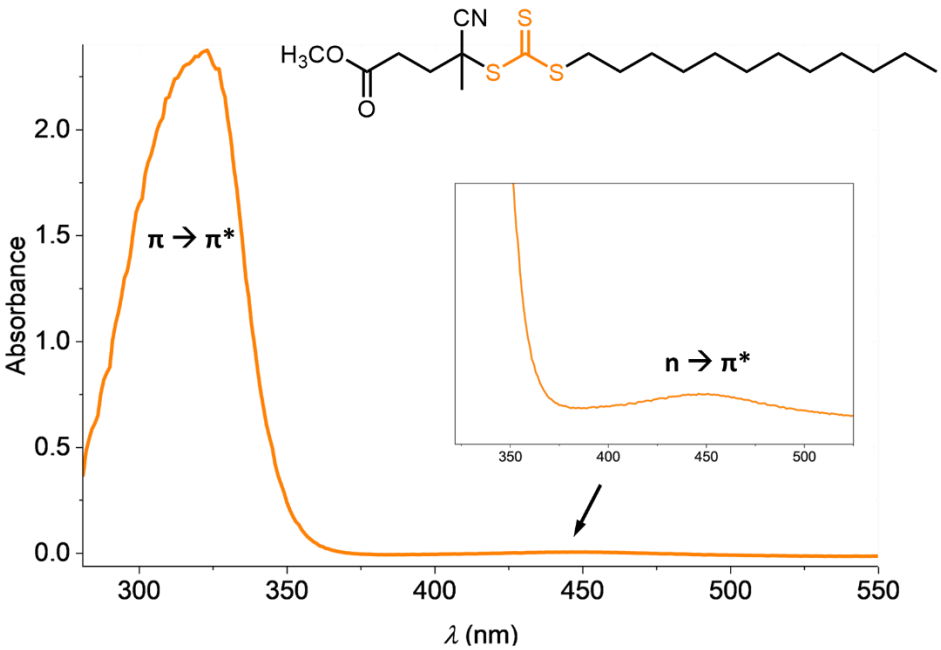

Figure 49 UV-Vis absorbance spectrum of MCDP.

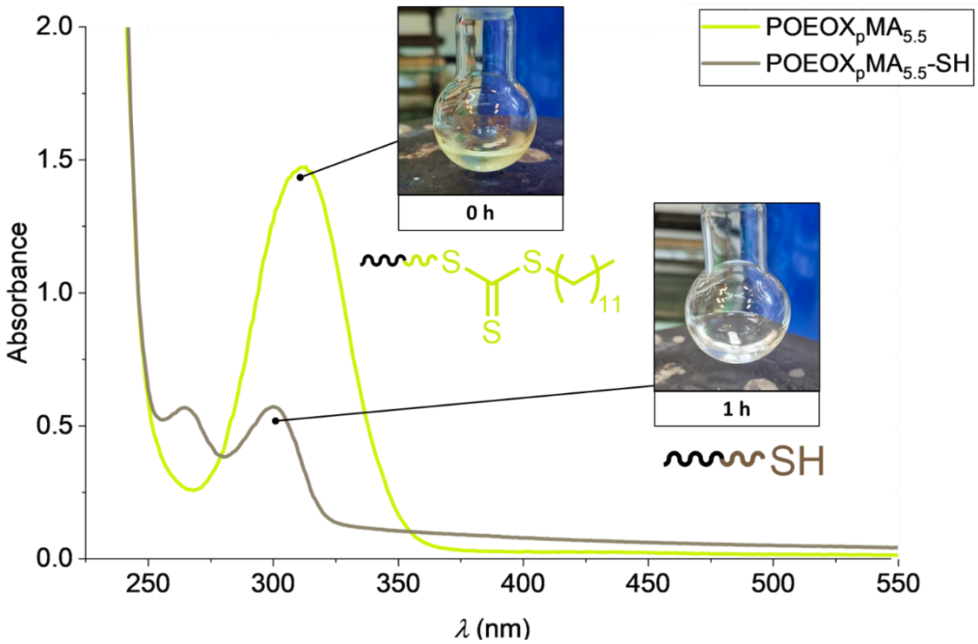

Figure 50 UV-Vis absorbance spectra of $POEOX_pMA_{5.5}$ before and after aminolysis.

The reaction gave rise to a byproduct, called dodecyl butylcarbamodithioate, which bears a dodecyl chain resulting from the nucleophilic attack of the amine on the trithiocarbonyl group. This byproduct could be easily removed through precipitation of the polymer in Et_2O, and the signals of the dodecyl chains were found in the ^{1}H-NMR spectrum of the supernatant liquid (Figure 51).

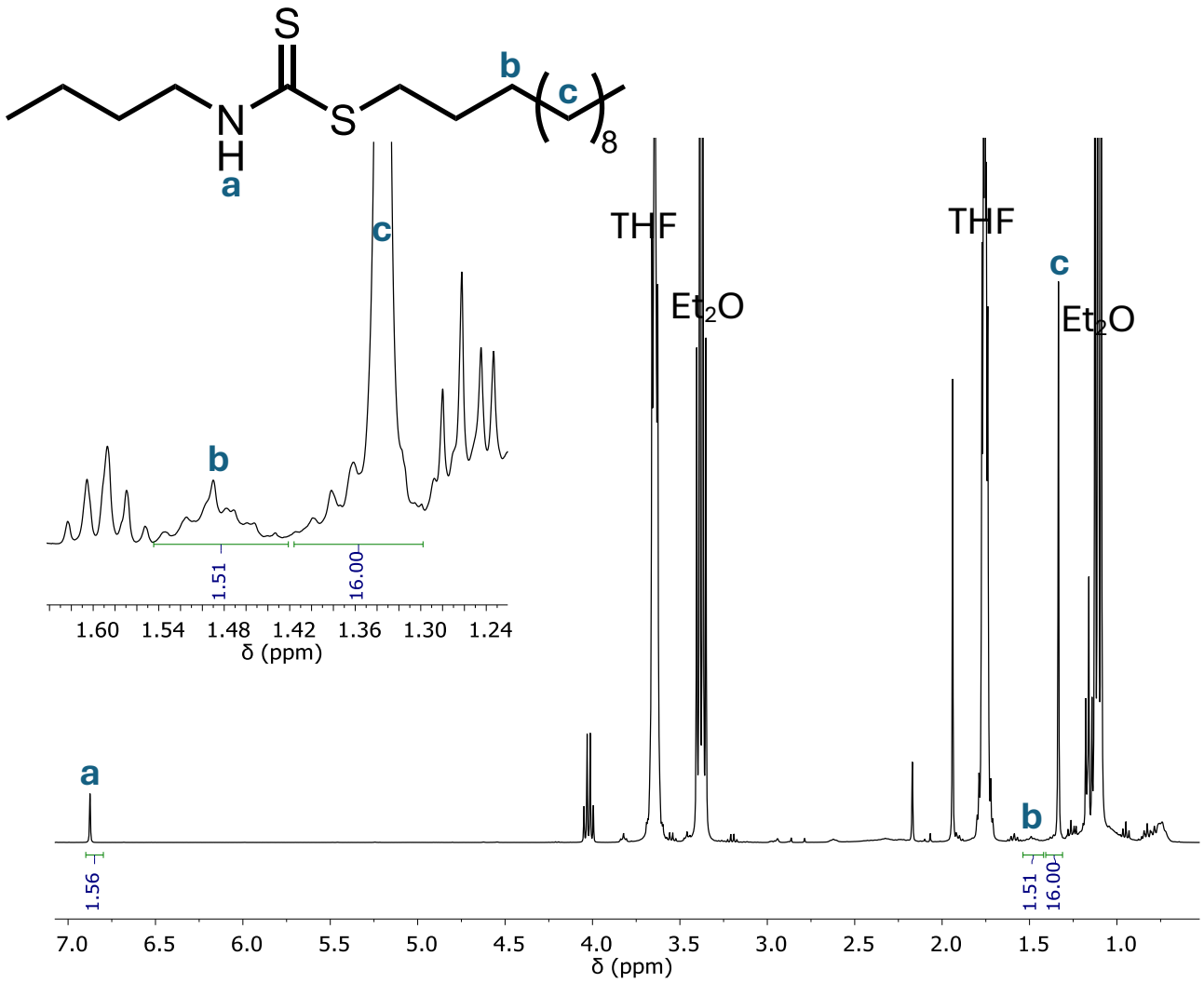

Figure 51 ^{1}H-NMR of supernatant liquid from precipitation of POEOX$_5$MA-SH.

3.7 LCST of POEOX$_n$MA-SH

For each polymer, two cloud point temperatures were measured:

- $T_{c,Heat}$ was the temperature corresponding to 50% of the transmittance at ambient temperature during heating;
- $T_{c,Cool}$ was the temperature corresponding to 50% of the transmittance at ambient temperature during cooling.

The cloud point temperatures were calculated by finding the inflection point of the sigmoid resulting from the temperature vs transmittance % plot. This was done by calculating the second derivative of the set of points corresponding to the sloped segment of the graph, then performing a linear fit for that data set and finding the zero of the function (see supporting information).

Polymer	$M_{n,exp}$ (kDa)	$\overline{DP}$ (NMR)	$\overline{DP}$ (GPC)	$T_{c,Heat}$ (°C)	$T_{c,Cool}$ (°C)
POEOX$_1$MA-SH	7.3	35	37	36.2	33.1
POEOX$_2$MA-SH	8.4	26	28	65.7	62.0
POEOX$_3$MA-SH	13.6	39	34	66.6	63.2
POEOX$_4$MA-SH	14.5	/	29	72.2	68.8
POEOX$_5$MA-SH	15.7	/	26	73.7	70.3
POEOX$_p$MA$_{4.5}$-SH	22.2	/	41	59.7	56.3
POEOX$_p$MA$_{5.5}$-SH	30.0	/	47	69.8	66.6

Table 5 Experimental number average molar mass, average DP (measured from ^{1}H-NMR), average DP (measured from GPC), clouding temperature during heating ($T_{c,Heat}$), clouding temperature during cooling ($T_{c,Cool}$) of all the thiol-capped polymers.

All the polymers showed reversible LCST behaviour, since after every cycle the transmittance rose back to the starting values. Even though the polymers synthesized had main chain lengths varying in a range of 26 to 47 repeating units (Table 5)., it was still possible to compare their cloud point temperatures, since it is reported in literature that there is an influence of backbone length on LCST only for POEOXMA comb brushes with high

molecular weight side-chains[59], while it is negligible for low molecular weight side-chains, similarly to POEGMA[60].

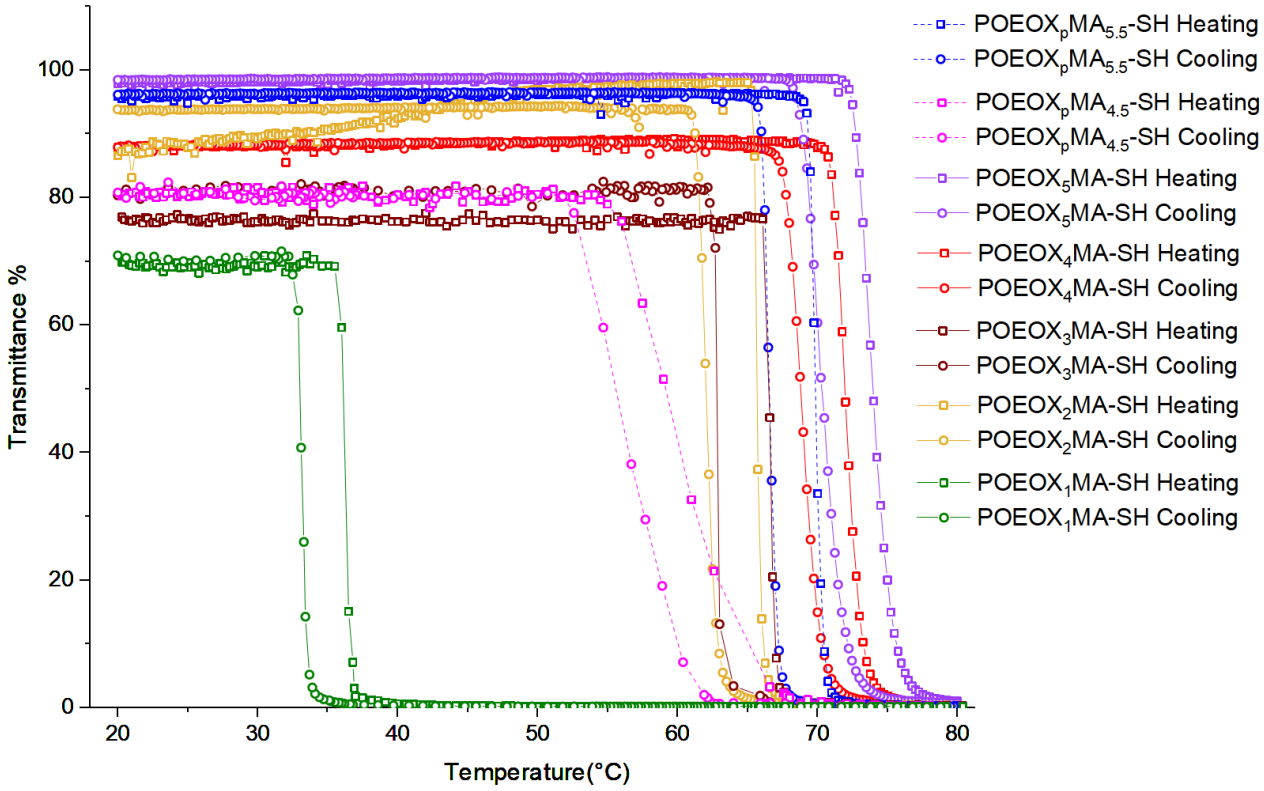

Figure 52 Plot of transmittance % vs temperature during heating and cooling cycle for all polymers (first measure).

From the plots obtained by performing a heating and cooling cycle (20°C ↔ 80 °C), it is possible to observe a hysteresis behaviour in all the curves, that resulted in a $T_{c,Cool}$ measured that was always 3 – 4 °C lower than the $T_{c,Heat}$ for the same polymer (Figure 52). This behaviour is extensively reported for many types of polymer chains that show aggregation in water, and its due to the formation of additional intermolecular or intramolecular interactions upon aggregation, which remain present during the cooling process at temperatures lower than the cloud point measured during heating.

In particular, for poly(*N*-isopropylacrylamide) (PNIPAM), this phenomenon is attributed to the formation of intrachain and interchain hydrogen bonds between carbonyl and amide moieties[61] (C=O---H-N), while for polymers that cannot form intramolecular hydrogen bond like poly(*N,N*-diethylacrylamide) (PDEAM), the hysteresis behaviour is dependent on the rate of heating, having a kinetic nature[62] (*i.e.*, chain contraction and association cannot follow the temperature change, being far from thermodynamic equilibrium). For the POEOXMA comb polymers synthetised in this work, since they have a structure similar to

PDEAM, (*i.e.*, tertiary amides), no additional inter/intramolecular hydrogen bonds can form, hence hysteresis could be attributed to the high heating rate at which the LCST experiments were performed (1 °C/min).

In some of the cycles, the polymer solutions showed partial clouding at room temperature, that slowly rose back to a stable value after the start of the analysis (like $POEOX_2MA$) or did not rose back at all (like $POEOX_1MA$). This could be due to an inadequate equilibration time at the beginning of the experiment, or to the partial insolubility of the polymer at room temperature (which is likely for $POEOX_1MA$, since it has the lowest T_c).

In literature, there are reported studies on how side-chain length on polydisperse $POEOX_pMA$ comb polymers influences LCST. In particular, for polymethacrylates with high molar weight OEOX side chains ($\overline{DP}$ > 5), there is no significant influence of the lateral side chain length on the cloud point temperature, since turbidity measures showed that $POEOX_pMA$ with same main-chain DP and different, high side-chain DP have almost the same T_c. On the other hand, this is not true for polymethacrylates with low molecular weight OEOX side chains ($\overline{DP}$ = 5), for which there is an influence of side chain DP on T_c, with a LCST behaviour similar to linear PEOXAs[59]. Indeed, $POEOX_pMA$s with a side chain $\overline{DP}$ = 5 showed higher cloud point temperatures than $POEOX_pMA$s with a side chain $\overline{DP}$ > 5. This can be rationalized by assuming that longer side chains becomes more and more difficult to hydrate, since the main chain becomes less accessible by water molecules, making $POEOX_pMA$s with smaller side chains more water-soluble, hence increasing their T_c (Figure 53). For these reasons, $POEOX_pMA$ comb polymers in solution behave more similar to linear PEOXAs than to their corresponding oligo(ethylene glycol) comb polymers (POEGMA).

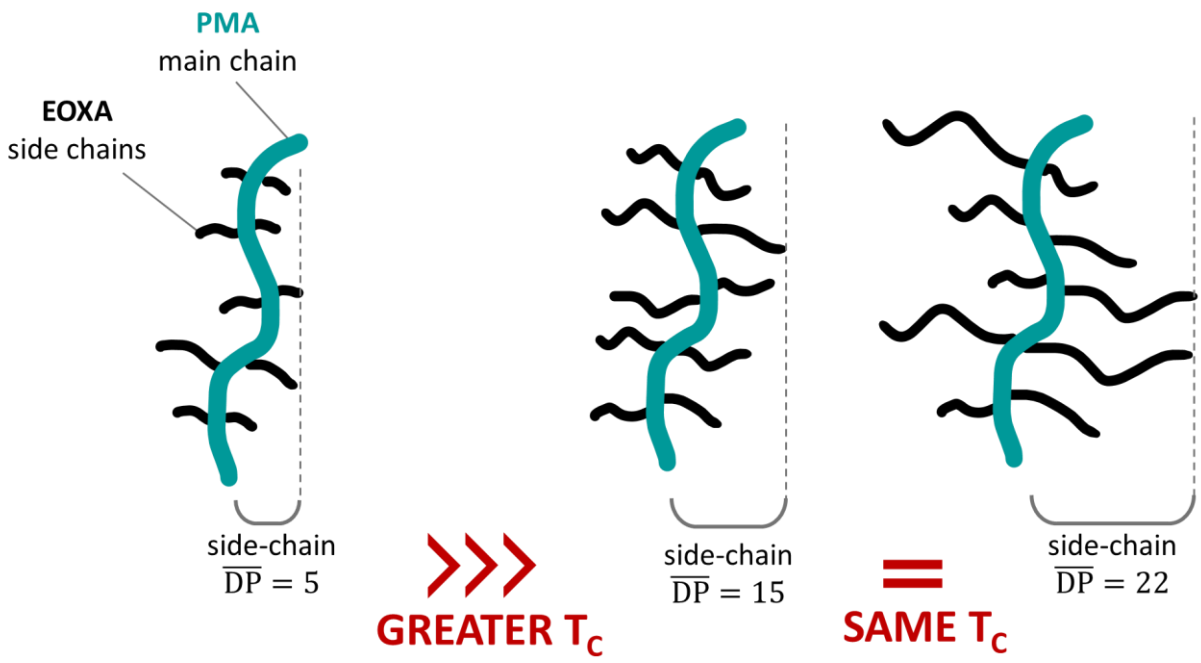

Figure 53 Influence of EOXA side-chain length on comb-like POEOXMA polydisperse polymers as reported by Weber et al.[59].

However, these studies do not investigate what happens to LCST when studying POEOXMA comb polymers with side chain $\overline{DP} \leq 5$, and furthermore with side chains of defined length (instead of a distribution centred around $\overline{DP}$). In this work, an interesting behaviour emerged when going from polydisperse to monodisperse, in terms of LCST and water solubility.

By comparing the $T_{c,Heat}$ plotted for discrete side chain lengths from n = 1 to n = 5 (Figure 54, full squares), a trend of increasing clouding temperatures among polymers bearing monodisperse side chains can be observed; in particular, $POEOX_1MA$ presents a much lower cloud point temperature than the other $POEOX_nMAs$, while the ones with lateral chain length from n = 2 to n = 5 have an almost linear increasing trend. This could mean that, when exploring a region of OEOX side chain length in the range of 1 to 5, discrete $POEOX_nMA$ comb polymers behave similar to discrete $POEG_nMA$ in terms of water-solubility.

The value of $T_{c,Heat}$ found for $POEOX_1MA$ is actually close to the T_c measured by Muljajew *et al.*[63] for PMMA-co-POEOXA comb polymers (copolymers obtained from RAFT polymerization of OEOXMA in the presence of MMA monomers), which resulted as T_c = 37 °C for a 17/83 OEOXMA/MMA ratio comb polymer (with a side chain $\overline{DP}$ = 5). This could mean that having discrete side chains of only one repeating unit of EOXA can drastically

reduce the hydrophilic contribution of oxazolines to the overall solubility of the polymer, making the hydrophobic contribution of the methacrylate main chain more predominant.

It is interesting to see that, as side chains size increases, the comb polymers become more water soluble and the cloud point of the solution increases, suggesting that longer monodisperse OEOX side chains make the polymer more hydrophilic. This behaviour is opposed to what was found for linear PEOXAs[64], which become less hydrophilic and less water-soluble as the chains become longer, and can be explained through a theoretical point of view, by considering two main factors:

1. For high molecular weight linear PEOXAs, water solubility decreases as the chain becomes longer due to bigger chains being more difficult to hydrate, since they might tend to assume coiled or globular conformations.
2. This effect is negligible for short linear OEOXAs (such as the oligomers produces in this work), since they are mostly water soluble and do not exhibit LCST behaviour, but there could be a trend of increasing polarity from n = 1 to n = 5 that might influence how they behave as side chains in a comb polymer. This observation is based on their interaction with a silica stationary phase, since in the column separation performed in this work, shorter oligomers seemed to elute better in less polar solvent (like DCM), while increasing the polarity by adding a percentage of MeOH in the mobile phase would better elute all the oligomers, specifically helping separate oligomers with higher chain length (*e.g.*, $OEOX_nMA$ with $n \geq 3$), that otherwise would not be eluted in a less polar mobile phase.

This might prove that, at least for $OEOX_nMA$s with n varying from 1 to 5, their polarity increases with increasing chain length, probably due to the increasing quantity of oxygen and nitrogen atoms that act as H-bond acceptor, making the chains more easily solvated by water molecules (*i.e.,* behaving more like small molecules than linear polymers). By extending this principle to the comb polymers obtained from the above mentioned $OEOX_nMA$s, the trend of water solubility of the final $POEOX_nMA$s can be rationalised: by increasing the discrete length of OEOX side chains from 1 to 5, the hydrophilic contribution of oxazoline moieties to the overall solubility of the polymer increases. Because of that, $POEOX_5MA$ will be the most hydrophilic comb polymer in the 1 to 5 series, while $POEOX_1MA$ will be the least hydrophilic one. It is important to note that there could be other, more complex, contribution to this behaviour, such as the less accessibility to the hydrophobic backbone in $POEOX_nMA$s with longer side chains. Moreover, the effect of longer discrete

side chain length with n > 5 must be further investigated, in order to determine to what extent side chain hydrophilicity can influence the overall polymer solubility, and if there is an actual inversion of the trend over a certain OEOX side chain length, making them behave like linear PEOXAs.

Focusing on polydisperse $POEOX_pMAs$ (Figure 54, half squares), an interesting behaviour seems to emerge. Their values of $T_{c,Heat}$ and $T_{c,Cool}$ are lower than expected, with $POEOX_pMA_{4.5}$ being less soluble than all the polymers except $POEOX_1MA$, and $POEOX_pMA_{5.5}$ being less soluble than $POEOX_4MA$ and $POEOX_5MA$. A comparison can be made based on a case reported in literature by Weber *et al.*[59], which measured values of T_c for $POEOX_pMAs$ with side chain $\overline{DP}$ = 5 at around 84 - 85 °C, hence being much higher than the T_c measured for both the polydisperse $POEOX_pMAs$ produced in this work. This difference might be deriving from how the polydisperse OEOX side chains are actually distributed around the central value indicated as $\overline{DP}$.

In this thesis, the relative quantities of each oligomer species present in the polydisperse mixtures were determined through MS analysis and, by assuming that every oligomer species reacted in the same amount to form the final polymers, the side-chain composition of $POEOX_pMA$ comb polymers should reflect the one of their parent oligomer mixtures. This could be verified by calculating the $\overline{DP}$ of the lateral chains on the polydisperse polymers through ^{1}H-NMR (normalized to the signal of O-CH_2- protons at 4.05 ppm) (see supporting information).

For $POEOX_pMA_{4.5}$, its low values of T_c can be explained by considering that, from MS analysis, there is a 7.7 % of $OEOX_1MAs$, which is not a negligible amount compared to the most present species (18.3 % of $OEOX_4MA$, 17.8 % of $OEOX_5MA$). This percentage of lateral chains with n = 1 might contribute to lower the cloud point temperature; indeed, the low value of T_c found for polymers bearing monodisperse $OEOX_1$ side chains might contribute to the final T_c of polymers bearing polydisperse side chains, making them less water-soluble in a way that is proportional to the relative quantity of $OEOX_1$ side chains present among the polydisperse mixture. However, further studies need to be performed, for example by isolating $OEOX_nMAs$ with n > 5, measuring the T_c of their resulting comb polymers, and verifying if the average of the T_c for $POEOX_nMAs$ with discrete side chains, weighted by their relative quantities present in the oligomer mixture with $\overline{DP}$ = 4.5, actually matches the T_c measured for the $POEOX_pMA_{4.5}$ polymer. The weighted average could be calculated with the formula:

$$T_c\left(POEOX_pMA_{4.5}\right) = \frac{I\%_1 T_{c,1} + I\%_2 T_{c,2} + I\%_3 T_{c,3} + \cdots}{T_{c,1} + T_{c,2} + T_{c,3} + \cdots}$$

where I% is the relative quantity of a certain oligomer present in the parent mixture and T_c is the cloud point temperature measured for the comb polymers obtained from that discrete oligomer.

The same effect is observed for $POEOX_pMA_{5.5}$ but, since its distribution is centred towards longer oligomer species, it has a lower quantity of $OEOX_1MA$ (6.1 %), and the contribute of longer side chain is higher (having higher dispersity), therefore the lowering effect of $OEOX_1$ in the lateral chains is reduced. Even in this case, an average of the cloud point temperatures weighted by the relative quantities of oligomers present in the mixture might help confirming these hypotheses.

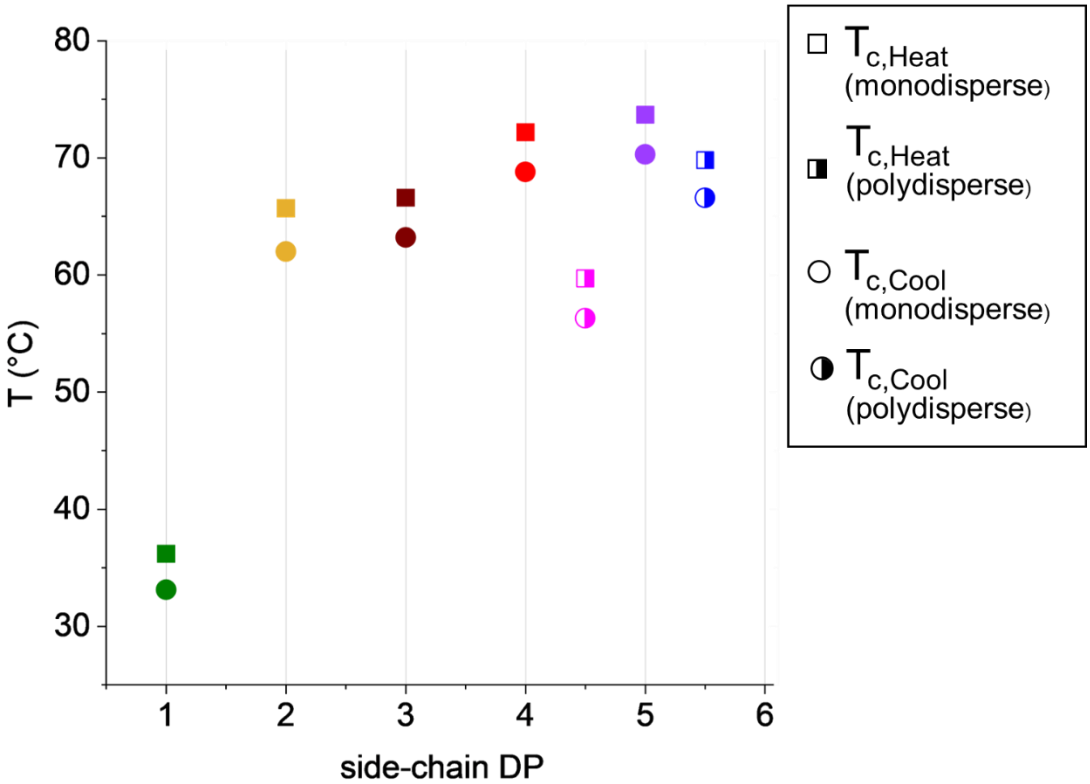

Figure 54 Plot of cloud point temperature during heating ($T_{c,Heat}$) and cooling ($T_{c,Cool}$) measured for $POEOX_nMAs$ with different discrete side chain length (full squares, full circles) and $POEOX_pMAs$ with different distribution of polydisperse side chain lengths (half squares, half circles).

All the statement made for the cloud point temperature during heating $T_{c,Heat}$ can be made for the cloud point temperature during cooling $T_{c,Cool}$, since it followed an almost identical trend.

In conclusion, by exploring how discrete, low molecular OEOX side chain in the range of 1 to 5 repeating units can influence the water-solubility of their respective comb polymers ($POEOX_nMA$, n discrete), a novel trend has been observed, since there is an increase of the hydrophilicity with increasing monodisperse side chain length, opposed to what was found for $POEOX_pMA$ comb polymers with polydisperse, high molecular weight OEOX side chain. Instead, $POEOX_nMA$ with $n \leq 5$ behaved similar to $POEG_nMA$ with discrete, low molecular weight OEG side chains. Moreover, the T_c of comb polymers with polydisperse, low molecular weight OEOX side chains ($POEOX_pMA$) seem to be influenced by the quantity of each oligomer species present and their contribution to water-solubility. Specifically, for the $POEOX_pMA_{4.5}$ and $POEOX_pMA_{5.5}$ synthetised in this work, their T_c ended up lower than most of the $POEOX_nMA$ examined due to the heavy contribute of $OEOX_1$ oligomers in the side chains, which lowers the overall water-solubility of the comb polymer.

CHAPTER 4: CONCLUSIONS AND FUTURE PERSPECTIVES

In this thesis, a library of poly[oligo(2-ethyl-2-oxazoline)methacrylate]s comb polymers were synthetised by first performing a CROP on 2-ethyl-2-oxazoline monomers, to obtain a mixture of polydisperse oligo(2-ethyl-2-oxazoline)methacrylate, and then separating them into discrete oligomers with defined chain length through flash column chromatography, focusing on $OEOX_nMAs$ with n from 1 to 5. Then, each discrete oligomer was polymerized through RAFT polymerization to obtain the final $POEOX_nMAs$, with n discrete. For comparison, RAFT polymerization was performed also on the polydisperse oligomer mixtures, to obtain two species of $POEOX_pMA$ with side chain $\overline{DP}$ of 4.5 and 5.5 respectively.

$OEOX_pMAs$ were successfully synthesized via cationic ring-opening polymerization of 2-ethyl-2-oxazoline, with conversions above 90% (almost complete monomer incorporation) and final $\overline{DP}$ that matched the expected monomer-to-initiator ratios, demonstrating reliable control over chain length. UHPLC-MS analysis confirmed the $\overline{DP}$ found and allowed to calculate the relative quantities of each oligomer species in the polydisperse mixtures, together with other important parameters like M_n, M_w and *Đ*. Overall, all batches exhibited high conversion, consistent molecular structure and reproducible synthesis, confirming that CROP of 2-ethyl-2-oxazoline is a reliable method for obtaining oligomers with controlled average chain lengths.

Flash column chromatography with DCM:MeOH gradient (100 % DCM to 95:5 DCM:MeOH) enabled quantitative separation of discrete $OEOX_nMAs$ from n = 1 to n = 5, and each species could be completely characterized through MS and ^{1}H-NMR, confirming the monodispersity of each oligomer obtained. Overall, the method proved effective for quantitative separation of $OEOX_nMAs$ but was limited to low molecular weight species and for crude mass of 1 - 2 g. Further optimization can be made by finely tuning the gradient or using high pressure, possibly employing automated instruments like automated high pressure column chromatography.

RAFT polymerization of $OEOX_nMAs$ was successfully achieved using a methylated CTA (MCDP), targeting a DP of 50. Conversions after 24 hours were over 70 %, with higher conversions (>90%) for polydisperse monomers ($OEOX_pMA_{4.5}$ and $OEOXpMA_{5.5}$). GPC analysis measured *Đ* in a range of 1.20 and 1.67, indicating a mostly controlled polymerization, and an increasing M_n with increasing side chain length, consistent with the expected trend. End capping of the polymers with thiols through aminolysis of terminal

trithiocarbonyl group was successful, as shown by the disappearing of the UV-Vis absorbance bands related to the trithiocarbonyl moieties.

Cloud point temperatures calculated through turbidity measurements showed a trend of increasing T_c with increasing side chain length for monodisperse $POEOX_nMA$ comb polymers, with $POEOX_1MA$ being far less water soluble than the other ones. Hysteresis was observed for all the POEOXMAs, deriving from the kinetic nature of the experiment, since at high heating rates the system is not fully at equilibrium. This resulted in values of cloud point temperatures during heating and cooling cycles that differed for 3 - 4 °C. Moreover, a comparison between $POEOX_nMA$ with monodisperse side chains and $POEOX_pMA$ with polydisperse side chains showed that having a discrete defined macromolecular structure can profoundly change proprieties like water-solubility. Indeed, $POEOX_nMA$ with n = 2, 3, 4 and 5 ended up being more water soluble than $POEOX_pMA_{4.5}$, while $POEOX_pMA_{5.5}$ still resulted less water-soluble than $POEOX_nMA$ with n = 4 and n = 5. This means that a precise control over side chain length and dispersity could help finely tune the thermoresponsiveness and hydrophilicity of comb polymers or graft polymers. However, to fully understand why polydisperse $POEOX_pMAs$ are much less water-soluble than their respective monodisperse $POEOX_nMAs$, further studies need to be performed, by isolating discrete oligomers with n > 5 and measuring the T_c of their resulting comb polymers.

In conclusion, further studies need to be performed to fully cover all the possible parameters that could influence water-solubility for this class of polymers, such as the influence of longer, discrete OEOX side chains, or the dispersity of the parent mixture of oligomers on T_c of $POEOX_pMA$ with polydisperse side chains. Another interesting system that could be studied would consist of polymers obtained from combining two species of discrete oligomers (*e.g.,* $OEOX_1MA$ and $OEOX_2MA$) in a RAFT co-polymerization, resulting in comb polymers with only two discrete side chain lengths, to verify if their resulting cloud point temperatures would fill the “gaps” of the T_c vs n plot presented in this work.

Other further applications of this study would be testing the interaction with water when POEOXMAs are grafted to gold surfaces (through the terminal -SH functionalities) and furthermore testing the interaction with proteins of the human serum. This could help studying how stealth proprieties in biological environment vary with different discrete side chain lengths. Indeed, going in this direction might help find the most optimal alternative to PEG, by modulating hydrophilicity, or even finding applications for the thermoresponsiveness of this comb polymers in drug delivery systems.

BIBLIOGRAPHY

[1] B. Jaquet, D. Wei, B. Reck, F. Reinhold, X. Zhang, H. Wu, M. Morbidelli, *Colloid Polym. Sci.* **2013**, *291*, 1659.

[2] A. Gaisinskaya, L. Ma, G. Silbert, R. Sorkin, O. Tairy, R. Goldberg, N. Kampf, J. Klein, *Faraday Discuss.* **2012**, *156*, 217.

[3] H. Yang, Y. Wang, L. Yao, J. Wang, H. Chen, *Langmuir* **2025**, *41*, 6471.

[4] K. B. Bjugstad, D. E. Redmond, K. J. Lampe, D. S. Kern, J. R. Sladek, M. J. Mahoney, *Cell Transplant.* **2008**, *17*, 409.

[5] A. A. D'souza, R. Shegokar, *Expert Opin. Drug Deliv.* **2016**, *13*, 1257.

[6] M. A. Bruusgaard-Mouritsen, J. D. Johansen, L. H. Garvey, *Clin. Exp. Allergy* **2021**, *51*, 463.

[7] P. Zhang, F. Sun, S. Liu, S. Jiang, *J. Controlled Release* **2016**, *244*, 184.

[8] N. J. Ganson, S. J. Kelly, E. Scarlett, J. S. Sundy, M. S. Hershfield, *Arthritis Res. Ther.* **2005**, *8*, R12.

[9] K. Aoi, *Prog. Polym. Sci.* **1996**, *21*, 151.

[10] R. W. Lenz, *Organic Chemisty of Synthetic High Polymers*, 1st edn., John Wiley & Sons: New York, **1967**.

[11] B. Verbraeken, B. D. Monnery, K. Lava, R. Hoogenboom, *Eur. Polym. J.* **2017**, *88*, 451.

[12] L. Trachsel, M. Romio, S. N. Ramakrishna, E. M. Benetti, *Adv. Mater. Interfaces* **2020**, *7*, 2000943.

[13] I. Yildirim, T. Bus, M. Sahn, T. Yildirim, D. Kalden, S. Hoeppener, A. Traeger, M. Westerhausen, C. Weber, U. S. Schubert, *Polym. Chem.* **2016**, *7*, 6064.

[14] J. Tong, X. Yi, R. Luxenhofer, W. A. Banks, R. Jordan, M. C. Zimmerman, A. V. Kabanov, *Mol. Pharm.* **2013**, *10*, 360.

[15] G. Morgese, E. Cavalli, M. Müller, M. Zenobi-Wong, E. M. Benetti, *ACS Nano* **2017**, *11*, 2794.

[16] T. Lorson, M. M. Lübtow, E. Wegener, M. S. Haider, S. Borova, D. Nahm, R. Jordan, M. Sokolski-Papkov, A. V. Kabanov, R. Luxenhofer, *Biomaterials* **2018**, *178*, 204.

[17] Protein adsorption on tailored oligo(ethylene glycol) surfaces - ProQuest. https://www.proquest.com/openview/2381a8b5524a06425328cd8173aa2e48/1?cbl=18750&diss=y&pq-origsite=gscholar (accessed March 26, 2025).

[18] P. Tang, School of Engineering and Materials science, Queen Mary University of London **2017**.

[19] T. Saegusa, H. Ikeda, *Macromolecules* **1973**, *6*, 808.

[20] O. Nuyken, G. Maier, A. Groß, H. Fischer, *Macromol. Chem. Phys.* **1996**, *197*, 83.

[21] G. H. Hsiue, A. X. Swamikannu, M. H. Litt, *J. Polym. Sci. Part Polym. Chem.* **1988**, *26*, 3043.

[22] B. Guillerm, S. Monge, V. Lapinte, J. Robin, *Macromol. Rapid Commun.* **2012**, *33*, 1600.

[23] S. Kobayashi, E. Masuda, S. Shoda, Y. Shimano, *Macromolecules* **1989**, *22*, 2878.

[24] J. M. Warakomski, B. P. Thill, *J. Polym. Sci. Part Polym. Chem.* **1990**, *28*, 3551.

[25] F. Wiesbrock, R. Hoogenboom, M. A. M. Leenen, M. A. R. Meier, U. S. Schubert, *Macromolecules* **2005**, *38*, 5025.

[26] S. Perrier, *Macromolecules* **2017**, *50*, 7433.

[27] D. J. Keddie, *Chem Soc Rev* **2014**, *43*, 496.

[28] T. N. Myers, in *Encyclopedia of Polymer Science and Technology* (Ed.: H. F. Mark), Wiley, **2002**.

[29] M. A. C. Stuart, W. T. S. Huck, J. Genzer, M. Müller, C. Ober, M. Stamm, G. B. Sukhorukov, I. Szleifer, V. V. Tsukruk, M. Urban, F. Winnik, S. Zauscher, I. Luzinov, S. Minko, *Nat. Mater.* **2010**, *9*, 101.

[30] C. Feng, X. Huang, *Acc. Chem. Res.* **2018**, *51*, 2314.

[31] C. W. Pester, E. M. Benetti, *Adv. Mater. Interfaces* **2022**, *9*, 2201439.

[32] D. Rana, T. Matsuura, *Chem. Rev.* **2010**, *110*, 2448.

[33] O. J. Uwaezuoke, P. Kumar, V. Pillay, Y. E. Choonara, *Drug Deliv. Transl. Res.* **2021**, *11*, 1903.

[34] J. L. Harding, M. M. Reynolds, *Trends Biotechnol.* **2014**, *32*, 140.

[35] W. Yang, Y. Gong, W. Li, *Front. Bioeng. Biotechnol.* **2021**, *8*, 622923.

[36] H. Okuyama, Y. Sugawara, T. Yamaguchi, *ACS Appl. Mater. Interfaces* **2024**, *16*, 25236.

[37] I. Szleifer, *Biophys. J.* **1997**, *72*, 595.

[38] *Polymer Surfaces and Interfaces*, Ed.: M. Stamm, Springer Berlin Heidelberg: Berlin, Heidelberg, **2008**.

[39] S. Wang, Z. Wang, J. Li, L. Li, W. Hu, *Mater. Chem. Front.* **2020**, *4*, 692.

[40] S. Chen, L. Li, C. Zhao, J. Zheng, *Polymer* **2010**, *51*, 5283.

[41] J. C. Conrad, M. L. Robertson, *JACS Au* **2023**, *3*, 333.

[42] K. E. B. Doncom, L. D. Blackman, D. B. Wright, M. I. Gibson, R. K. O'Reilly, *Chem. Soc. Rev.* **2017**, *46*, 4119.

[43] A. Lo Bocchiaro, C. Pavón, F. Lorandi, E. M. Benetti, *Prog. Polym. Sci.* **2025**, *167*, 101992.

[44] F. P. B. Van Der Maeden, M. E. F. Biemond, P. C. G. M. Janssen, *J. Chromatogr. A* **1978**, *149*, 539.

[45] E. A. Murphy, C. Zhang, C. M. Bates, C. J. Hawker, *Acc. Chem. Res.* **2024**, *57*, 1202.

[46] Y. Wang, X. Tan, Y. Zhang, D. J. T. Hill, A. Zhang, D. Kong, C. J. Hawker, A. K. Whittaker, C. Zhang, *Macromolecules* **2024**, *57*, 11753.

[47] N. D. Ogbonna, M. Dearman, C.-T. Cho, B. Bharti, A. J. Peters, J. Lawrence, *JACS Au* **2022**, *2*, 898.

[48] M. Romio, B. Grob, L. Trachsel, A. Mattarei, G. Morgese, S. N. Ramakrishna, F. Niccolai, E. Guazzelli, C. Paradisi, E. Martinelli, N. D. Spencer, E. M. Benetti, *J. Am. Chem. Soc.* **2021**, *143*, 19067.

[49] B. Van Genabeek, B. A. G. Lamers, C. J. Hawker, E. W. Meijer, W. R. Gutekunst, B. V. K. J. Schmidt, *J. Polym. Sci.* **2021**, *59*, 373.

[50] R. V. Iozzo, L. Schaefer, *Matrix Biol.* **2015**, *42*, 11.

[51] J. Seror, Y. Merkher, N. Kampf, L. Collinson, A. J. Day, A. Maroudas, J. Klein, *Biomacromolecules* **2011**, *12*, 3432.

[52] S. Joshi, M. Kaushik, M. Agarwal, M. Daruka, *IP Int. J. Periodontol. Implantol.* **2023**, *8*, 65.

[53] C. Pavón, A. Grigoletto, V. Kempkes, A. Eguskiza, M. Morbidelli, R. Fiammengo, E. Papini, A. Mattarei, G. Pasut, K. Matyjaszewski, F. Lorandi, E. M. Benetti, *JACS Au* **2025**, *5*, 4519.

[54] T. K. Kwei, T. T. Wang, in *Polymer Blends*, Elsevier, **1978**, pp 141.

[55] K. Van Durme, G. Van Assche, E. Nies, B. Van Mele, *J. Phys. Chem. B* **2007**, *111*, 1288.

[56] D. R. Paul, *Polymer Blends Volume 1*, Elsevier, **2012**.

[57] Q. Zhang, C. Weber, U. S. Schubert, R. Hoogenboom, *Mater. Horiz.* **2017**, *4*, 109.

[58] C. Weber, R. C. Becer, A. Baumgaertel, R. Hoogenboom, U. S. Schubert, *Des. Monomers Polym.* **2009**, *12*, 149.

[59] C. Weber, C. R. Becer, R. Hoogenboom, U. S. Schubert, *Macromolecules* **2009**, *42*, 2965.

[60] J. Lutz, *J. Polym. Sci. Part Polym. Chem.* **2008**, *46*, 3459.

[61] Y. Ding, X. Ye, G. Zhang, *Macromolecules* **2005**, *38*, 904.

[62] Y. Lu, K. Zhou, Y. Ding, G. Zhang, C. Wu, *Phys. Chem. Chem. Phys.* **2010**, *12*, 3188.

[63] I. Muljajew, C. Weber, I. Nischang, U. S. Schubert, *Materials* **2018**, *11*, 528.

[64] R. Hoogenboom, H. M. L. Thijs, M. J. H. C. Jochems, B. M. Van Lankvelt, M. W. M. Fijten, U. S. Schubert, *Chem. Commun.* **2008**, 5758.

SUPPORTING INFORMATIONS

^{1}H-NMR spectra of purified OEOX$_p$MAs

<u>OEOX$_p$MA$_{1.7}$</u>

^{1}H-NMR (400 MHz, $CDCl_3$): δ 6.06 (s, 1H), 5.60 (m, 1H), 4.26 (m, 2H), 3.50 (m), 3.01 (m, 3H), 2.32 (m), 1.91 (s, 3H), 1.10, (m).

$$\overline{\mathrm{DP}}\,(\mathrm{CH_2}) = \frac{3.24}{2} \approx 1.6$$

$$\overline{\mathrm{DP}}\,(\mathrm{CH_3}) = \frac{4.90}{3} \approx 1.6$$

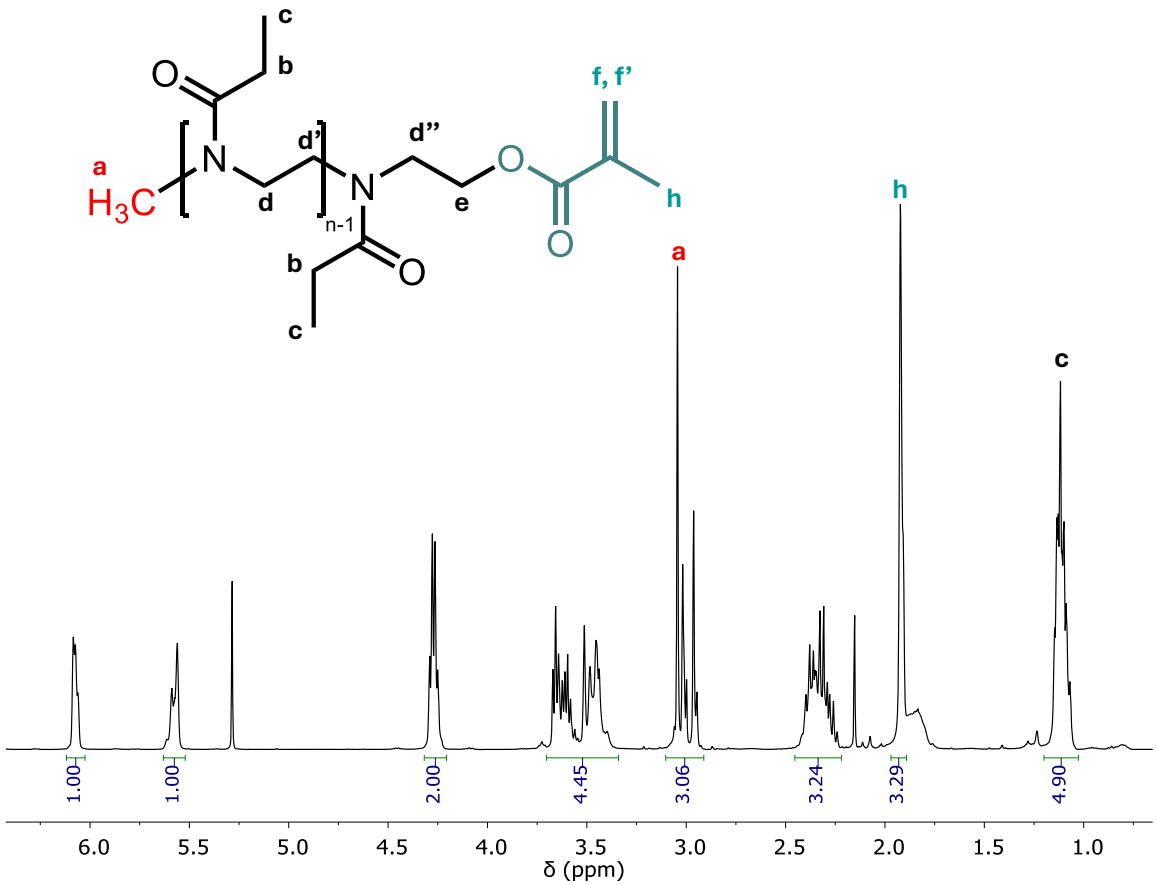

Figure 55 ^{1}H-NMR spectrum of OEOX$_p$MA$_{1.7}$.

OEOX$_p$MA$_{5.5}$

^{1}H-NMR (400 MHz, $CDCl_3$): δ 6.06 (s, 1H), 5.60 (m, 1H), 4.26 (m, 2H), 3.50 (m), 3.01 (m, 3H), 2.32 (m), 1.91 (s, 3H), 1.10, (m).

$$\overline{\mathrm{DP}}\,(\mathrm{CH_2}) = \frac{11.53}{2} \approx 5.8$$

$$\overline{\mathrm{DP}}\,(\mathrm{CH_3}) = \frac{16.96}{3} \approx 5.6$$

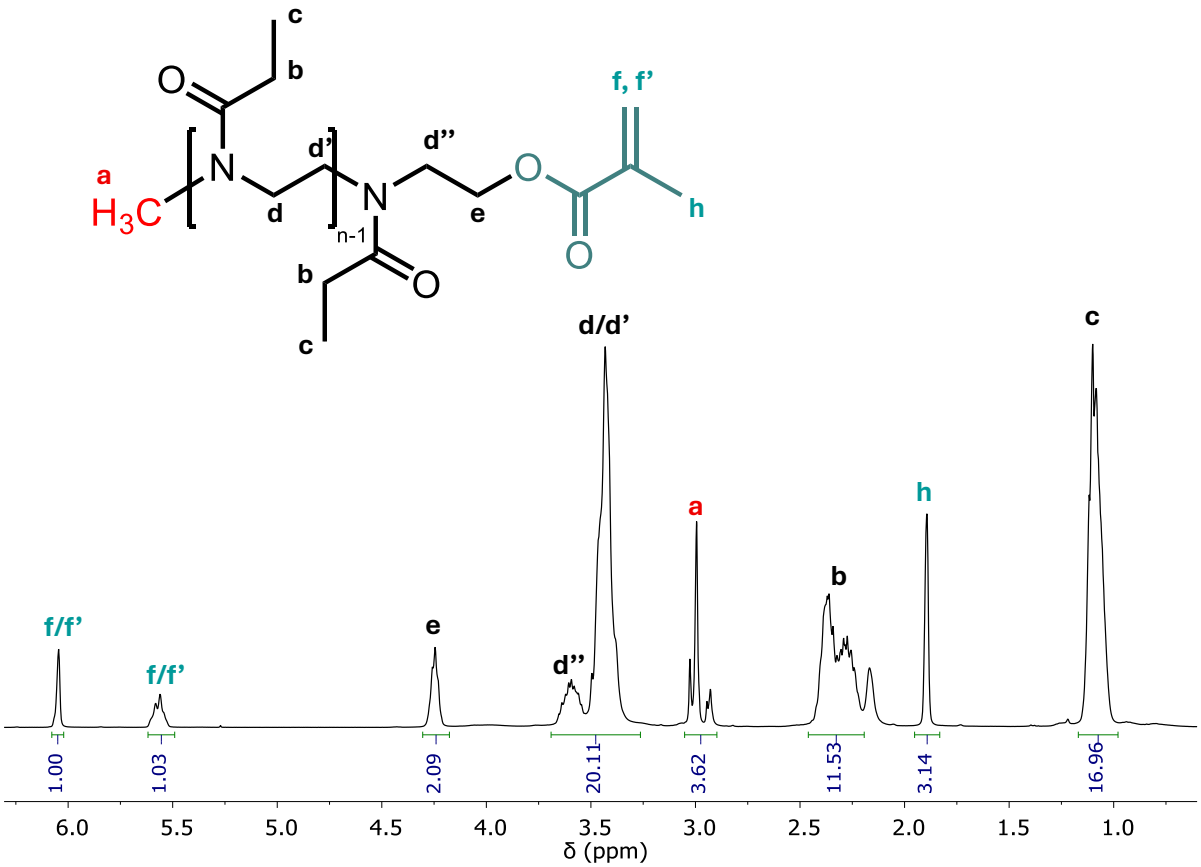

Figure 56 ^{1}H-NMR spectrum of OEOX$_p$MA$_{5.5}$.

OEOX$_p$MA$_{4.5}$

^{1}H-NMR (400 MHz, $CDCl_3$): δ 6.06 (s, 1H), 5.60 (m, 1H), 4.26 (m, 2H), 3.50 (m), 3.01 (m, 3H), 2.32 (m), 1.91 (s), 1.10, (m).

$$\overline{\mathrm{DP}}\,(\mathrm{CH_2}) = \frac{8.87}{2} \approx 4.4$$

$$\overline{\mathrm{DP}}\,(\mathrm{CH_3}) = \frac{13.93}{3} \approx 4.6$$

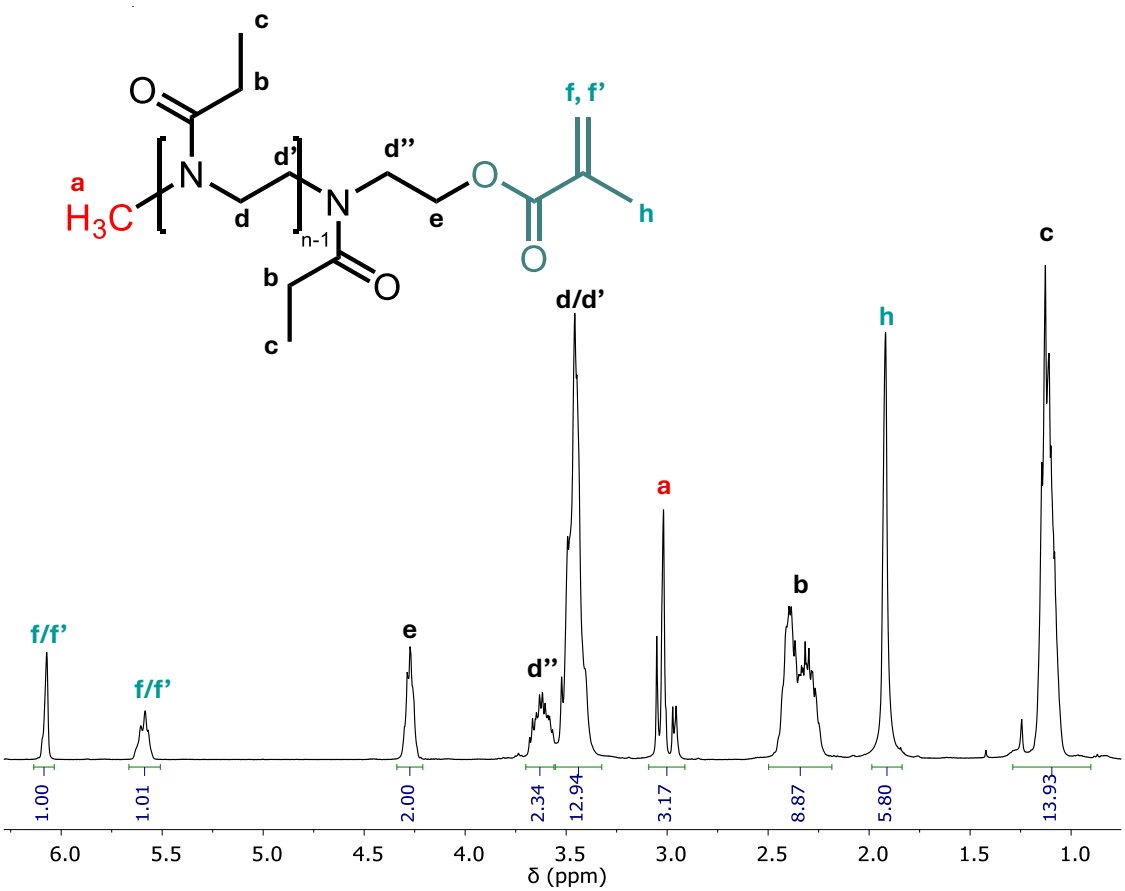

Figure 57 ^{1}H-NMR spectrum of OEOX$_p$MA$_{4.5}$.

MS analysis of OEOX$_p$MAs

DAD elugrams

OEOX$_p$MA$_{1.7}$

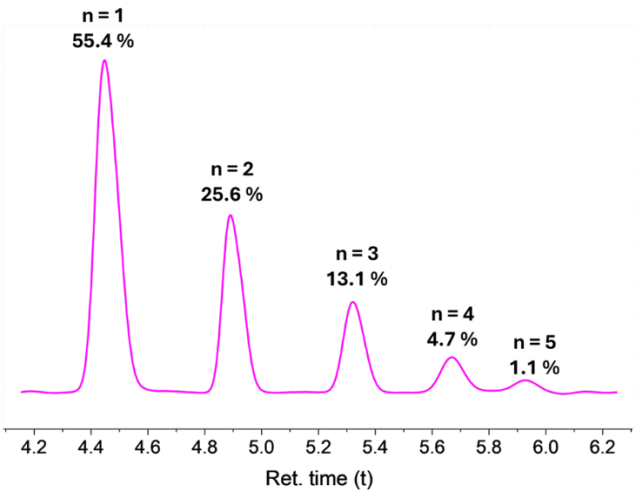

Ret. Time (min)	Integrals	Relative ratios (%)	Exact mass $[M+H]^+$	n
4.45	1455.82	55.4	200.1281	1
4.89	672.92	25.6	299.1969	2
5.32	345.30	13.1	398.2657	3
5.67	122.70	4.7	497.3342	4
5.93	30.15	1.1	596.4023	5

M_n	M_w	Đ	$\overline{DP}$
270.0	119.5	/	1.7

Figure 58 DAD elugram (left), peaks table and calculated parameters for OEOX$_p$MA$_{4.5}$ (right).

OEOX$_p$MA$_{4.5}$

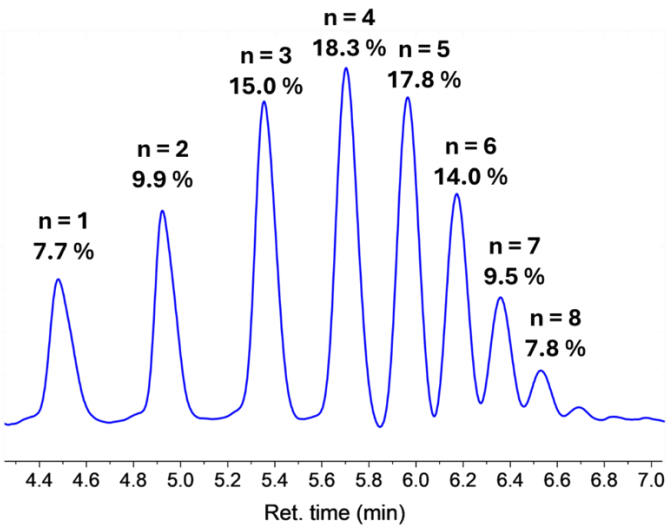

Ret. Time (min)	Integrals	Relative ratios (%)	Exact mass $[M+H]^+$	n
4.48	188.16	7.7	200.1281	1
4.92	241.29	9.9	299.1969	2
5.35	366.34	15.0	398.2657	3
5.70	444.74	18.3	497.3342	4
5.96	434.44	17.8	596.4023	5
6.18	340.85	14.0	695.4717	6
6.36	230.37	9.5	794.5393	7
6.54	190.2	7.8	893.6079	8

M_n	M_w	Đ	$\overline{DP}$
544.3	613.8	1.13	4.5

Figure 59 DAD elugram (left), peaks table and calculated parameters for OEOX$_p$MA$_{4.5}$ (right).

OEOX$_p$MA$_{5.5}$

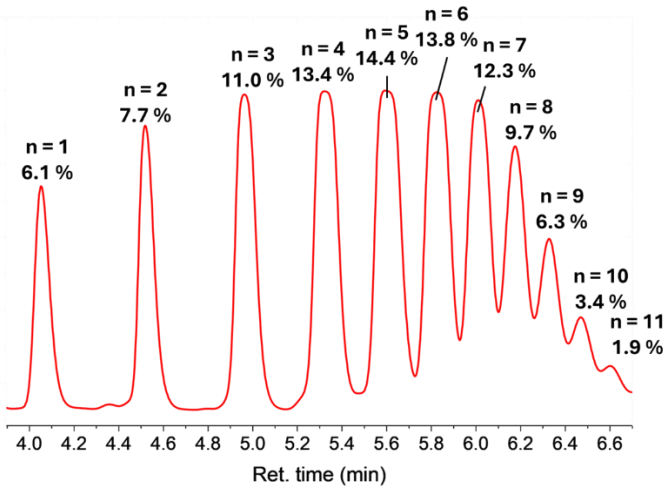

Ret. Time (min)	Integrals	Relative ratios (%)	Exact mass $[M+H]^+$	n
4.05	6048.00	6.1	200.1281	1
4.52	7700.09	7.7	299.1969	2
4.96	10972.35	11.0	398.2657	3
5.33	13337.39	13.4	497.3342	4
5.60	14336.39	14.4	596.4023	5
5.83	13757.85	13.8	695.4717	6
6.01	12236.38	12.3	794.5393	7
6.20	9678.96	9.7	893.6079	8
6.32	6245.12	6.3	922.6755	9
6.48	3341.44	3.4	1091.7435	10
6.60	1920.56	1.9	1190.8131	11

M_n	M_w	Đ	$\overline{DP}$
634.1	729.1	1.15	5.4

Figure 60 DAD elugram (left), peaks table and calculated parameters for OEOX$_p$MA$_{5.5}$ (right).

MS elugrams

OEOX$_p$MA$_{1.7}$

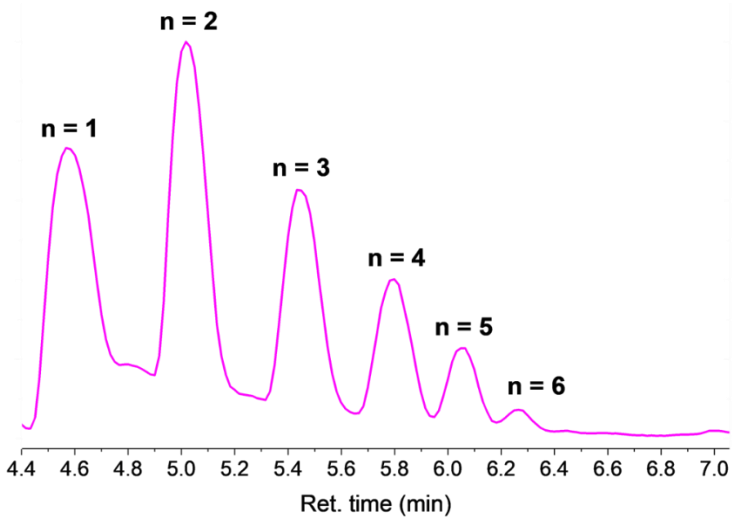

Ret. Time (min)	Exact mass $[M+H]^+$	n
4.57	200.1281	1
5.02	299.1969	2
5.45	398.2657	3
5.80	497.3342	4
6.05	596.4023	5
6.27	695.4717	6

Figure 61 MS elugram (left) and peaks table (right) for OEOX$_p$MA$_{1.7}$.

OEOX$_p$MA$_{4.5}$

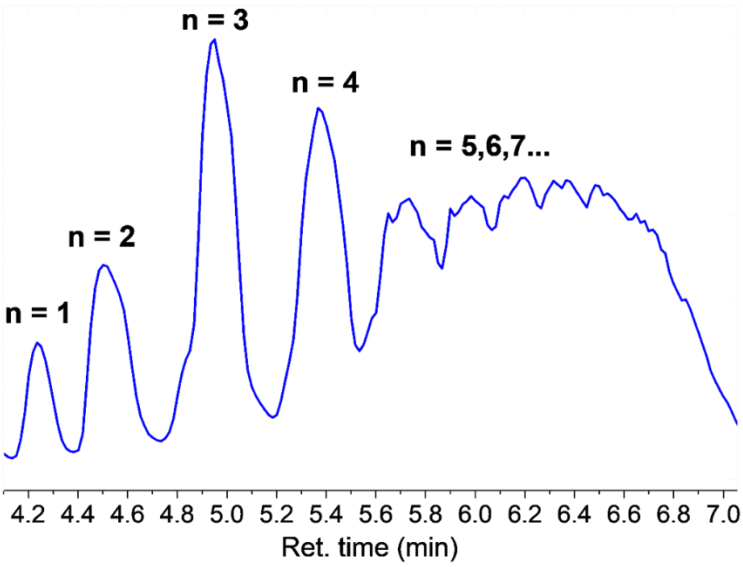

Ret. Time (min)	Exact mass $[M+H]^+$	n
4.24	200.1281	1
4.50	299.1969	2
4.95	398.2657	3
5.38	497.3342	4

Figure 62 MS elugram (left) and peaks table (right) for OEOX$_p$MA$_{4.5}$.

OEOX$_p$MA$_{5.5}$

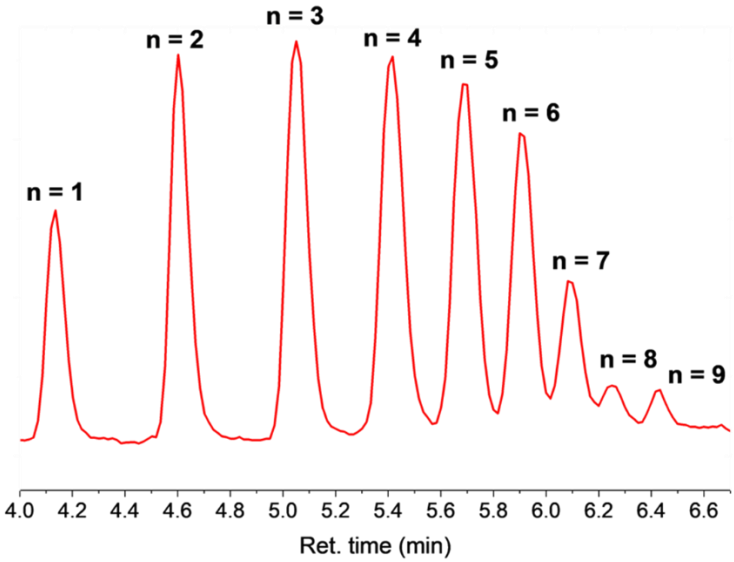

Ret. Time (min)	Exact mass $[M+H]^+$	n
4.13	200.1281	1
4.60	299.1969	2
5.05	398.2657	3
5.42	497.3342	4
5.69	596.4023	5
5.91	695.4717	6
6.09	794.5393	7
6.25	893.6079	8
6.43	922.6755	9

Figure 63 MS elugram (left) and peaks table (right) for OEOX$_p$MA$_{5.5}$.

^{1}H-NMR and MS spectra of isolated OEOX$_n$MAs

OEOX$_1$MA:

^{1}H-NMR (400 MHz, $CDCl_3$): δ 6.06 (s, 1H), 5.60 (s, 1H), 4.26 (t, 2H), 3.62 (dt, 2H), 3.01 (d, 3H), 2.32 (m, 2H), 1.91 (s, 3H), 1.10, (m, 3H).

MS-ESI (MeOH/H$^+$), signals from $C_{10}H_{17}NO_3$: [M+Na]$^+$ 222 m/z, [(M+1)+Na]$^+$ 223 m/z

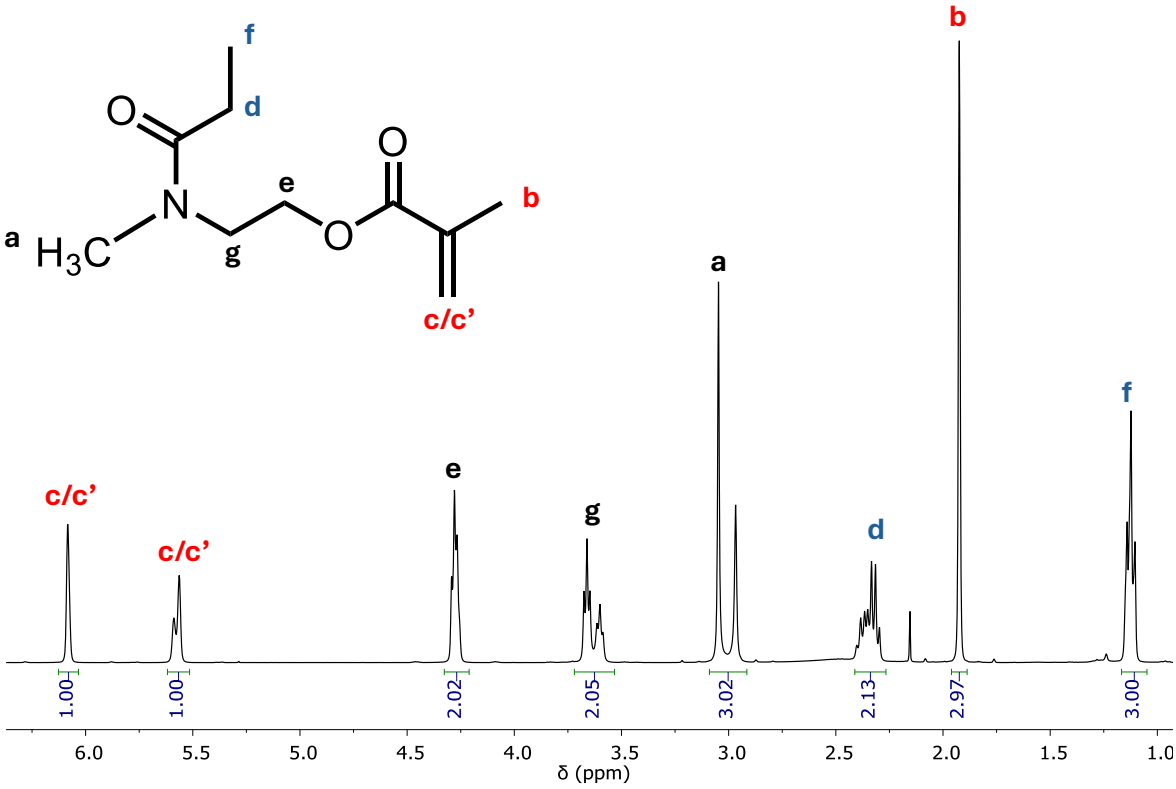

Figure 64 ^{1}H-NMR of OEOX$_1$MA.

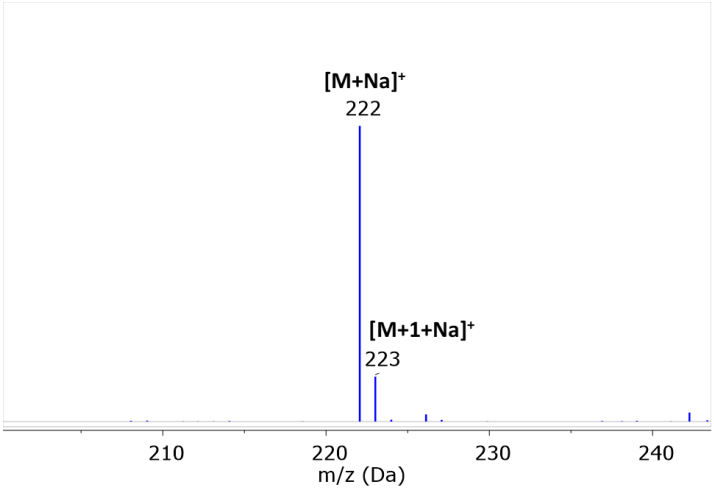

Figure 65 MS-ESI of OEOX$_1$MA.

OEOX$_2$MA:

^{1}H-NMR (400 MHz, $CDCl_3$): δ 6.06 (s, 1H), 5.60 (s, 1H), 4.25 (m, 2H), 3.50 (m, 6H), 3.00 (m, 3H), 2.30 (m, 4H), 1.91 (s, 3H), 1.10, (m, 6H).

MS-ESI (MeOH/H$^+$), signals from $C_{15}H_{26}N_2O_4$: $[M+H]^+$ 299 m/z, $[(M+1)+H]^+$ 300 m/z, $[M+Na]^+$ 321 m/z, $[(M+1)+Na]^+$ 322 m/z

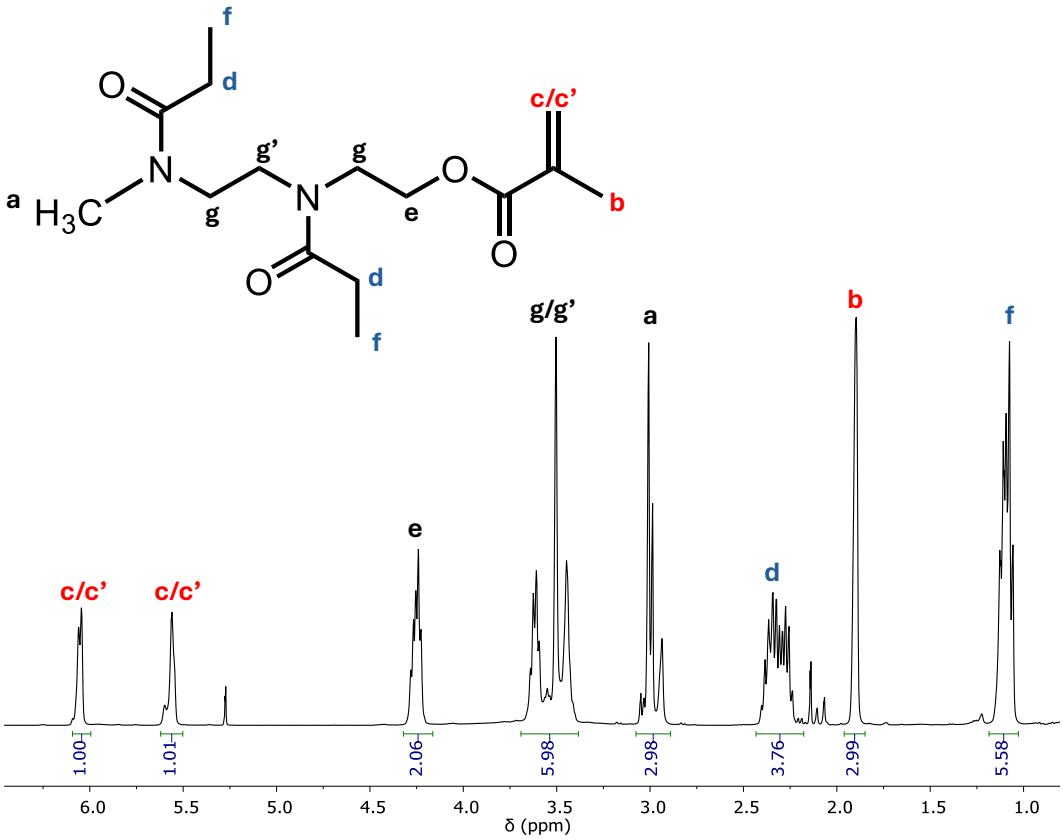

Figure 66 ^{1}H-NMR of OEOX$_2$MA.

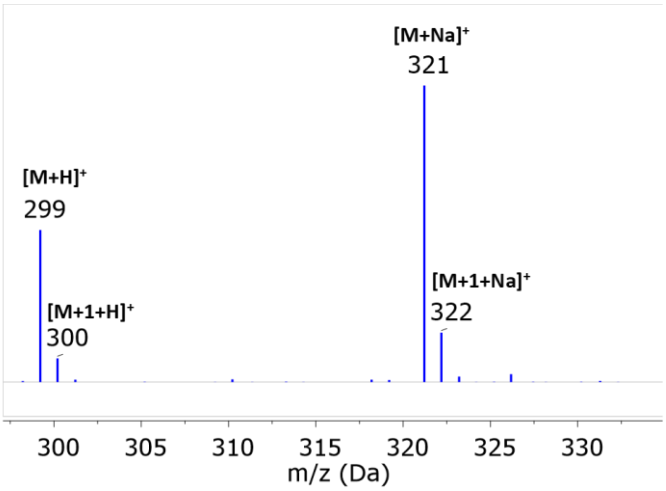

Figure 67 MS-ESI of OEOX$_2$MA.

OEOX$_3$MA:

^{1}H-NMR (400 MHz, $CDCl_3$): δ 6.06 (s, 1H), 5.60 (m, 1H), 4.25 (m, 2H), 3.50 (m, 10H), 3.00 (m, 3H), 2.30 (m, 6H), 1.91 (s, 3H), 1.10, (m, 9H).

MS-ESI (MeOH/H$^+$), signals from $C_{20}H_{35}N_3O_5$: $[M+H]^+$ 398 m/z, $[M+Na]^+$ 420 m/z

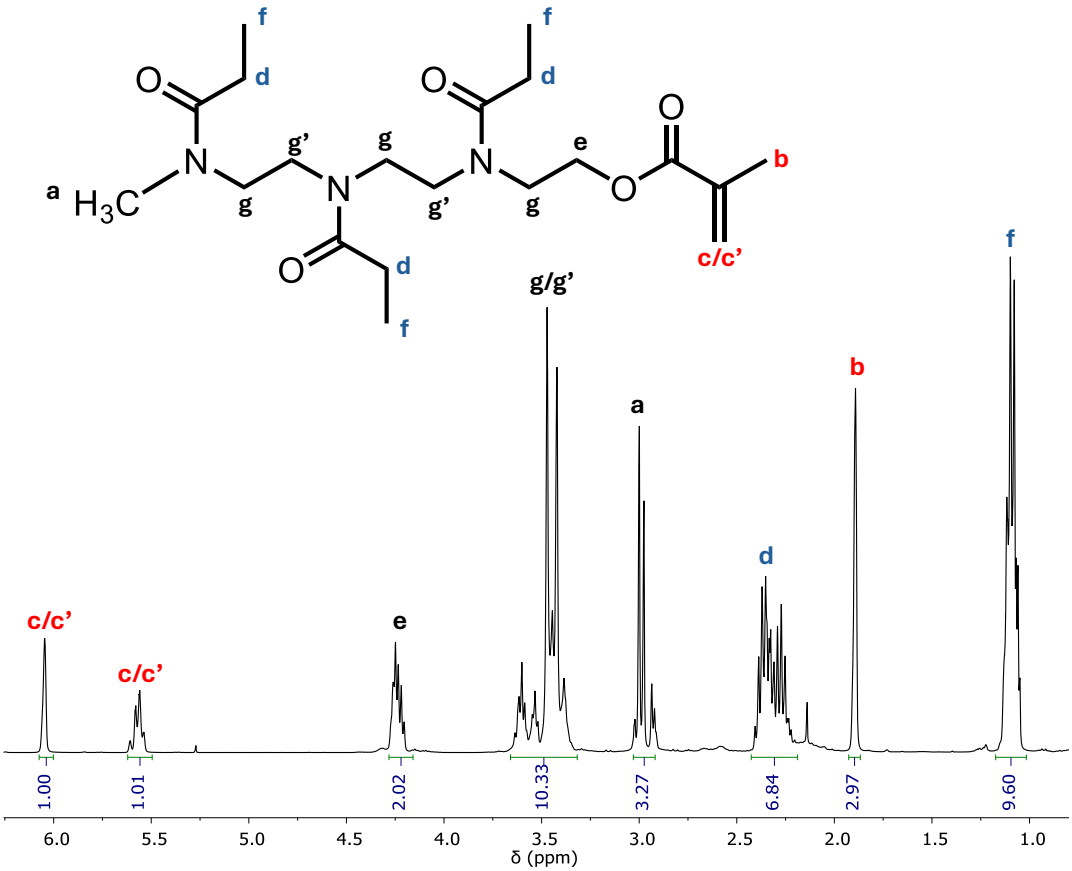

Figure 68 ^{1}H-NMR of OEOX$_3$MA.

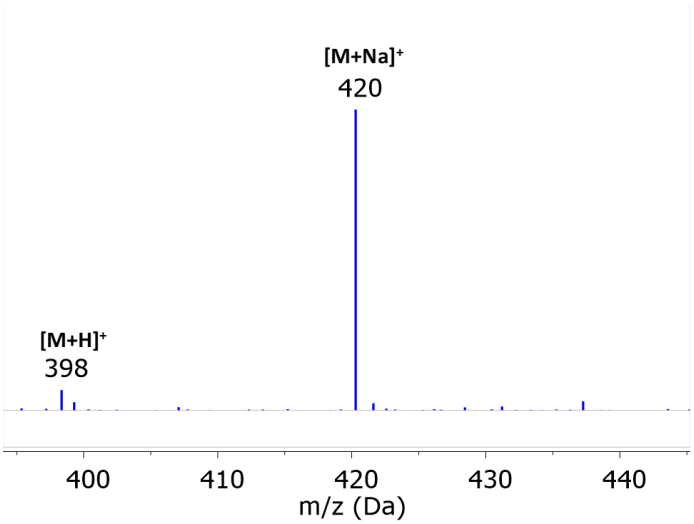

Figure 69 MS-ESI of OEOX$_3$MA.

OEOX$_4$MA:

^{1}H-NMR (400 MHz, $CDCl_3$): δ 6.10 (s, 1H), 5.60 (m, 1H), 4.26 (m, 2H), 3.50 (m, 14H), 3.00 (m, 3H), 2.30 (m, 8H), 1.91 (s, 3H), 1.10, (m, 12H).

MS-ESI (MeOH/H$^+$), signals from $C_{25}H_{44}N_4O_6$: [M+Na]$^+$ 519 m/z, [(M+1)+Na]$^+$ 520 m/z, [(M+2)+Na]$^+$ 521 m/z

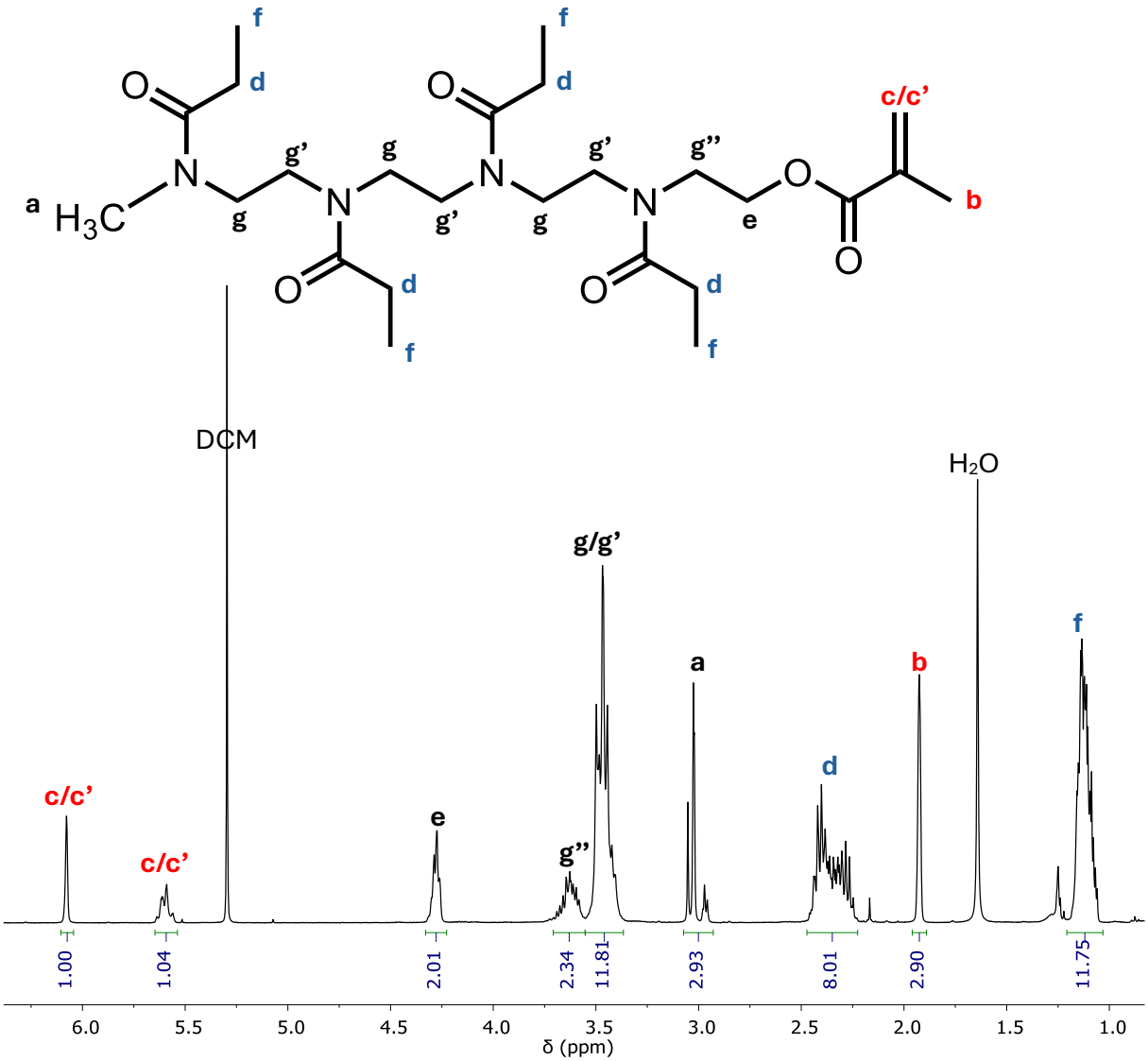

Figure 70 ^{1}H-NMR of OEOX$_4$MA.

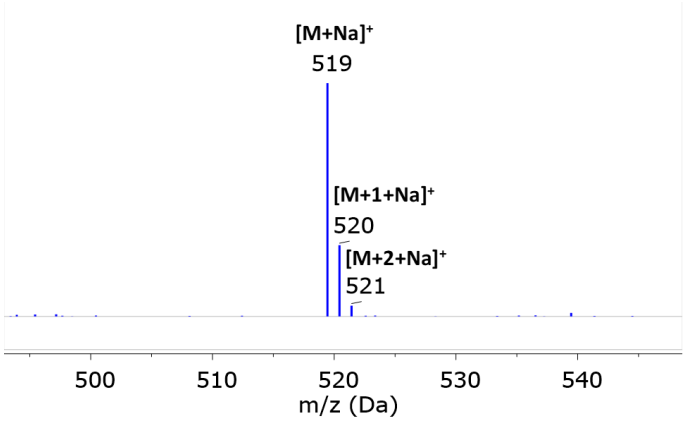

Figure 71 MS-ESI of OEOX$_4$MA.

<u>OEOX$_5$MA:</u>

^{1}H-NMR (400 MHz, $CDCl_3$): δ 6.10 (s, 1H), 5.60 (m, 1H), 4.26 (m, 2H), 3.50 (m, 18H), 3.00 (m, 3H), 2.30 (m, 10H), 1.91 (s, 3H), 1.10, (m, 15H).

MS-ESI (MeOH/H$^+$), signals from $C_{30}H_{53}N_5O_7$: [M+Na]$^+$ 618 m/z, [(M+1)+Na]$^+$ 619 m/z, [(M+2)+Na]$^+$ 620 m/z

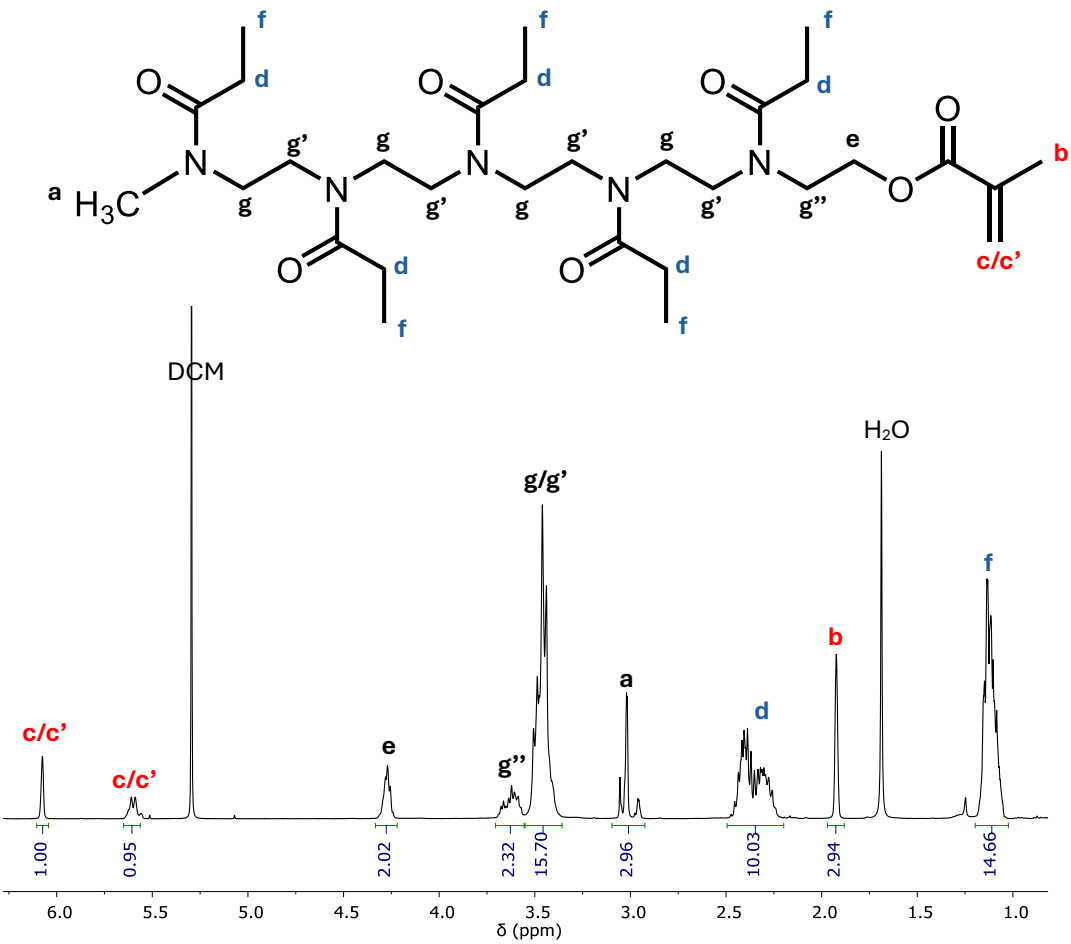

Figure 72 ^{1}H-NMR of OEOX$_5$MA.

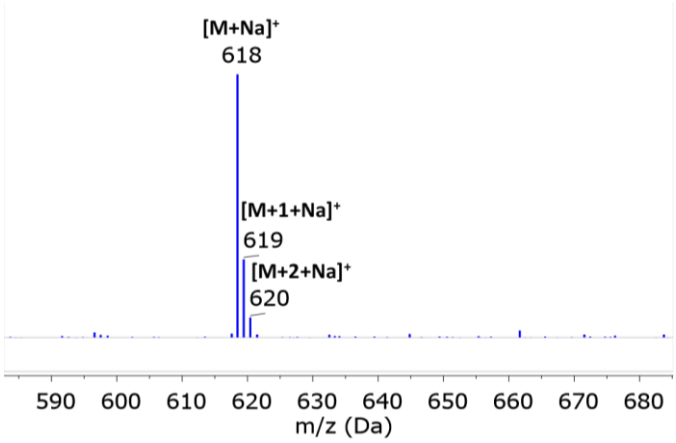

Figure 73 MS-ESI of OEOX$_5$MA.

^{1}H-NMR spectra and GPC elugrams of purified POEOX$_n$MAs

POEOX$_1$MA

^{1}H-NMR (400 MHz, $CDCl_3$): δ 4.05 (68H), 3.70 (s, 3H), 3.65 (66H), 3.01 (105H), 2.40 (73H), 1.85 (66H), 1.15 (113H), 0.90 (105H).

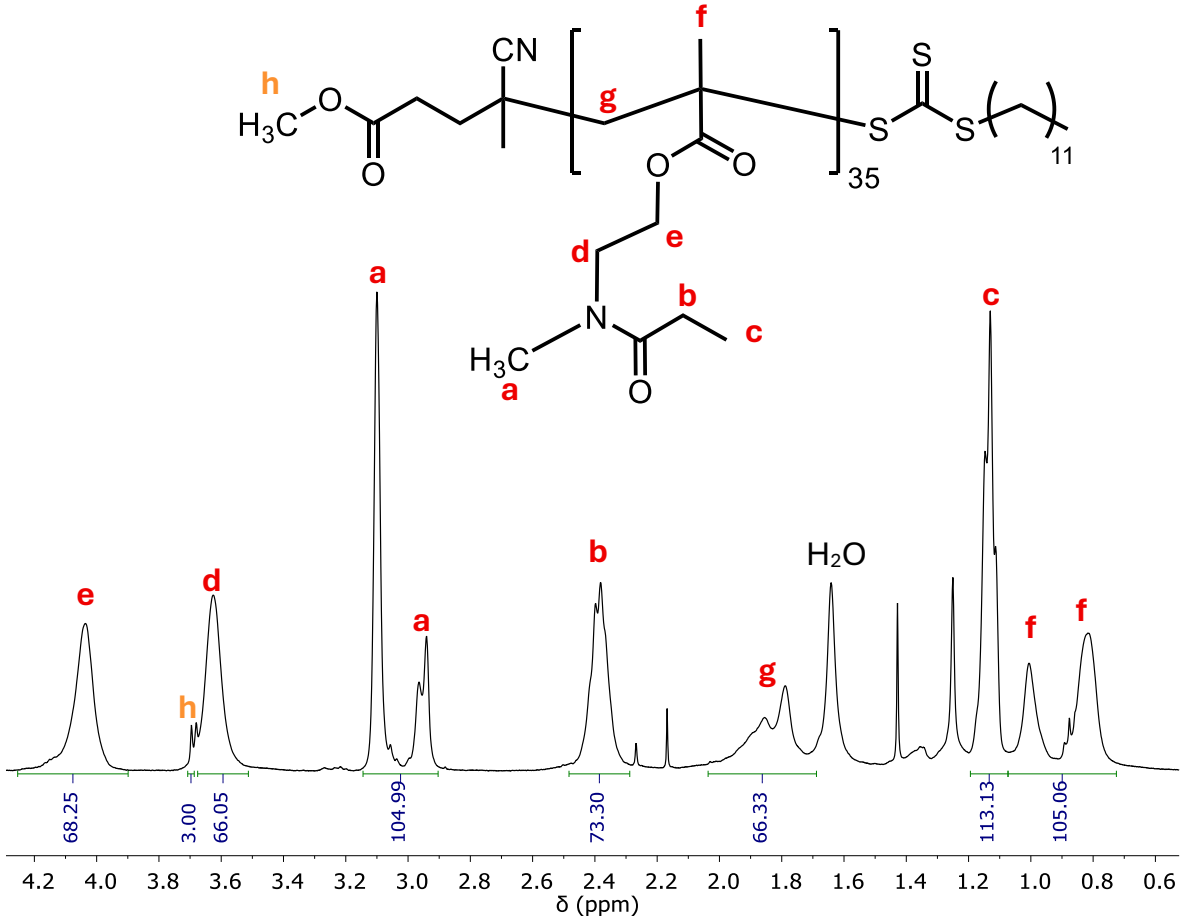

δ (ppm)	nH	integral	DP
4.05	2	68.25	34
3.65	2	66.05	33
3.00	3	104.99	35
2.40	2	73.30	37
1.85	2	66.33	33
1.15	3	113.13	38
0.90	3	105.06	35

$\overline{DP}$	35

Figure 74 ^{1}H-NMR and peaks table for DP calculation of POEOX$_1$MA.

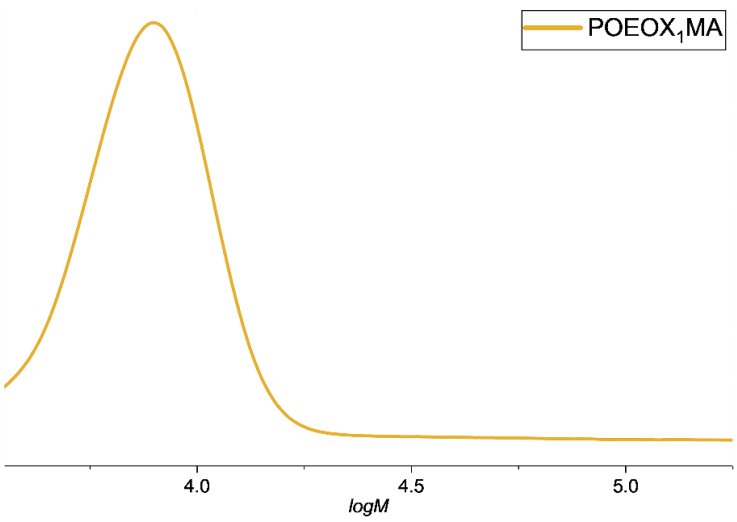

Figure 75 GPC trace of POEOX$_1$MA.

POEOX$_2$MA

^{1}H-NMR (400 MHz, $CDCl_3$): δ 4.05 (53H), 3.70 (s, 3H), 3.55 (154H), 3.01 (79H), 2.35 (103H), 1.15 (161H), 0.90 (74H).

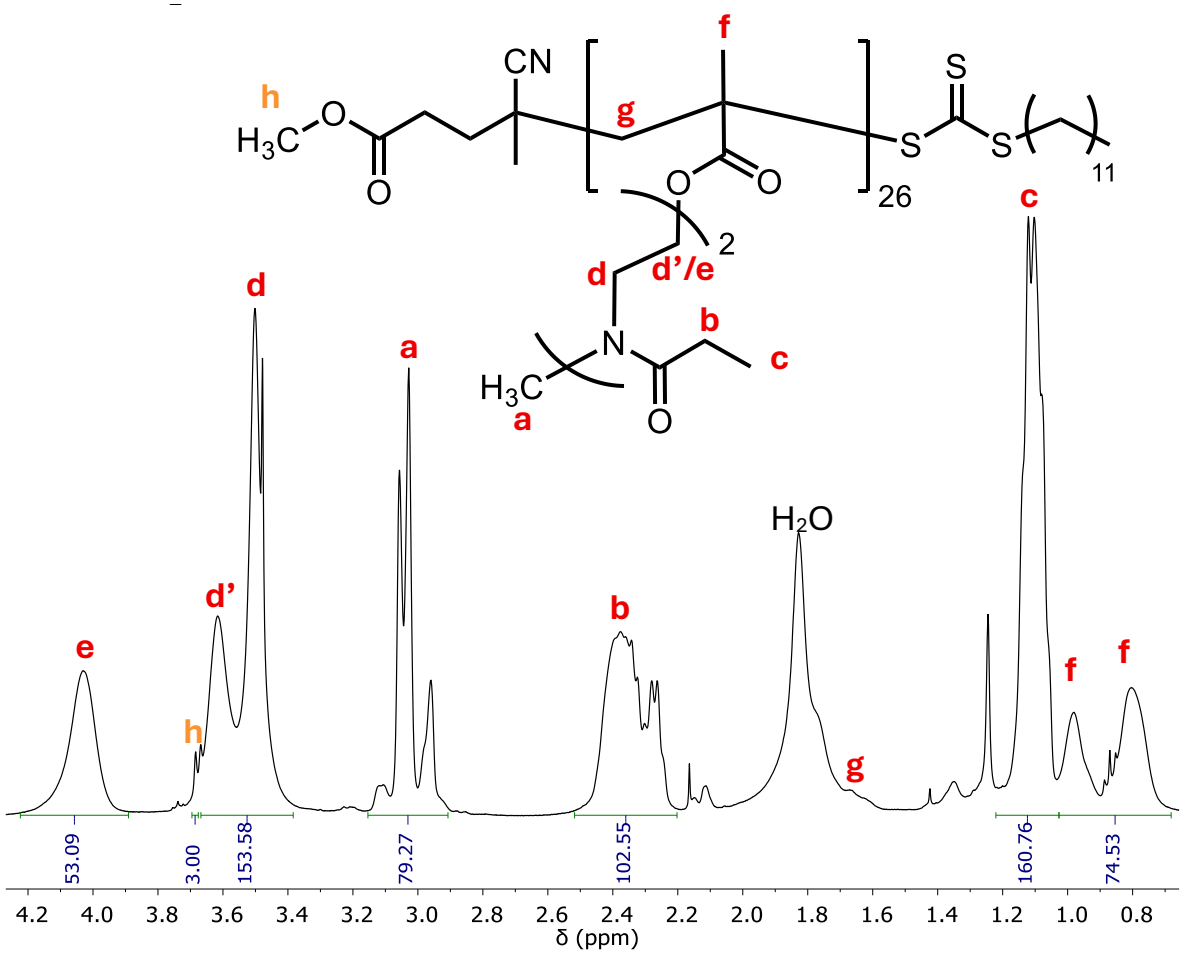

δ (ppm)	nH	integral	DP
4.05	2	53.09	27
3.65	6	153.58	26
3.05	3	79.27	26
2.35	4	102.55	26
1.10	6	160.76	27
0.90	3	74.53	25

$\overline{DP}$	26

Figure 76 ^{1}H-NMR and peaks table for DP calculation of POEOX$_2$MA.

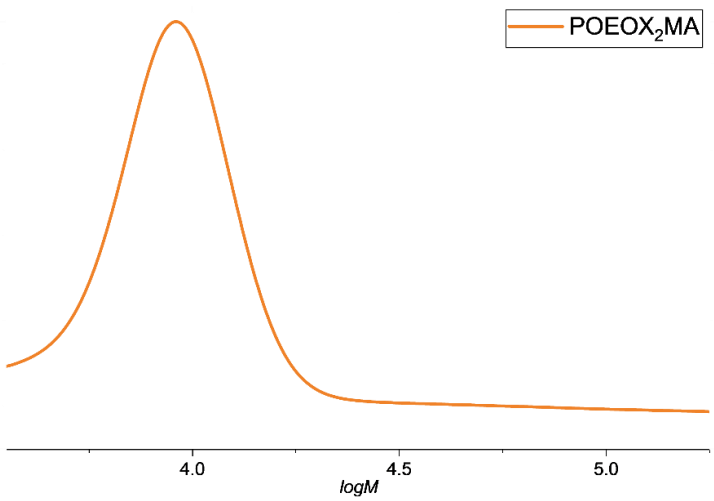

Figure 77 GPC trace of $POEOX_2MA$.

POEOX$_3$MA

^{1}H-NMR (400 MHz, $CDCl_3$): δ 4.05 (72H), 3.67 (s, 3H), 3.55 (381H), 3.01 (118H), 2.35 (243H), 1.15 (374H), 0.90 (112H).

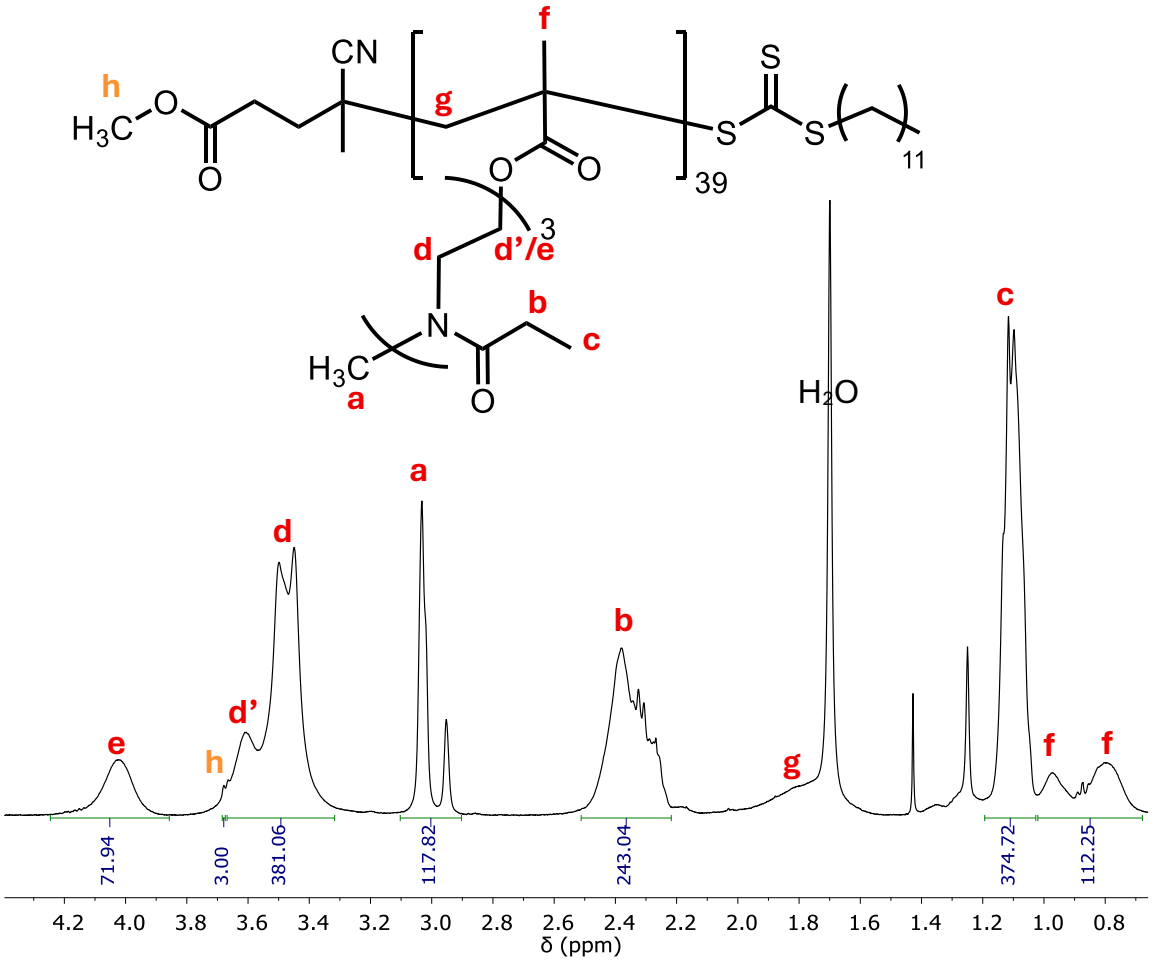

δ (ppm)	nH	integral	DP
4.05	2	71.94	36
3.65	10	381.06	38
3.05	3	117.82	39
2.35	6	243.04	41
1.10	9	374.72	42
0.90	3	112.25	37

$\overline{DP}$	39

Figure 78 ^{1}H-NMR and peaks table for DP calculation of POEOX$_3$MA.

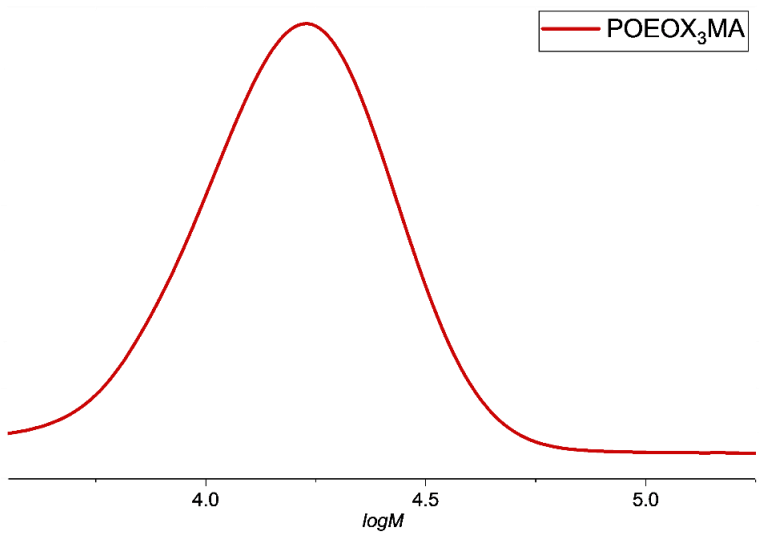

Figure 79 GPC trace of POEOX$_3$MA.

<u>POEOX$_4$MA</u>

^{1}H-NMR (400 MHz, $CDCl_3$): δ 4.05, 3.55, 3.01, 2.35, 1.75, 1.15, 0.85.

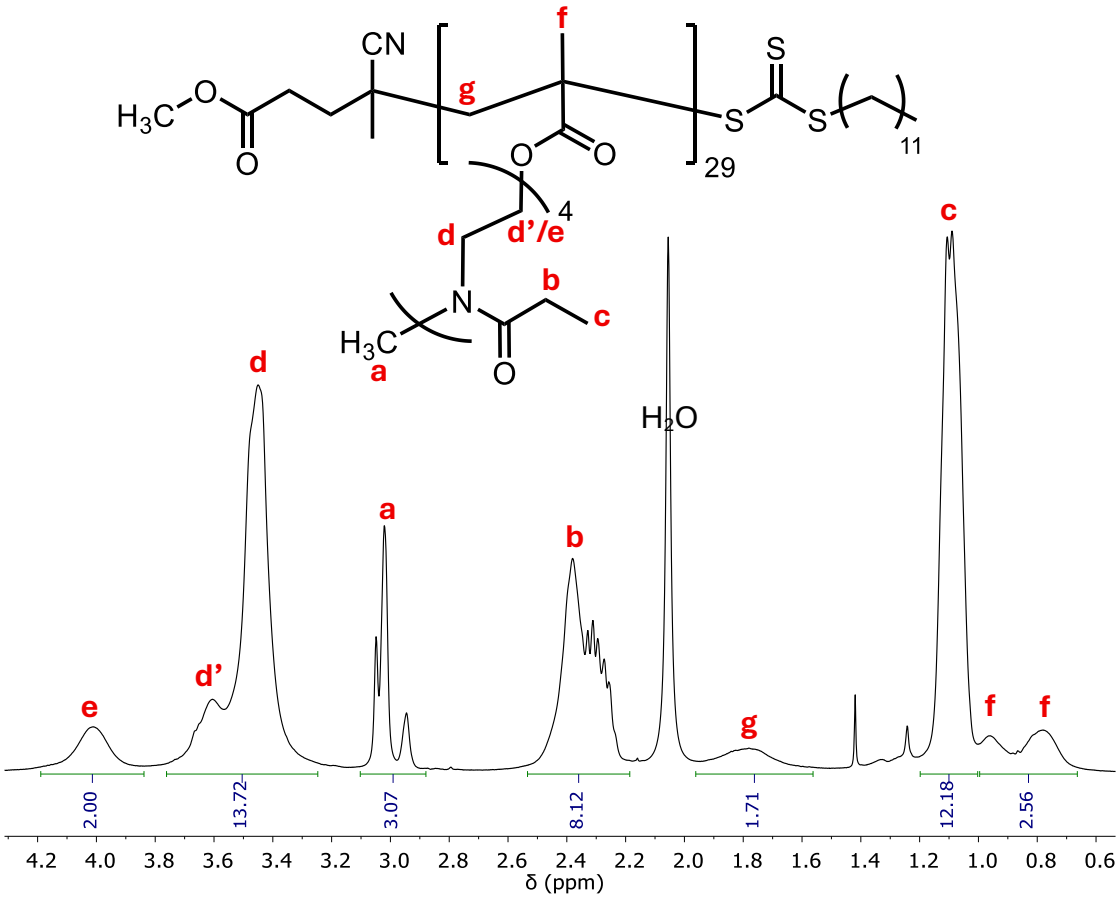

Figure 80 ^{1}H-NMR of POEOX$_4$MA.

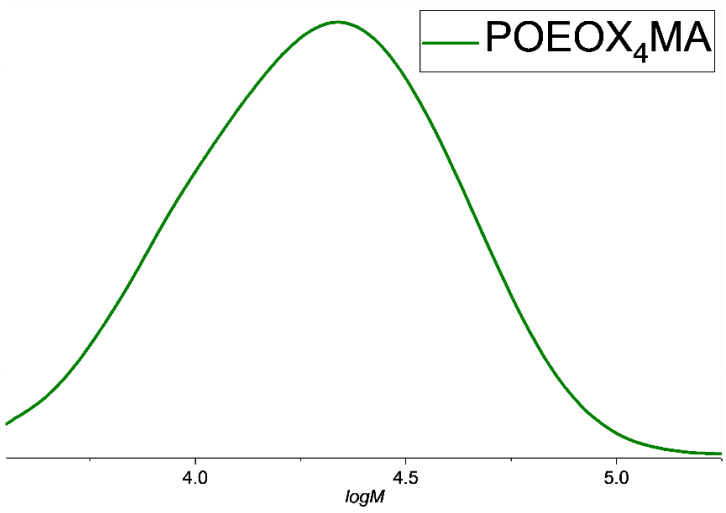

Figure 81 GPC trace of POEOX$_4$MA.

<u>POEOX$_5$MA</u>

^{1}H-NMR (400 MHz, $CDCl_3$): δ 4.05, 3.55, 3.01, 2.35, 1.80, 1.15, 0.90.

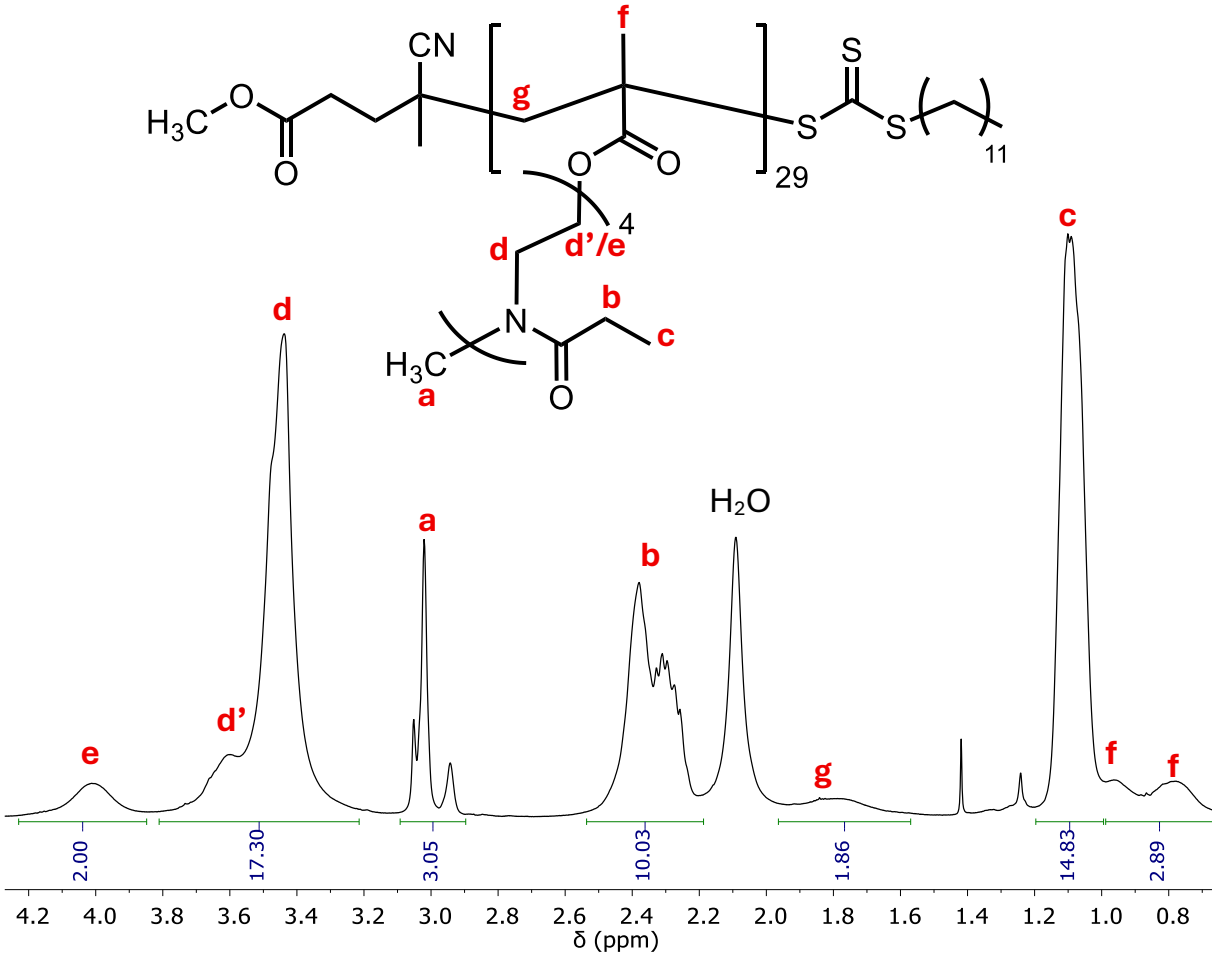

Figure 82 ^{1}H-NMR of POEOX$_5$MA.

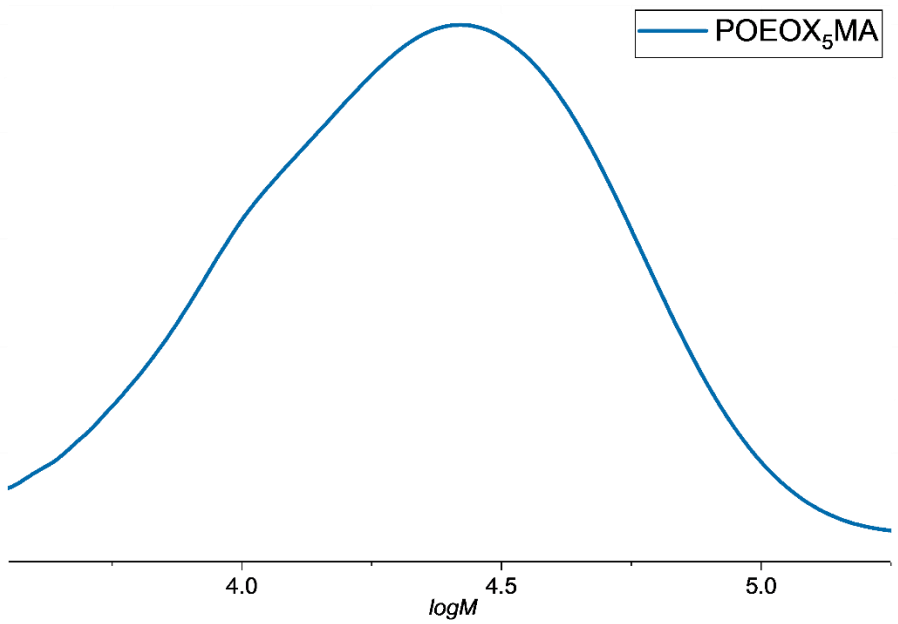

Figure 83 GPC trace of POEOX$_5$MA.

POEOX$_p$MA$_{4.5}$

^{1}H-NMR (400 MHz, $CDCl_3$): δ 4.05, 3.55, 3.01, 2.35, 1.80, 1.15, 0.90.

$$\overline{DP}_{\text{side chains}}\,(CH_3) = \frac{13.28}{3} \approx 4.4$$

$$\overline{DP}_{\text{side chains}}\,(CH_2) = \frac{9.02}{2} \approx 4.5$$

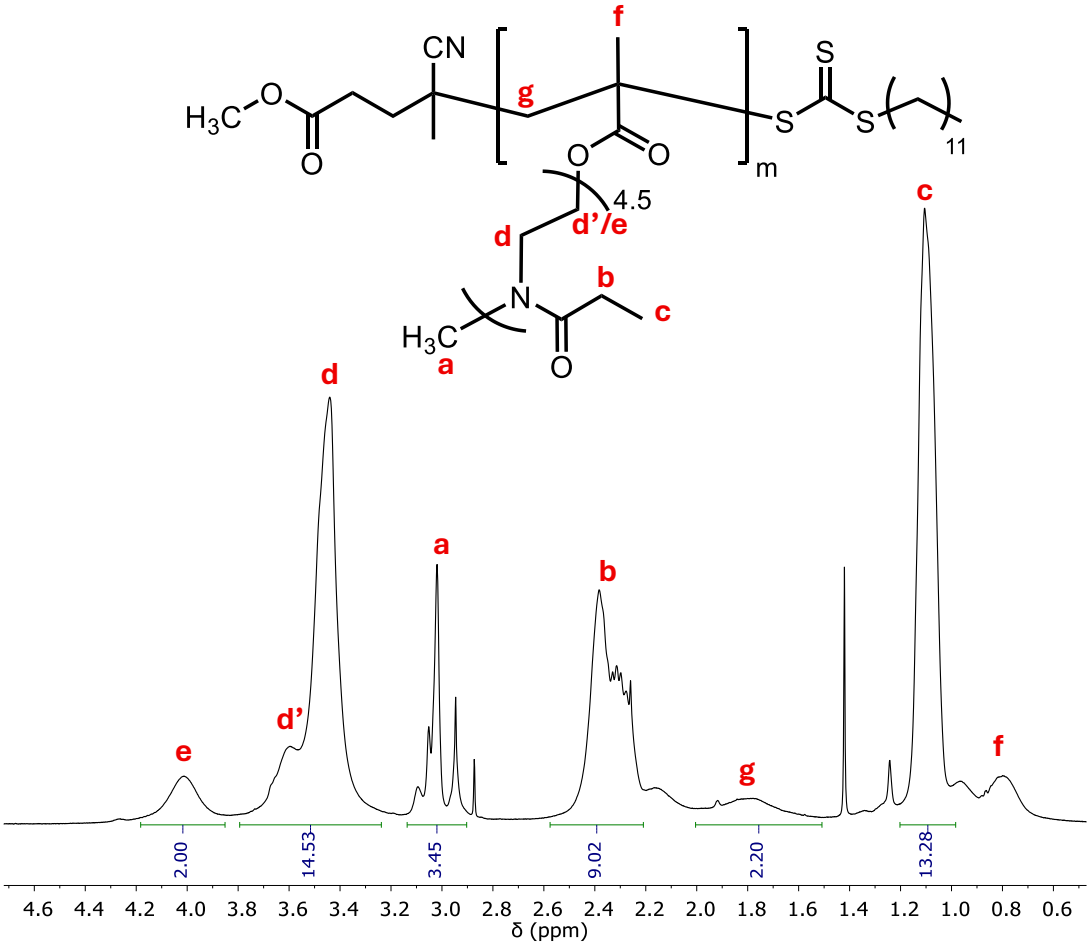

Figure 84 ^{1}H-NMR of POEOX$_p$MA$_{4.5}$.

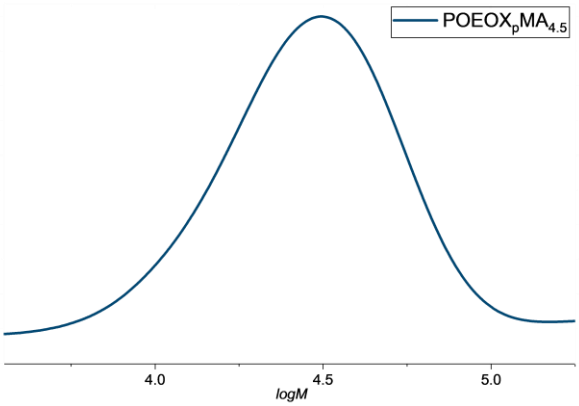

Figure 85 GPC trace of POEOX$_p$MA$_{4.5}$.

POEOX$_p$MA$_{5.5}$

^{1}H-NMR (400 MHz, $CDCl_3$): δ 4.05, 3.50, 3.01, 2.35, 1.80, 1.15, 0.90.

$$\overline{\mathrm{DP}}_{\text{side chains}}\,(\mathrm{CH_3}) = \frac{14.56}{3} \approx 4.9$$

$$\overline{\mathrm{DP}}_{\text{side chains}}\,(\mathrm{CH_2}) = \frac{9.64}{2} \approx 4.8$$

In this case, side chain $\overline{\mathrm{DP}}$ resulted lower than expected. This could due to a reduced reactivity of high molar mass oligomer species, or to an error in the integral calculation caused by the broadening of the NMR peaks.

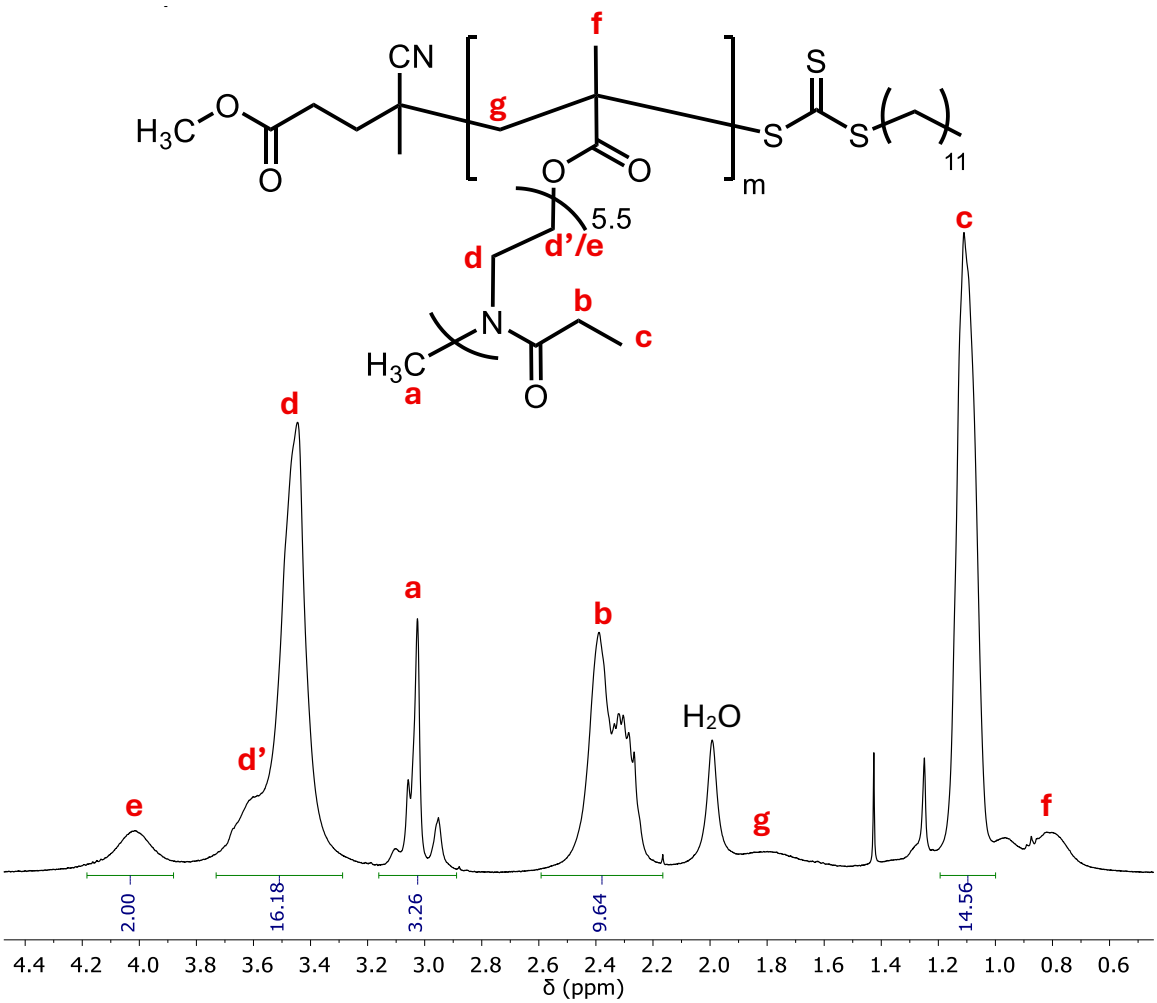

Figure 86 ^{1}H-NMR of POEOX$_p$MA$_{5.5}$.

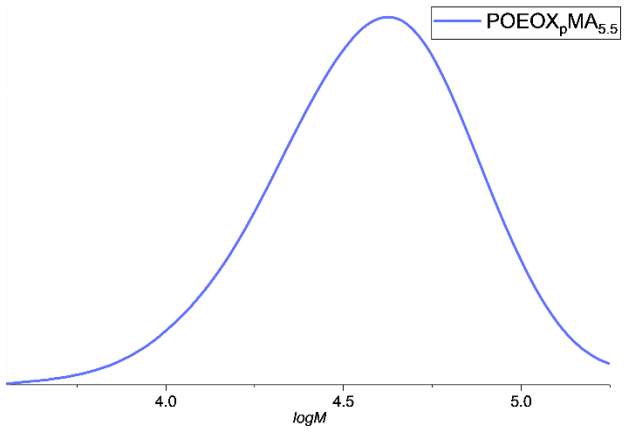

Figure 87 GPC trace of POEOX$_p$MA$_{5.5}$.

UV-Vis absorbance spectra of POEOX$_n$MA and POEOX$_n$MA-SH (superimposed)

<u>POEOX$_1$MA, POEOX$_1$MA-SH</u>

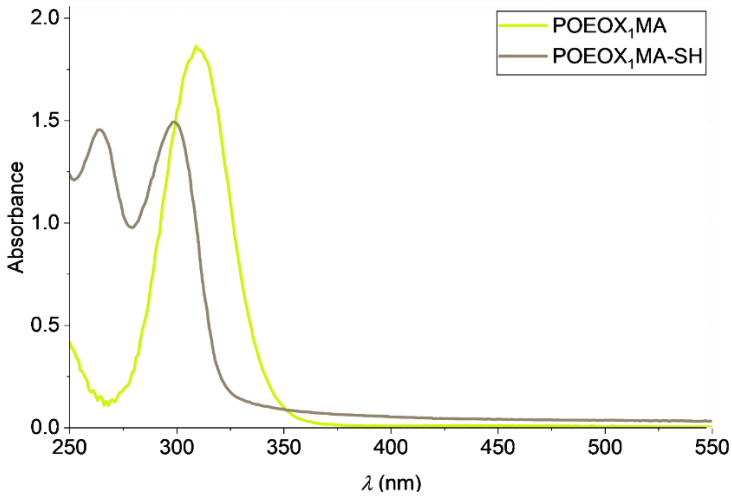

Figure 88 UV-Vis absorbance spectra of POEOX$_1$MA and POEOX$_1$MA-SH.

POEOX$_2$MA, POEOX$_2$MA-SH

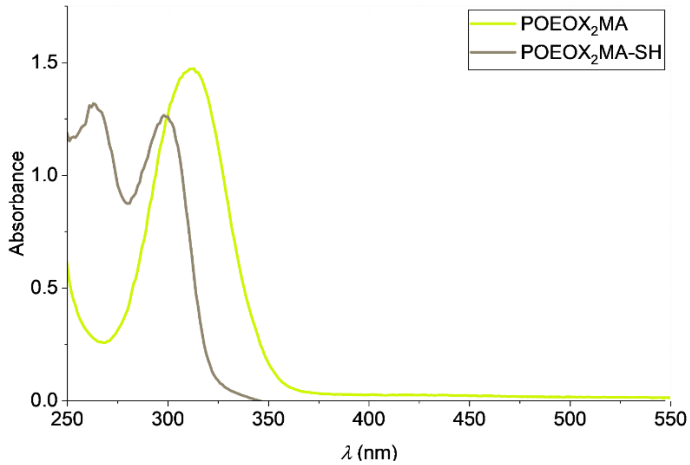

Figure 89 UV-Vis absorbance spectra of POEOX$_2$MA and POEOX$_2$MA-SH.

POEOX$_3$MA, POEOX$_3$MA-SH

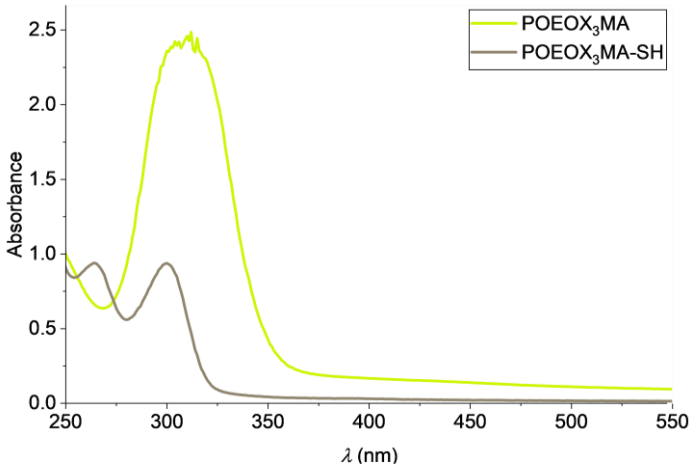

Figure 90 UV-Vis absorbance spectra of POEOX$_3$MA and POEOX$_3$MA-SH.

POEOX$_4$MA, POEOX$_4$MA-SH

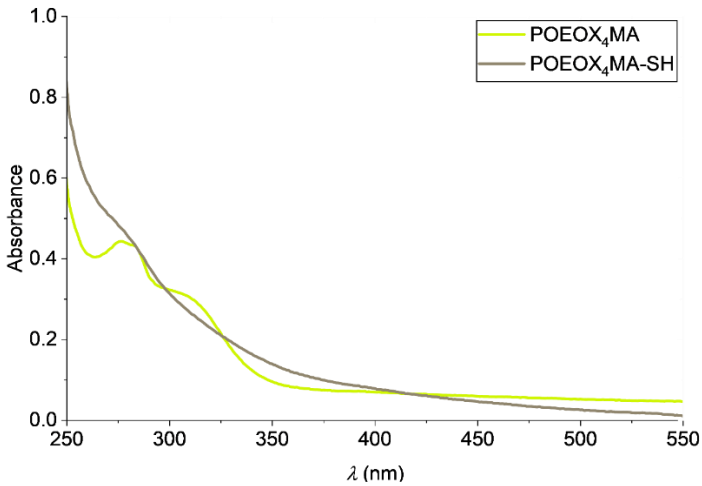

Figure 91 UV-Vis absorbance spectra of POEOX$_4$MA and POEOX$_4$MA-SH.

POEOX$_5$MA, POEOX$_5$MA-SH

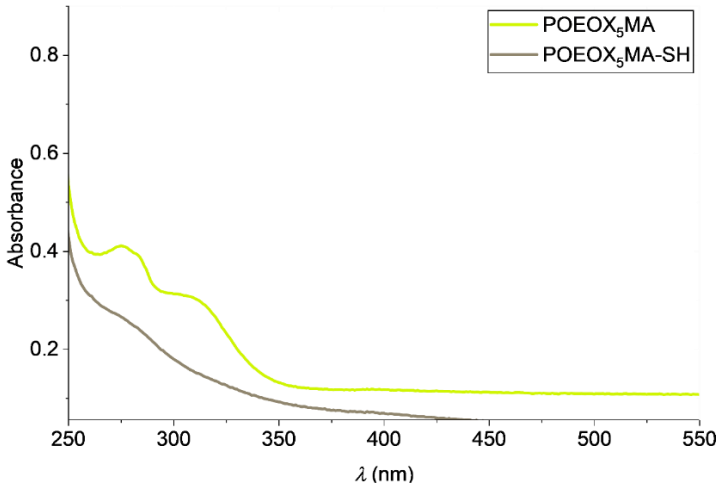

Figure 92 UV-Vis absorbance spectra of POEOX$_5$MA and POEOX$_5$MA-SH.

POEOX$_{4.5}$MA, POEOX$_{4.5}$MA-SH

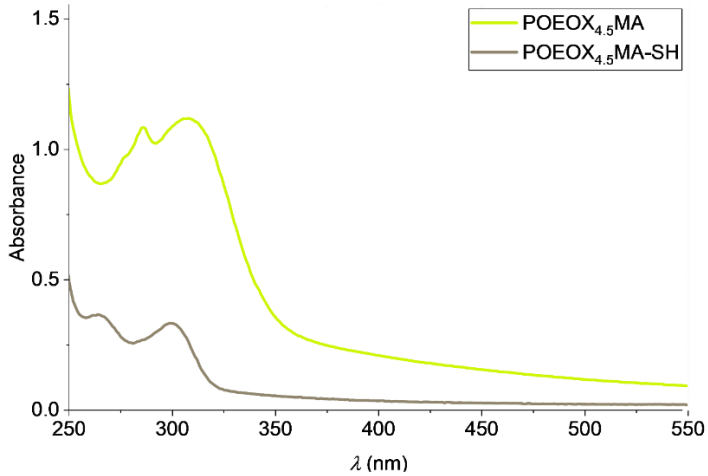

Figure 93 UV-Vis absorbance spectra of POEOX$_p$MA$_{4.5}$ and POEOX$_p$MA$_{4.5}$-SH.

POEOX$_{5.5}$MA, POEOX$_{5.5}$MA-SH

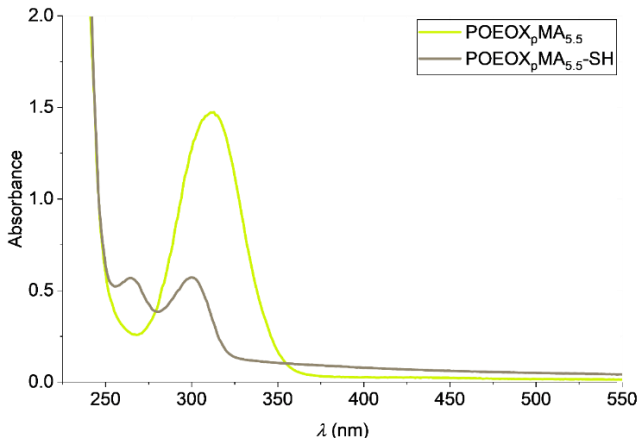

Figure 94 UV-Vis absorbance spectra of POEOX$_p$MA$_{5.5}$ and POEOX$_p$MA$_{5.5}$-SH.

Fitting of T_c for $POEOX_nMA$-SH

POEOX$_1$MA-SH

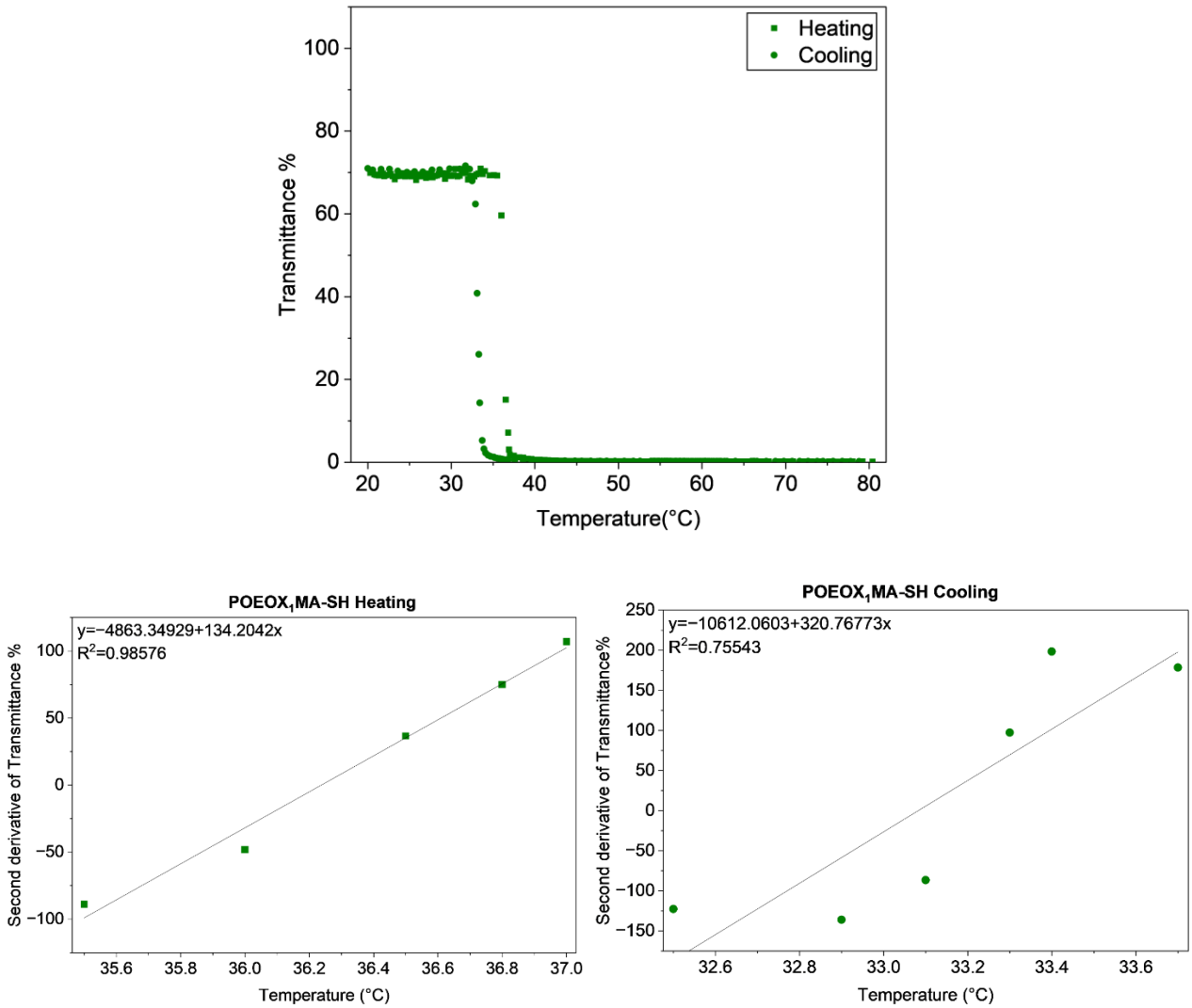

Figure 95 Transmittance % vs temperature plot (up) and linear fit for the inflection data sets (down) for POEOX$_1$MA-SH.

POEOX$_2$MA-SH

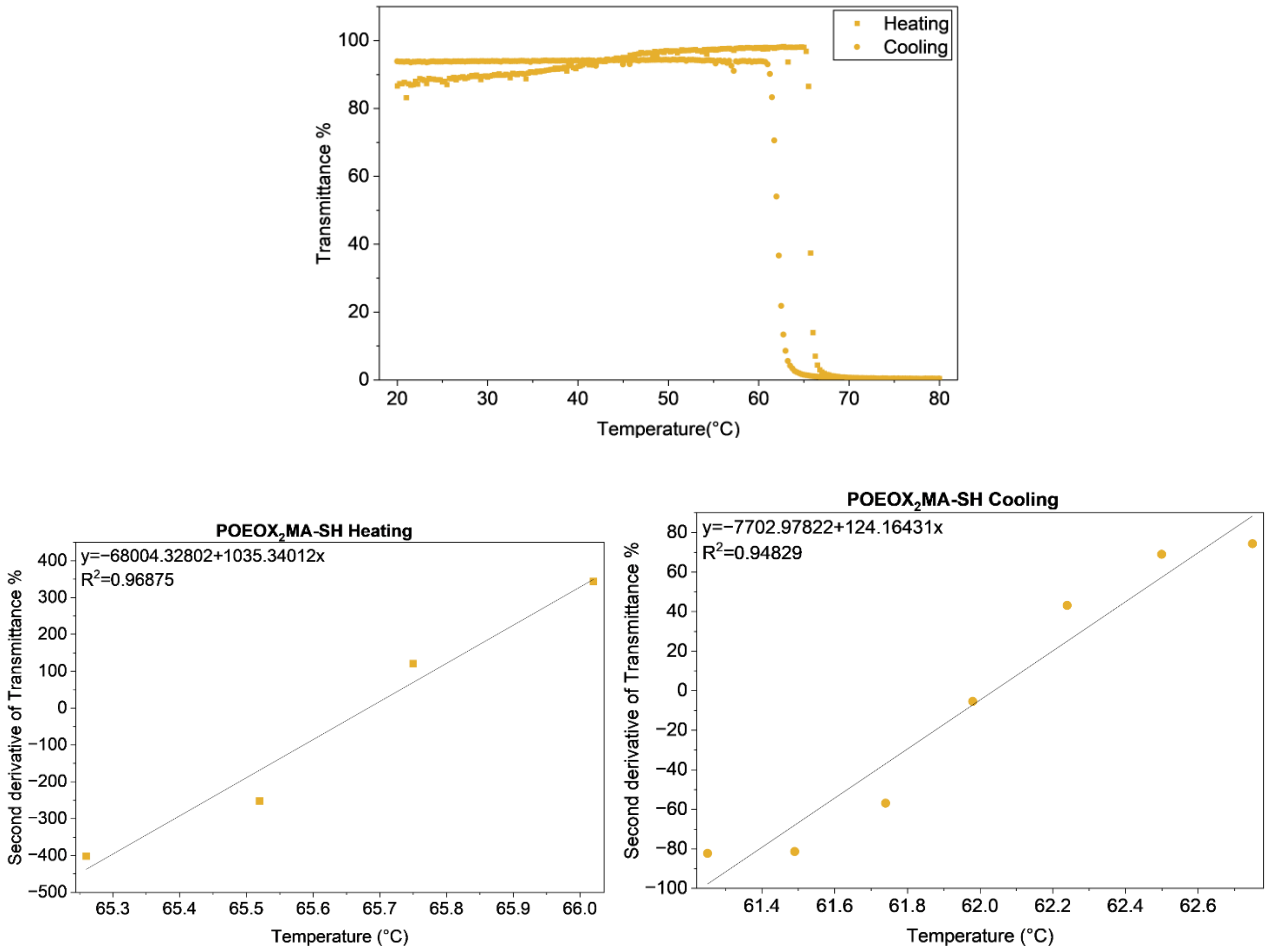

Figure 96 Transmittance % vs temperature plot (up) and linear fit for the inflection data sets (down) for POEOX$_2$MA-SH.

POEOX$_3$MA-SH

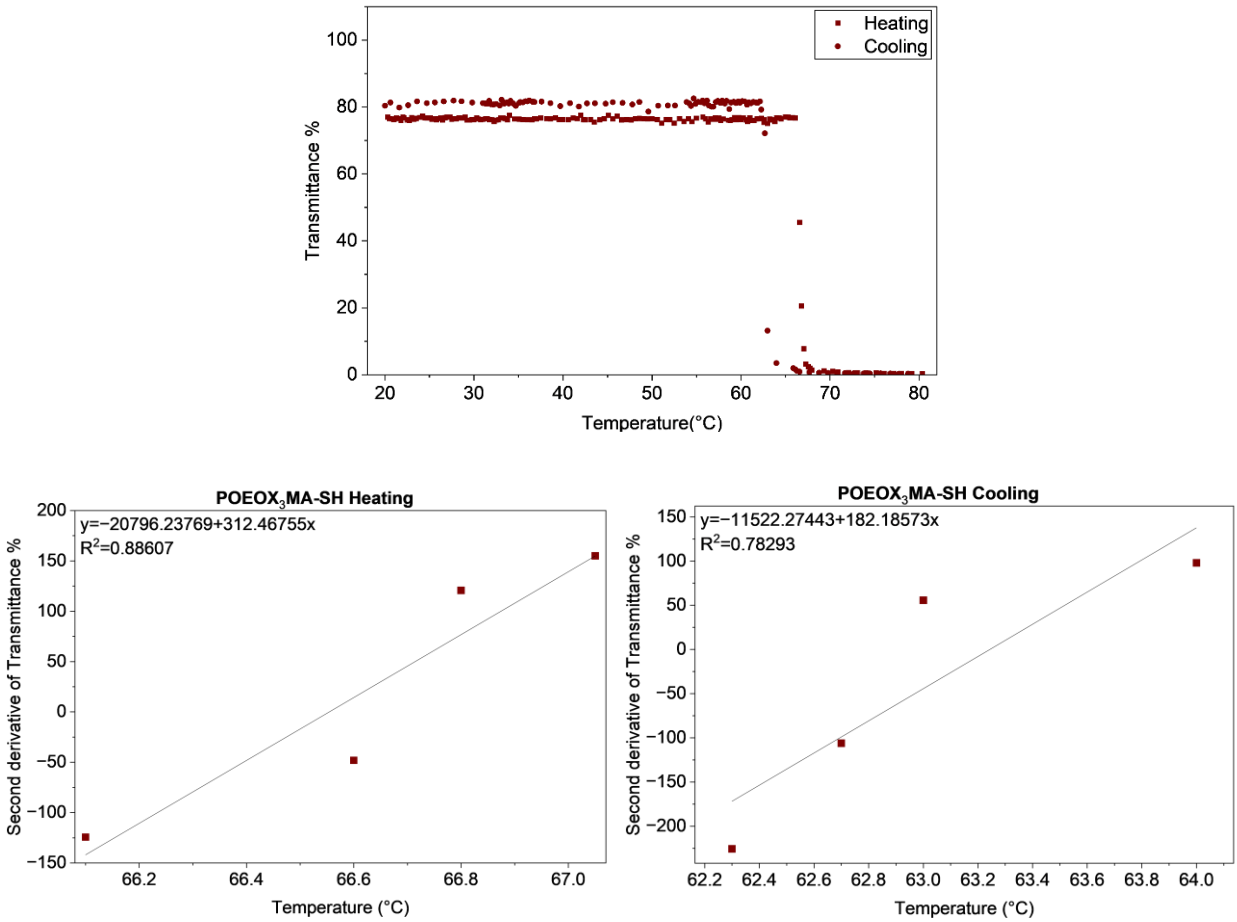

Figure 97 Transmittance % vs temperature plot (up) and linear fit for the inflection data sets (down) for POEOX$_3$MA-SH.

POEOX$_4$MA-SH

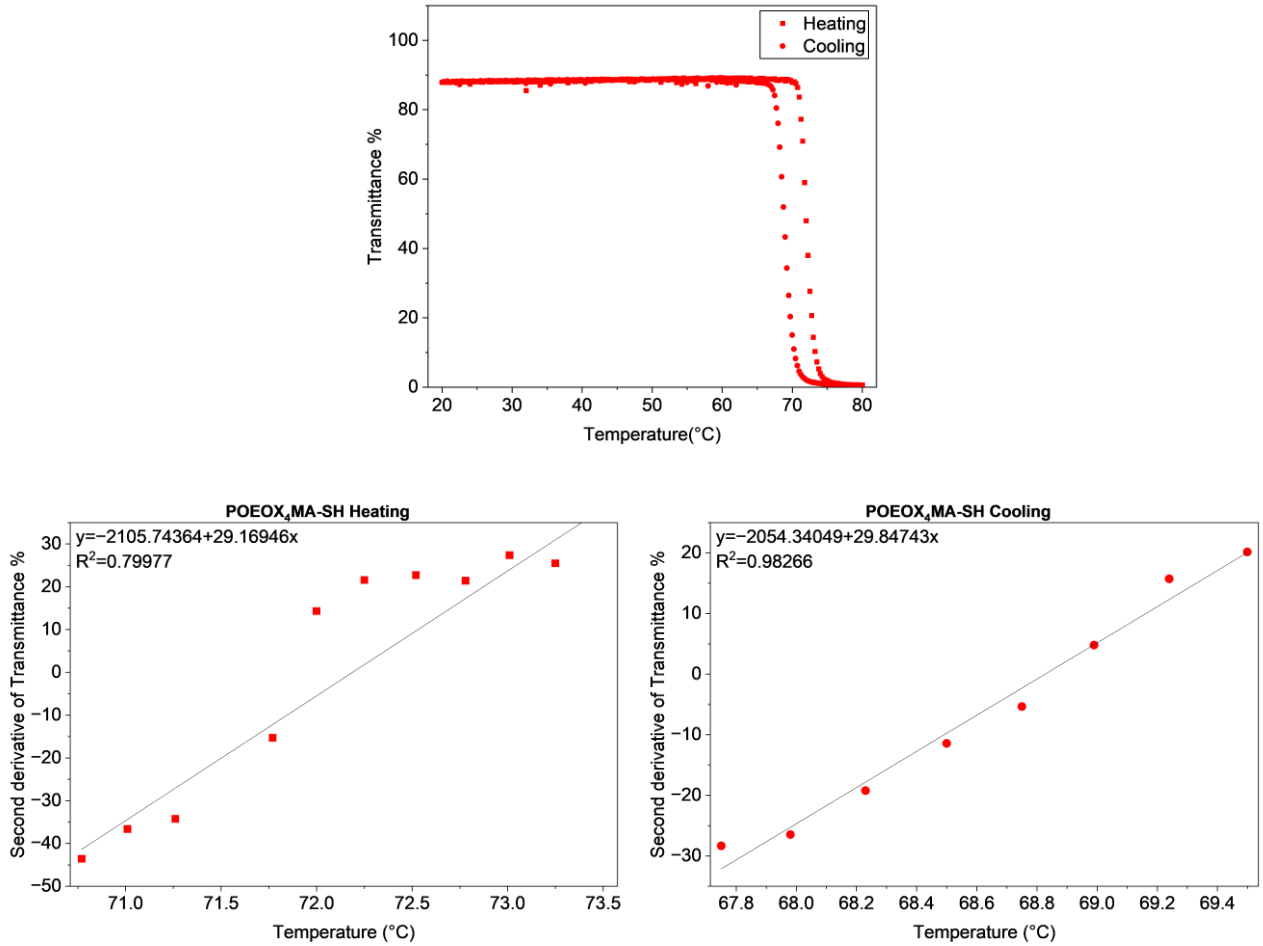

Figure 98 Transmittance % vs temperature plot (up) and linear fit for the inflection data sets (down) for POEOX$_4$MA-SH.

POEOX$_5$MA-SH

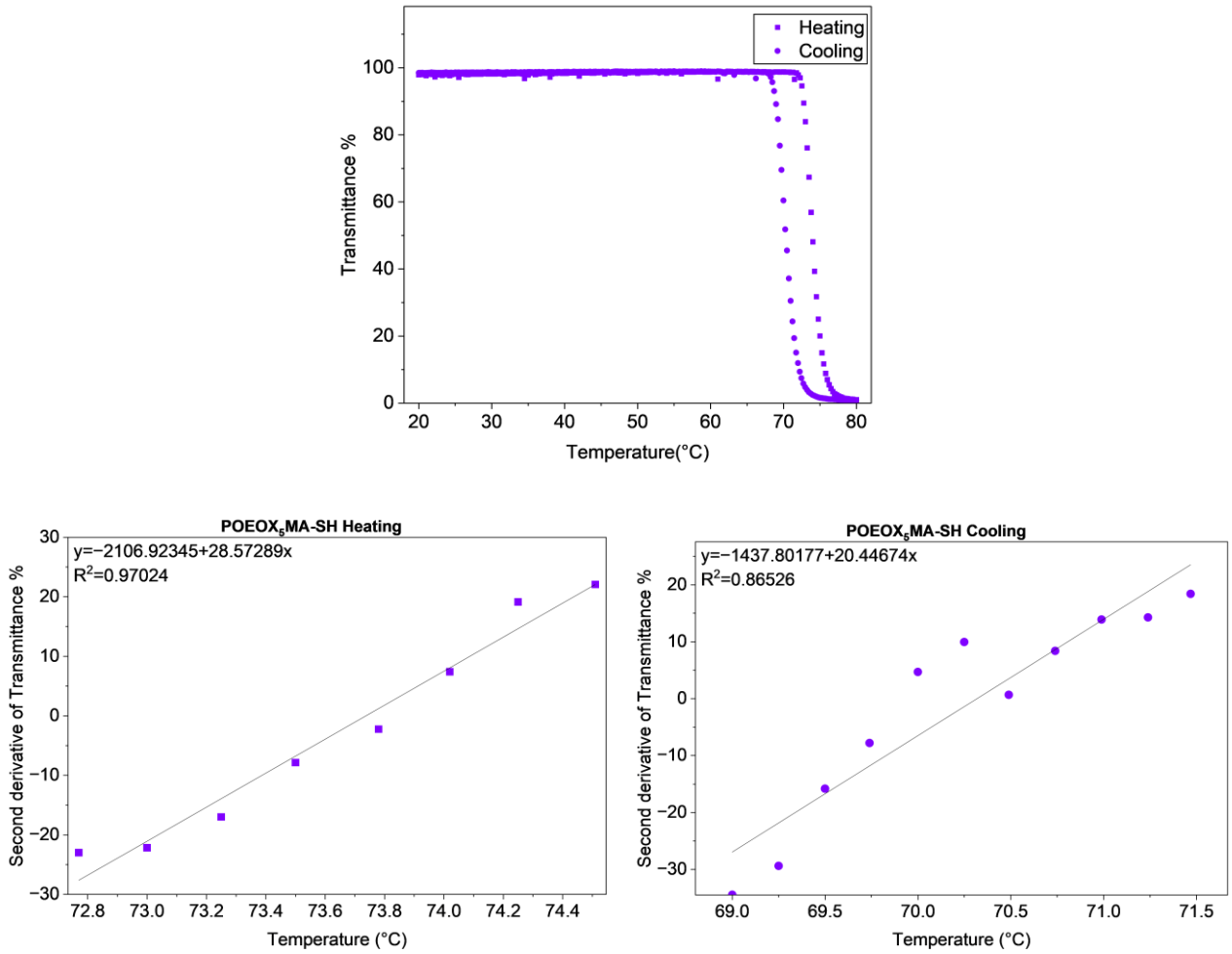

Figure 99 Transmittance % vs temperature plot (up) and linear fit for the inflection data sets (down) for POEOX$_5$MA-SH.

POEOX$_p$MA$_{4.5}$-SH

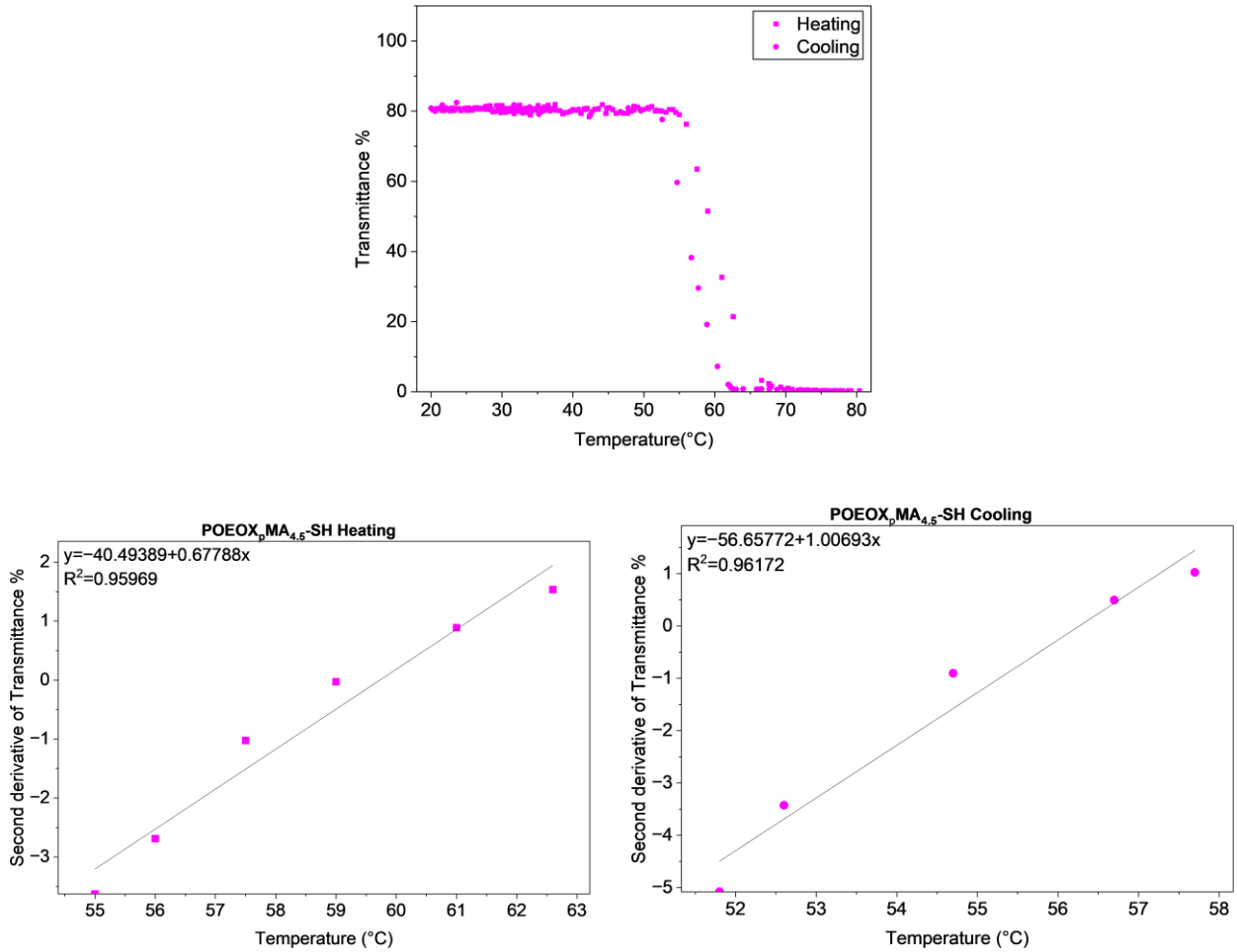

Figure 100 Transmittance % vs temperature plot (up) and linear fit for the inflection data sets (down) for POEOX$_p$MA$_{4.5}$-SH.

POEOX$_p$MA$_{5.5}$-SH

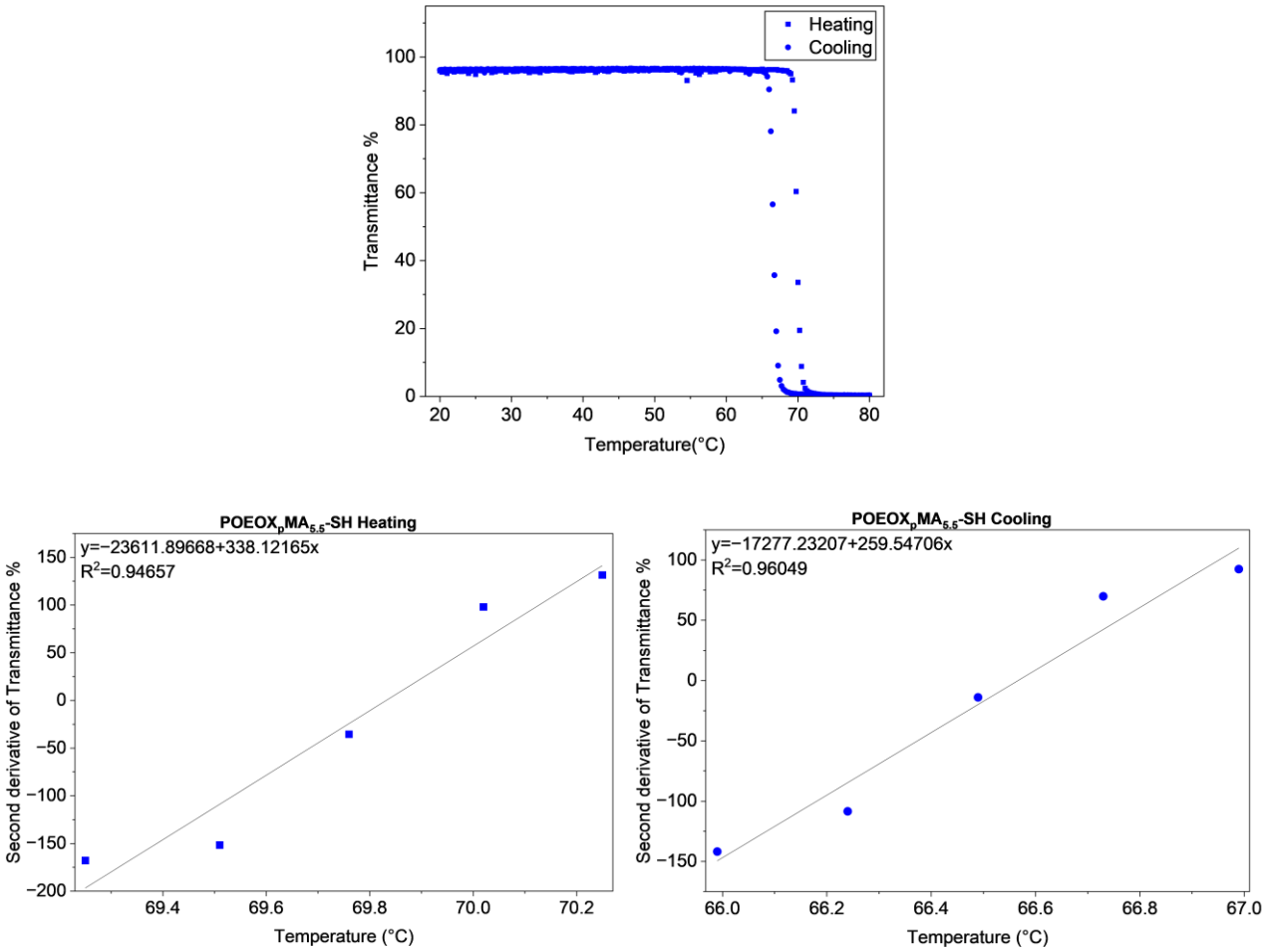

Figure 101 Transmittance % vs temperature plot (up) and linear fit for the inflection data sets (down) for POEOX$_p$MA$_{5.5}$-SH.

Quantities used for the synthesis of $OEOX_pMAs$

Chemical	*MW* (g/mol)	m (g)	n (mmol)	ρ (g/L)
EOXA	99.13	5.09	51.4	0.982
MeOTs	186.23	2.66	14.3	1.234
MAA	86.09	2.65	30.8	1.015
TEA	101.19	2.97	29.4	0.728

Table 6 Quantities used for the synthesis of $OEOX_pMA_{4.0}$.

Chemical	*MW* (g/mol)	m (g)	n (mmol)	ρ (g/L)
EOXA	99.13	8.07	81.4	0.982
MeOTs	186.23	4.93	26.5	1.234
MAA	86.09	4.56	53.0	1.015
TEA	101.19	5.26	52.0	0.728

Table 7 Quantities used for the synthesis of $OEOX_pMA_{3.4}$.

Chemical	*MW* (g/mol)	m (g)	n (mmol)	ρ (g/L)
EOXA	99.13	6.00	60.5	0.982
MeOTs	186.23	4.94	26.5	1.234
MAA	86.09	5.28	61.3	1.015
TEA	101.19	6.11	60.4	0.728

Table 8 Quantities used for the synthesis of $OEOX_pMA_{1.7}$.

Chemical	*MW* (g/mol)	m (g)	n (mmol)	ρ (g/L)
EOXA	99.13	13.02	131.4	0.982
MeOTs	186.23	4.90	26.3	1.234
MAA	86.09	4.57	53.1	1.015
TEA	101.19	5.32	52.6	0.728

Table 9 Quantities used for the synthesis of $OEOX_pMA_{5.5}$.

Chemical	*MW* (g/mol)	m (g)	n (mmol)	ρ (g/L)
EOXA	99.13	11.30	114.0	0.982
MeOTs	186.23	5.18	27.8	1.234
MAA	86.09	4.79	55.6	1.015
TEA	101.19	5.63	55.6	0.728

Table 10 Quantities used for the synthesis of $OEOX_pMA_{4.5}$.

Quantities used for the synthesis of $POEOX_nMAs$

Chemical	*MW* (g/mol)	m (mg)	n (mmol)	ρ (g/L)
$OEOX_1MA$	199.13	142.6	0.716	/
MCDP	417.70	5.9	0.014	/
AIBN	164.21	0.5	0.003	/

Table 11 Quantities used for the synthesis of $POEOX_1MA$.

Chemical	*MW* (g/mol)	m (mg)	n (mmol)	ρ (g/L)
$OEOX_2MA$	298.20	320.0	1.070	/
MCDP	417.70	8.8	0.021	/
AIBN	164.21	0.7	0.004	/

Table 12 Quantities used for the synthesis of $POEOX_2MA$.

Chemical	*MW* (g/mol)	m (mg)	n (mmol)	ρ (g/L)
$OEOX_3MA$	397.26	116.8	0.294	/
MCDP	417.70	2.5	0.006	/
AIBN	164.21	0.2	0.001	/

Table 13 Quantities used for the synthesis of $POEOX_3MA$.

Chemical	*MW* (g/mol)	m (mg)	n (mmol)	ρ (g/L)
$OEOX_4MA$	496.33	315.0	0.635	/
MCDP	417.70	5.4	0.013	/
AIBN	164.21	0.5	0.003	/

Table 14 Quantities used for the synthesis of $POEOX_4MA$.

Chemical	*MW* (g/mol)	m (mg)	n (mmol)	ρ (g/L)
$OEOX_5MA$	595.40	250.0	0.420	/
MCDP	417.70	3.8	0.009	/
AIBN	164.21	0.3	0.002	/

Table 15 Quantities used for the synthesis of $POEOX_5MA$.

Chemical	*MW* (g/mol)	m (mg)	n (mmol)	ρ (g/L)
$OEOX_pMA_{4.5}$	~544.28	514.5	0.945	/
MCDP	417.70	7.9	0.019	/
AIBN	164.21	0.7	0.004	/

Table 16 Quantities used for the synthesis of $POEOX_pMA_{4.5}$.

Chemical	*MW* (g/mol)	m (mg)	n (mmol)	ρ (g/L)
$OEOX_pMA_{5.5}$	~634.11	443.9	0.700	/
MCDP	417.70	5.8	0.014	/
AIBN	164.21	0.5	0.003	/

Table 17 Quantities used for the synthesis of $POEOX_pMA_{5.5}$.